DOKUZ EYLÜL UNIVERSITY
GRADUATE SCHOOL OF NATURAL AND APPLIED SCIENCES

INVESTIGATING ADDED VALUE OF IMPROVED DEM, RIVER GEOMETRY AND MODEL PARAMETER DEFINITIONS ON FLOOD INUNDATION MAPPING

by
Mohamed NAJAR

August, 2015
İZMİR

INVESTIGATING ADDED VALUE OF IMPROVED DEM, RIVER GEOMETRY AND MODEL PARAMETER DEFINITIONS ON FLOOD INUNDATION MAPPING

A Thesis Submitted to the
Graduate School of Natural and Applied Sciences of Dokuz Eylül University In Partial Fulfillment of the Requirements for the Degree of Master of Science in Geographical Information Systems

by
Mohamed NAJAR

August, 2015
İZMİR

M.Sc THESIS EXAMINATION RESULT FORM

We have read the thesis entitled **"INVESTIGATING ADDED VALUE OF IMPROVED DEM,RIVER GEOMETRY AND MODEL PARAMETER DEFINITIONS ON FLOOD INUNDATION MAPPING"** completed by **Mohamed NAJAR** under supervision of **ASST.PROF.DR. Ali GÜL** and we certify that in our opinion it is fully adequate, in scope and in quality, as a thesis for the degree of Master of Science.

....

Asst.Prof.Dr. Ali GÜL

Supervisor

Doç.Dr. Okan Fıstıkoğlu | Asst.Prof.Dr. Ayşegül Özgenç Aksoy

Jury Member | Jury Member

Prof. Dr. Ayşe OKUR

Director

Graduate School of Natural and Applied Sciences

ACKNOWLEDGEMENTS

I would like to express my deep appreciation to my great supervisor Asst.Prof.Dr. Ali GÜL for his constant support, time and guidance. I would also like to thank Assoc.Prof.Dr. Okan FISTIKOĞLU and Asst.Prof.Dr. Ayşegül ÖZGENÇ AKSOY for serving on my committee.

I also would like to extend my appreciation to the Director of Geographical Information Systems Department, and GIS Department staff who give me energy and knowledge to become better and better.

Thanks still goes to Assoc.Prof.Dr. Gülay ONUŞLUEL GÜL, who also provided practical advice with what is related to hydraulic modeling executing.

Mohamed NAJAR

INVESTIGATING ADDED VALUE OF IMPROVED DEM, RIVER GEOMETRY AND MODEL PARAMETER DEFINITIONS ON FLOOD INUNDATION MAPPING

ABSTRACT

Digital Elevation Model (DEM) constitutes an essential topographic dataset, which have been used to derive hydrological features forming inputs to various models. Elevation datasets are available from several major sources (remote sensing and land survey based techniques) and at different spatial resolutions. In particular, the resolution of DEM plays an important role in securing the expected accuracy of flood plain inundation maps as one of the major determinants.

In general, most of floodplain inundation maps are created using high resolution topographic datasets such as the DEMs derived from Light Detection and Ranging data. Although these datasets provide high accuracy (1.5 m grid size), they are relatively more expensive and not fully available in Turkey covering greater areas. Therefore, coarser topographic datasets with less accuracy are used to create the floodplain inundation maps.

This study applied a methodology framework in order to determine and quantify the "loss of attribute" issue when reducing the resolution of DEM as well as to understand the impact of changing DEM resolution on the floodplain hydraulic model outputs. In the study, HEC-RAS was used for the Iyidere Basin and the results clearly indicated that varying the resolution of DEMs would make significant impacts on both the depth and the extent characteristics observed in the corresponding floodplain for the river.

Keywords: Floodplain modeling, HEC-RAS, DEM resolution, İyidere river

GELİŞTİRİLMİŞ SYM, AKARSU GEOMETRİSİ VE MODEL PARAMETRE TANIMLAMALARININ TAŞKIN ALANI BELİRLENMESİ ÜZERİNE KATKILARININ İNCELENMESİ

ÖZ

Çeşitli modellere girdi oluşturan hidrolojik nesnelerin belirlenmesinde kullanılan Sayısal Yükselti Modeli (SYM), gerekli bir topografik veri seti olarak ifade edilmektedir. Yükselti verileri belirli farklı kaynaklardan (uzaktan algılamaya ve arazi çalışmalarına dayalı yöntemler) ve değişen mekansal çözünürlüklerde elde edilebilmektedir. SYM çözünürlüğü özellikle temel belirleyicilerden birisi olarak taşkın haritalarında arzu edilen doğruluğun yakalanması noktasında büyük önem taşımaktadır.

Genel olarak taşkın haritalarının büyük bölümü, Laser Interferometry Detection and Ranging (LIDAR) verilerinden türetilen SYMler gibi yüksek çözünürlüklü topografik veri setlerinden türetilmektedir. Bu veri setleri, kazanılan doğruluk artışına rağmen, nisbeten yüksek maliyetlere sahip olup, Türkiye'de kapsam bakımından yaygın olarak temin edilememektedir. Bu itibarla taşkın haritalamasında, daha düşük doğruluğa sahip ve daha az çözünürlüklü topografik veri setlerinden sıkça yararlanılmaktadır.

Sunulan çalışma, SYM çözünürlüğünün azaltılması neticesinde, çözünürlük farklılaşmalarının taşkın amaçlı hidrolik model çıktıları üzerinde oluşturabileceği etkilerin anlaşılmasının yanı sıra, oluşabilecek bilgi kaybının belirlenmesi ve değerlendirilmesi amacıyla da bir yöntem çerçevesi ortaya koymaktadır. Çalışma kapsamında, İyidere Havza örneği için HEC-RAS modeli kullanılmış olup sonuçlar, değişen SYM çözünürlüğünün taşkın yatağında gözlemlenen taşkın su derinliği ve su basma alanı göstergelerinin ikisi üzerrinde de belirgin etkilere yol açtığına işaret etmektedir.

Anahtar kelimeler: Taşkın yatağı modellemesi, HEC-RAS, SYM çözünürlüğü, İyidere akarsuyu

CONTENTS

LIST OF FIGURES

Pages

LIST OF TABLES

Pages

CHAPTER ONE
INTRODUCTION

1.1 Background and Study Objective

“One should consider preventive and protective measures before disaster hits. It is futile to lament after the disaster hits.” Mustafa Kemal Atatürk

Changes in regional and global hydrological conditions are among the major consequences of climate change that people have to cope with. One of the major challenges with climate change is its impact on water resources and extreme hydrological events (Andersson, Samuelsson, & Kjellström, 2011).

Turkey is among the countries most affected from disasters on a global scale due to its tectonic movement of the crust plate, topographic and climactic structure. Earthquakes take the first place when evaluated in terms of their devastating effects despite of disasters such as floods, landslides and fires are common in turkey. Based on statistics the last 60 years, the direct and indirect economic of turkey suffered from 3% downgrade in Gross national product (GNP), this is a sign of the importance of disaster management for turkey (Disaster And Emergency Management Presidency [AFAD], 2012).

Flood Inundation Mapping involves the steps of analysis of river flow, hydrologic/hydraulic model executing and topographical surveys. Water surface elevations (WS El.) and flood inundation extents are the two key components of flood inundation mapping. Hydraulic modeling is mainly carried out using one dimensional Hydrologic Engineering Center-River Analysis System (HEC-RAS) which has been designed and developed by United States Army Corps of Engineers(United States Army Corps of Engineers [USACE], 2010a).

Topography considers the main factor in determining the accuracy of hydraulic modeling and flood inundation mapping (Brandt, 2005). DEM is a digital grid which represents the ground surface topography. A DEM can be represented as a raster or as a Triangular Irregular Network (TIN) model. They are commonly acquired by remote sensing; however, they might also be built from land surveying. DEMs are often used in Geographic Information Systems (GIS) for which they serve as the basis for digital relief maps, and are used as a main prerequisite to hydraulic modeling.

A hydraulic model aids in forecasting the expected river flow pattern of a flooding event. DEMs are used to generate cross sections for open channel conduits representing rivers, water surface elevation and flood extents. Resolution and accuracy are the two main properties of a DEM that affect hydraulic and hydrologic modeling results (Vaze, Teng, & Spencer, 2010).

The quality of a DEM is a measure of how accurate elevation is at each pixel, spatial resolution and vertical accuracy resolution play the essential role for quality of DEMs. The spatial resolution of a DEM is the size of a pixel that is recorded in a raster image. According to the Environmental Systems Research Institute, it refers to the area covered on the ground surface by a single cell which suggests that a higher resolution DEM has more number of cells per unit area and thus represents the topography more accurately as compared to a coarser resolution DEM (Environmental Systems Research Institute [ESRI], 2014a). Resolutions of DEMs can affect the parameters and attributes derived from them and influence models associated with them (Haile & Rientjes, 2005; Omer, Nelson, & Zundel, 2003). The vertical accuracy of a DEM is the probability distribution of digital elevation values measured with respect to the true value. It is measured by the amount of linear error in elevation (ESRI, 2014b).

The accuracy of a DEM has a significant impact on the hydraulic modeling results (Darnell, Tate, & Brunsdon, 2008). Therefore, Digital Elevation Model resolution and accuracy have a direct influence on water surface elevations and flood extents.

In most studies and research, the water surface elevations and flood maps calculated using DEMs obtained from LIDAR data. Due to those DEMs are more accurate than the other widely used DEMs present in the world (Charlton, Large, & Fuller, 2003; Schumann et al., 2008)

However, LIDAR data are still unavailable for any region in Turkey as several areas around the world; hence, the land survey techniques were used to obtain DEM instead of the techniques based on remote sensing approach. This thesis focuses on the impact of the key attribute of topographic data – resolution – on modeling and flood inundation mapping. The study of resolution seeks to understand the vacillation between the resolution and the hydraulic output. Thus, two main research objectives of the study based on different DEM resolutions are:

- Investigating the impact of DEM resolution or grid size on water surface elevations and flood inundation extents
- Studying the impact of DEM errors on water surface elevations and flood inundation extents.

With the intention to accomplish these research objectives, the method of DEM resampling and error analysis is used. The thesis also aims to find a threshold for DEM grid sizes above which the hydraulic analysis results may seem to be unacceptable considering the study areas as such.

However, it should be noted here that the inference gathered from the specific outputs of this presented study is validated only for the presented case-study and some variations can be expected on different implementations over different topographies despite the fact the generally concluded relationships between the flood characteristics and the varying grid sizes should still be obtained.

1.2 Approach

The objectives of this thesis are accomplished by analyzing the results obtained from flood inundation mapping for Iyidere River in the northeast of turkey. Flood mapping for this river is carried out by one dimensional HEC-RAS modeling using topographic datasets which obtained from 20 meter interval contour lines. Several flow hydrographs associated with different recurrence intervals (return period) are adapted from an earlier study(Ousluel Gul G. et al., 2013), where hydrographs had been generated for the 2, 5, 10, 25, 50 and 100-year precipitation events estimated over the basin through hydrologic modeling efforts on the Hydrologic Engineering Center - Hydrologic Modeling System (HEC-HMS) software. The first task to attain the objectives of this study involves creating the DEM datasets from the contour lines with different resolutions, followed then by using those topographical datasets for hydraulic modeling. The results for the second objective are obtained by introducing elevation error of different magnitudes into the produced DEMs for the reach. The results are compared with flood inundation maps obtained from the high resolution DEM (i.e., the reference DEM 10-meter resolution) as the base map.

The assumption with this approach is that the 10-m. resolution DEM dataset is the topographically most accurate. However, the accuracy of the predicted flood map is not validated due to the absence of observed flood inundation map.

The high resolution DEMs generate superior output results in estimating the flood inundation area and extracting river networks when the cell sizes are less than 10 m (J. Li & Wong, 2010; Rayburg, Thoms, & Neave, 2009).

1.3 Thesis Organization

This thesis is organized in six chapters. Chapter one presents a general overview for the study problem and the study objective. Chapter Two presents a review of previous carried out studies on the impact of varying Spatial Resolution of DEMs on hydraulic modeling. This chapter also presents previous studies on Vertical Errors of DEMs analysis. Chapter three describes the study area and the hydraulic/hydrology data used for this study. Chapter four illustrates the methodology used in this study analysis. Techniques used for different variables. The methodology used to create different topographic datasets is explained first followed by a description of extraction the river network for each different DEM. A detail deception of hydraulic model execution is also presented. Chapter five presents the results obtained from this study. The results are divided into three parts discussing the impact of DEM resolution, DEM error and resample algorithms on hydraulic outputs. The chapter also shows the result obtained from vulnerability weighted indices analysis, chapter six presents the conclusions and discussion for this study.

CHAPTER TWO
LITERATURE REVIEW

The effect of added value of improved DEM, changing the river geometry and model parameters are analyzed in this thesis. DEMs with larger grid sizes have less detailed information as they have one elevation value for a larger area. DEMs with high resolution or smaller grid sizes represent elevations of smaller areas and can better represent the smaller topographic details. Previous studies on the impact of altering DEMs' resolution and the accompanying variations of vertical error in the elevations are discussed in Section 2.1. The effect of varying the accuracy of DEMs and the previous case studies discussing the importance of the errors on hydraulic modeling are presented in Section 2.2.

2.1 Effect of DEM's Spatial Resolution on Hydraulic Modeling

With the advent of GIS based techniques to obtain channel cross-sections, topographic datasets have become essential in flood mapping. The technological advances provided by GIS and the increasing availability and quality of DEMs have greatly expanded the application potential of DEMs to many hydrologic, hydraulic, water resources and environmental investigations (Moore, Grayson, & Ladson, 1991).

The cross-section elevations obtained from topographic datasets are used for hydraulic modeling in HEC-RAS to produce water surface elevations. Flood extent is obtained by subtracting the topography from the interpolated water surface obtained through hydraulic modeling (Tate, Maidment, Olivera, & Anderson, 2002).

The following two sections provide reviews of the past studies that have established the importance of (1) the spatial resolution and (2) the accuracy and errors of the DEMs.

To understand the significance of using various DEMs on hydraulic modeling, it is essential to look at the key roles properties for DEMs; which are: (1) sources of the DEMs, (2) DEM production, (3) special resolution and (4) vertical errors of the DEMs.

The National Elevation Dataset (NED) provided by the United States Geological Survey (USGS) considers the most widely used DEMs in the world; which it's provide 30 m resolution DEMs for the United States and 90 m resolution for the rest of world. The NED 30 m resolution DEMs are often obtained from cartography or photogrammetry and are of low quality due to the existence of artifacts (Gesch et al., 2002).

However, The DEMs of higher resolution and accuracy are obtained through the LiDAR remote sensing technology. The quality of LiDAR DEMs depends upon the sampling and filtering methods (Chu, Chen, Tseng, & Wang, 2014). The technology LiDAR serves as an accurate survey tool for obtaining highly accurate topographic datasets (Charlton et al., 2003); Nevertheless, Turkey as in many places around the world does not have the resources to obtain LiDAR data, and therefore, DEMs of coarser resolutions like USGS DEMs are used for hydraulic modeling where LiDAR DEMs are unavailable.

To understand the variation of hydraulic modeling results based on changing DEMs produced by the remote sensing technology. Sanders (2007) carried out a study by comparing the performances of four on-line DEMs (LiDAR, NED, SRTM and IfSAR) on flood inundation modeling for Santa Clara River in Texas. The results of this study clearly show DEMs based on airborne LiDAR are preferred because of horizontal resolution, vertical accuracy and the ability to separate bare-earth from built structures and vegetation. DEMs produced on airborne Interferometric Synthetic Aperture Radar Technique (IfSAR) have good horizontal resolution but existing of building and vegetation reflected in the gridded elevation therefor further process may be required before the flood modeling. The study also suggests that IfSAR and Shuttle Radar Topography Mission (SRTM) DEMs suffers from some errors such as radar speckle, or noise, so flood plains may predicted with no accurate results. DEMs based on national elevation data NED are remarkably smooth in comparison to IfSAR and SRTM. However, using NED, flood predictions may overestimate flood extent. In addition to this, the study highlights the utility of SRTM as a global source of terrain data for flood modeling.

With the intention to evaluate the remote sensing technology DEMs when compared to ground survey techniques DEMs, Casas, Benito, Thorndycraft, and Rico (2006) carried out a study of accuracy of topographic dataset sources in hydraulic modeling for Ter River near Sant Juliá de Ramis, which consisted of Digital Terrain Models (DTMs) from three different sources: high resolution LiDAR, global positioning system (GPS) survey and vectorial cartography. Hydraulic modeling was carried out using HEC-RAS and water surface elevations and delineated flooded area were analyzed. The study reveals that LiDAR dataset have the highest accuracy with less than 1% variation followed by GPS-based DTMs by less than 8% variation. The contour-based DTM performed with the least accuracy with a variation of 50% in the flood inundation determination from the observed data.

The hydraulic modeling for the two studies described above (Sanders, 2007 and Casas, Benito, Thorndycraft, & Rico, 2006) was performed using HECRAS. These studies showed that the performance of LiDAR DEMs was superior to the other available DEMs (USGS, IfSAR and SRTM) as well as DEMs derived from different sources (GPS survey, photogrammetry and cartography).

One of the most important properties of a DEM affecting hydraulic modeling results is its spatial resolution. In order to increase the prediction accuracy of DEMs, it is essential to understand the effectiveness of DEM resolution on flood mapping. Many studies were carried out analyzing the effect of varying DEM resolution on hydraulic modeling which concluded that DEM resolution played a significant role in predicting hydraulic outputs.

One of the first studies by Werner (2001) to analyze the impact of grid size on accuracy of predicted flood areas showed that hydraulic controls such as embankments have a significant effect on the accuracy of flood extents. Local elevations around the hydraulic controls averaged out on using a coarser resolution DEM while the use of higher resolution DEMs increased the computational time significantly.

This study reveals that the main disadvantage of using coarse DEMs to perform hydraulic model was the inaccuracy in determining correct elevations for bridges, embankments and levees. However this problem could be corrected by using field surveyed elevations and locations for hydraulic controls, the effect of increasing the grid size or decreasing DEM resolutions on predicted flood extents is still significant and further studies were carried out to evaluate this effect.

In order to understand the effect changing DEM resolution for an urban area, Haile and Rientjes (2005) carried out study for the city Tegucigalpa in Honduras which, severely has been affected by flood events as caused by extreme rainfall events. For the study area, a DEM with 1.5 m grid size resolution was generated and consider as reference base for the various resample DEMs. The reference 1.5 m base DEM was resampled by decreasing the resolution up to 15 m. As a result of resampling, losing attributes from cross section, which affects the flood analysis, was realized.

The study concluded that the DEM resolution has significant effect on flood inundation mapping. Flood simulation characteristics that are affected are inundation extent, flow velocity, flow depth and flow patterns across the model domain. It has however not become clear by this study what generic aspect of the applied flood model approach has caused the significant differences. In this study three possible causes are identified. Firstly, the hydraulic gradient at the downstream boundary could have an impact on the computed flood characteristics. Secondly, in general decreasing the resolution has a significant impact on the flood simulation. Thirdly, at larger grid elements flow direction delineation becomes more arbitrary particular when rectangular grid DEM structure is applied which is also specific to the SOBEK flood model approach.

In order to recognize the causes of over-predictions of flood extents by coarser resolution DEMs, a study on the effect of cell resolution on depressions was carried out by Zandbergen (2006) for a 6-meter LIDAR DEM for a watershed in North Carolina was used to determine the relationship of DEM resolution and occurrence of depressions. With smaller cell sizes the number of depressions was found in increasing and following an inverse power relationship. At coarse resolution, the topography is much smoother, the terrain variability is no longer reliably represented, an extensive number of large and sometimes deep artificial depressions are generated. The study also reveals that the use of the highest resolution and most accurate data, such as a LIDAR derived DEM, may not result in the most reliable estimates of terrain derivatives unless proper consideration is given to the scale-dependency of the parameters being studied.

Based on the studies mentioned above, most studies advocate that a coarser resolution DEMs have negative correlation with accuracy as well as resulted over-predicted flood extents. In addition of that using coarser resolution DEMs to extract cross section resulting obvious smoothing in the cross sections profile.

The presented study introduces a method to quantify and assess the change in hydraulic modeling outputs resulting from varying spatial resolution of DEMs, which is not established in the previous studies.

2.2 Effect of DEM’s Accuracy and Errors in Hydraulic Modeling

On the other hand, with the aim of understanding the impact of the accuracy and errors of the DEMs on the hydraulic modeling, it’s essential to investigate several parameters which may lead to generate these errors.

In order to compare and quantify the magnitude of error inclusion in different DEMs, a study by Gonga-Saholiariliva, Gunnell, Petit, and Mering (2011) carried out to conduct a comparative analysis of DEMs derived from six different sources (airborne, radar, optical and composite) for Wasatch Mountain Front in Utah. These DEMs included LiDAR (2 m), CODEM (5 m), NED (10 m), ASTER DEM (15 m), GDEM (30 m) and SRTM (90 m). The results show that LiDAR DEMs have the least errors followed by NED 10 which is generated from composite data sources. CODEM and ASTER DEM show high magnitude of errors even after having high ground resolutions. This study highlighted the importance of source-study before processing and delivering the final product.

Even though a significant percentage of DEM error are random, F. J. Aguilar, M. A. Aguilar, Agüera, and Sánchez (2006) carried out study in order to develop model which determines the error that occurs when modeling the terrain surface from randomly spaced data points that are converted into regularly gridded data points using triangulation with linear interpolation. Nevertheless, the linear interpolation does not positively correlate with the creation of DEM.

Therefore, Aguilar et al. (2010) carried out a follow up study for data for 29 study sites, 200 × 200 m in size, belonging to different areas around Almeria province, south-east Spain. In contrast the study which carried out in 2006, inverse distance weighed interpolation method was used to develop the error in LIDAR based DEMs of non-point terrain. The study suggests that the DEM's errors are a combination of the error from LiDAR data capture of ground sampled points in open terrain, in addition to a non-negligible error that refer as gridding error that produced by interpolation methods used for infilling gaps. The result of this study reveals a very good agreement between predicted and observed data ($R^2 = 0{:}9856$; $P < 0{:}001$).

Regarding the validation results, Bristol in United Kingdom observed vertical errors, corresponding to different LiDAR point densities, which suggest a reasonable fit to predicted errors. Better result even achieved in Gador mountain topographic dataset which has rugged morphology than Bristol area. However, the results of this study were encouraging, it is complicated to apply the model for different DEM resources as well as is consider time-consuming.

Another advanced approach to model the spatial distribution of DEM errors was followed by Erdoğan (2010). In this study, accuracy is discussed by examining the magnitudes and spatial patterning of elevation errors for the area of Sahitler Hill area, Afyonkarahisar, Turkey. This study investigated the size and spatial patterning of errors in a large-scale area approximately 29,65265 acres, by comparing three different interpolation algorithms. Finally, ordinary least squares and geographically weighted regression models were used to model the relationship between error and surface characteristics. Geographically weighted regression modeling gave better results than ordinary least-squares regression modeling.

A study to determine the accuracy of interpolation techniques used to derive DEMs was carried out by Chaplot et al. (2006) for a total of six sites, three from those site in the mountainous region of northern Laos and the other three selected to be in more gentle landscape of western France, the surface areas various from micro-plots, hillslopes, and catchments. Several interpolation techniques include (1) inverse distance weighting (IDW), (2) ordinary kriging (OK), (3) universal kriging (UK), (4) Multi-Quadratic Radial basis function (MRBF), and Regularized Spline with Tension (RST) were used to create DEMs based on point height data with density values from 4 (low density) to 109 (high density) points/km^2.

The study reveals that if the sampling density was high regardless the spatial scales or the variability and spatial structure of altitude, few differences were observed between the interpolation methods, although MRBF offered slightly better results. However, at lower sampling densities, the best estimation yielded from kriging, for the three mountainous regions of northern Laos which high variation of altitude IDW performed slightly better than the other method.

Heritage, Milan, Large, and Fuller (2009) carried out a study to investigate another factor which has an impact on DEM accuracy, this factor is surveying strategy. The study quantifies survey strategy and interpolation error for the River Nent, Blagill, Cumbria, UK. Five sampling strategies were compared: (i) cross section; (ii) bar outline only; (iii) bar and chute outline; (iv) bar and chute outline with spot heights; and (v) aerial LiDAR equivalent, derived from degraded Terrestrial Laser Scan (TLS) data. Then Digital Elevation Models were produced by using five different common interpolation algorithms. The study concludes that DEM error is strongly influenced by the position of survey points relative to the morphology being surveyed, while choice of the interpolation algorithm is less important.

2.3 Summary

To sum up, a detailed study of effects of DEM resolution and vertical errors was presented in this chapter. It can be clearly seen that the error in DEMs exists due to several factors: Sources of DEMs, DEM production which include resampling and interpolation technique as well as the survey strategy.

All the studies mentioned above conclude that the higher accuracy and spatial resolution of DEMs the better result of hydraulic modeling. In addition, the studies suggest that using courser resolution DEMs resulted over-predicted flood extent.

CHAPTER THREE
STUDY AREA AND DATA

This chapter provides an extensive overview of the Iyidere River which is used in this study. A description of the data used for flood modeling and model parameters used for hydraulic modeling in HEC-RAS is also presented. Land use data used for classification of Manning's n values and cross-sections extraction are included. All Manning's n values are extracted using Corine land cover 2006 - Version 17 (12/2013) (Appendix B) - published by the European Commission programme to Coordinate information on the Environment (Corine). A detailed description of the topographic data used for these sites is also presented in this section.

3.1 Description of Iyidere River

Iyidere River at Trabzon, Turkey is located in Eastern north of turkey. The study area is about 55 kilometers (50 mi) long, and between 10 and 38 kilometers (9 and 35 mi) wide, with a total area of 1035 square kilometers (405 mi^2) (Figure 3.1).

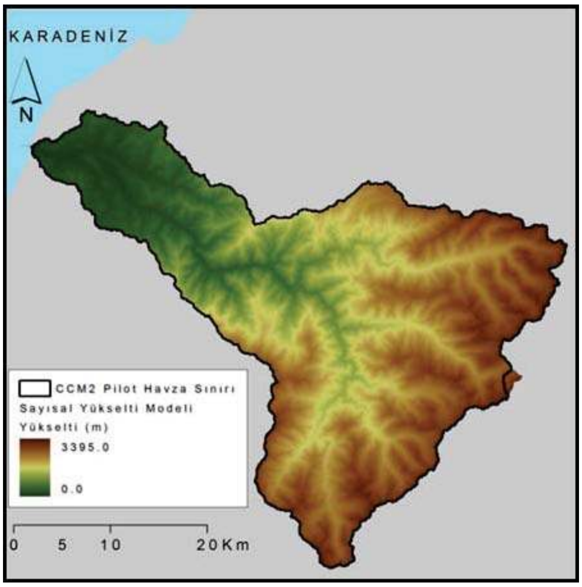

Figure 3.1 İyidere river location

3.2 Description of Topographic Data Set

Topographic datasets generated using contour lines are used for study area. 20 meter interval contour lines with scale of 1:50000 provide by General Command of Mapping (GCM). GCM is by law the National Mapping Agency for TURKEY and is responsible for the official topographical mapping of the country in hard-copy and digital forms for all the uses sectors such as military, government, administrative and educational. 10 m spatial resolution DEM was produced using 20 m contour lines. With the assumption that 10m contour based DEM dataset are the most accurate topographic dataset; therefor, this study considers it as the reference base for all other generated DEM (Figure 3.2).

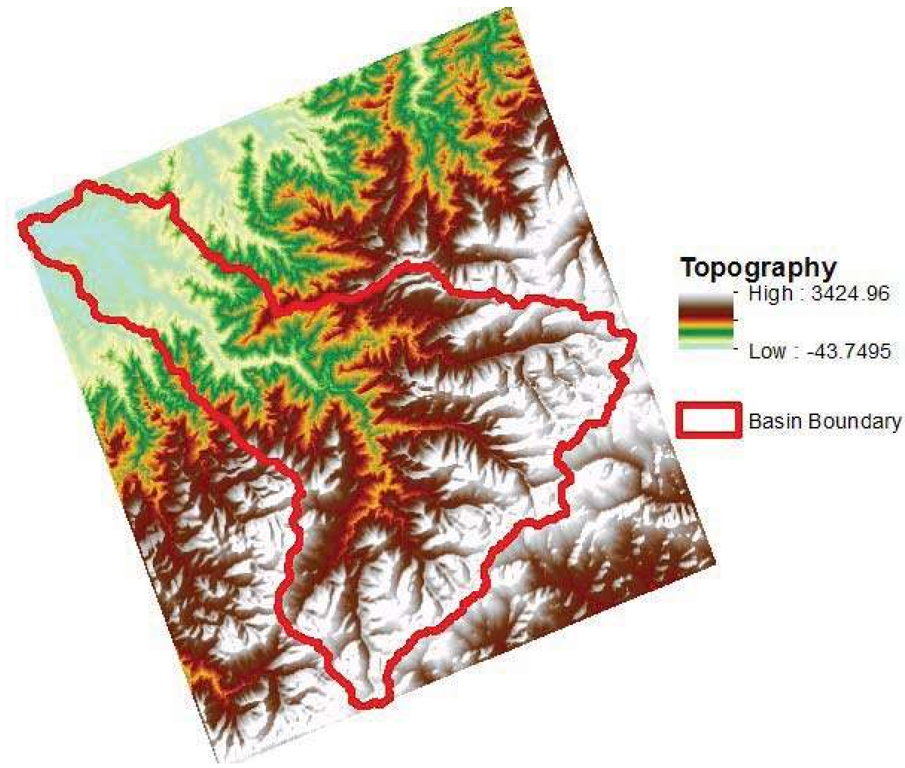

Figure 3.2 Basin topography

CHAPTER FOUR
METHODOLOGY

This chapter explains in detail the methodology applied in floodplain mapping. The traditional process of floodplain mapping based on the hydraulic calculations of water surface elevations was adopted for the local data conditions. The main objective is to bring the process into digital format for use of software tools for spatial analyses. The methodology used in this study consists of three steps: (i) Pre-processing of geometric data for HEC-RAS, using HEC-GeoRAS; (ii) Hydraulic analysis in HEC-RAS (model Execution); and (iii) Post-processing of HEC-RAS results and floodplain mapping, using HEC-GeoRAS. Process flowchart for using HEC-GeoRAS is shown in (Figure 4.1), Flow data are added to the HEC-RAS project files as a part of model execution and the data obtained through HEC-RAS is exported to ArcGIS for post-processing to obtain flood maps (Merwade, 2012; Tate & Maidment, 1999). These processes are repeated using different topographic datasets as inputs during terrain pre-processing.

4.1 Creation of Digital Elevation Models

With the main aim of this study, which is to understand the relationship between grid size and DEM errors with water surface elevations and flood extents, DEMs with different resolution are created starting from 10m up to 100m resolution with by 10 m interval jumps in order to extract elevations using HEC-GeoRAS in ArcGIS. This leads to the creation of geometry files with different elevations for river centerline, cross-sections and flow lines.

Data for this project was collected from the GCM, a 20 m contour line is used to create DEMs. The Topo to Raster tool runs on contour data. The tool is an interpolation process design to create hydrologically conditioned DEMs based on its parent product ANUDEM-algorithms developed by Dr. Michael Hutchinson at the Australian National University. Topo to Raster operates within both the 3D Analyst Tool set and the Spatial Analyst Tool Set. Topo to raster tool is run 10 time with the

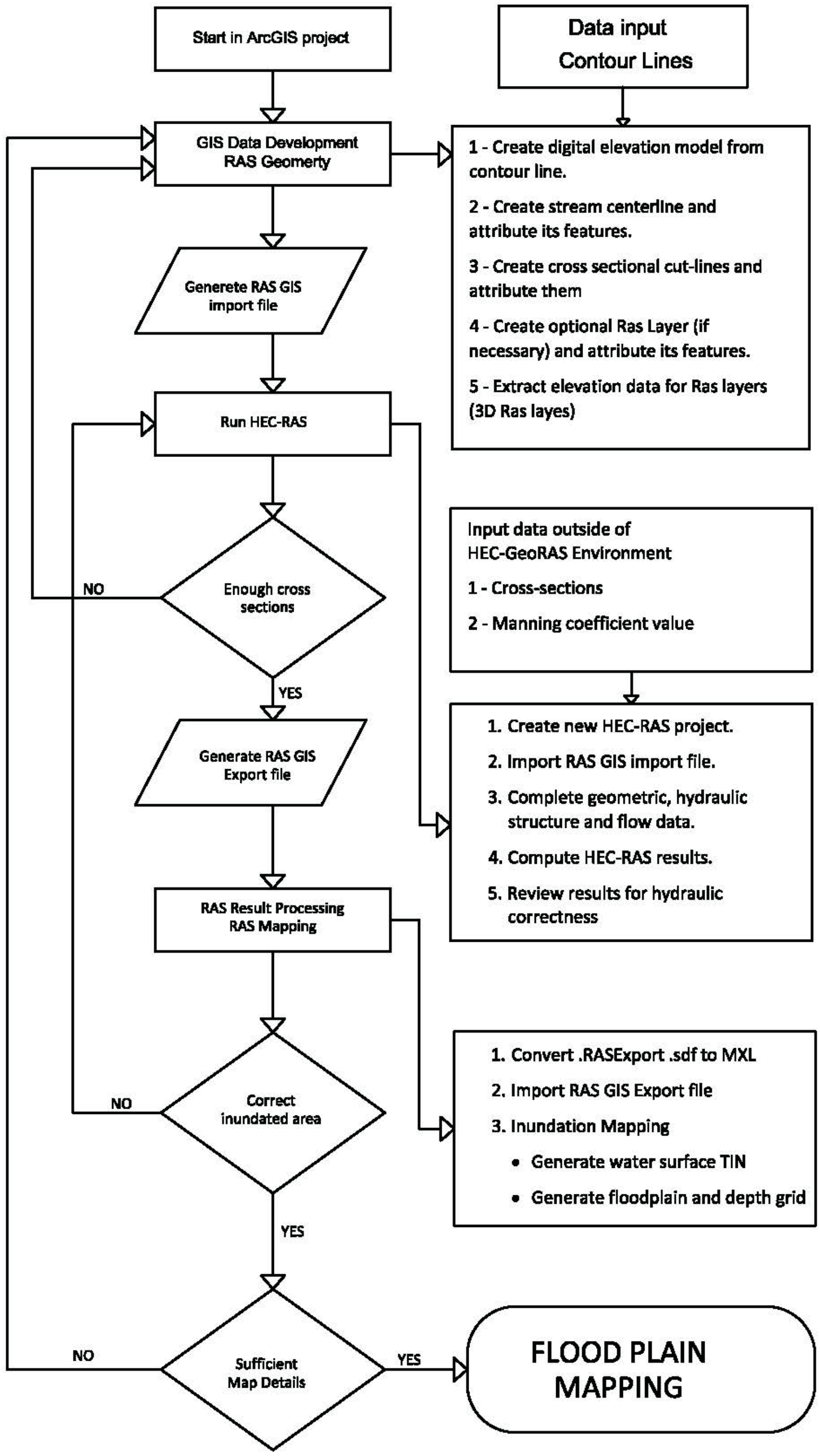

Figure 4.1 Process flow diagram for using HEC-GeoRAS (after (USACE, 2011))

same input file as contour line 20 m interval and changing is in output cell size, which is set up ascending from 10m to 100m (20, 30, 40, 50, 60, 70, 80, 90 and 100 m), considering the assumption that the 10 m DEM resolution is the most accurate one and is used as reference for all the other relativity coarse DEMs. Topo to Raster technique was selected because it considers the most realistic method to use DEM produced by raw data as contour lines.

Another approached used is to investigate the effect of DEM resolution on hydraulic modeling; in this approach a resampling technique is used. The original contour-based DEM which, is produced by topo to raster tools is resampled into different grid sizes using the Data Management Toolbox in ArcGIS for all the study areas. Resampling is a technique of changing the proportions of a discrete raster into a continuous raster and subsequently interpolating it into a discrete raster of different grid size (Parker, Kenyon, & Troxel, 1983).

Resampling datasets into larger grid sizes often leads to loss in quality and accuracy of the dataset. Resampling in ArcGIS can be done through three methods: (1) nearest neighbor; (2) bilinear; and (3) cubic.

The functions for the three resample methods; Nearest Neighbor, Bilinear Interpolation and Cubic Convolution, is to determine how the value of the cells in the output raster are calculated after a geometric operation done. The determination of the method better to be used depends upon the usage of input raster and the expected value after the operation is performed. For categorical data such as land-use classification or slope classification, Nearest Neighbor is preferred for use. Since the value of the output cell is determined again by the nearest neighborhood algorithm, its cell value will still remain the same as the input grid.

While Bilinear Interpolation uses a weighted average of the four nearest cell centers. As the closer an input cell center is to the output cell center, as higher influence of input cell value is on the output cell value. This means that there is the possibility of the output value to be different from the nearest cell input, however, the new calculated value still remains within the same range of values as input. Due to the output value may be changed, Bilinear is not recommended for categorical data. However, it is strongly recommended to use when dealing with continuous data such as elevation and raw slope values.

Cubic Convolution considers the 16 nearest cell centers to the output cell then fits a smooth curve through the cells to find the value. The value of output cell significantly changes when use Cubic algorithm even so the output value can be out the range of the input cells value. This method is also not recommended for categorical data, nevertheless does fit the case of smoothing continuous data. Therefore, for the analysis, Bilinear Interpolation is used because this study deals with continuous data like elevation.

For the Iyidere River, the 10 m resolution reference DEM is resampled into different coarser gird sizes of 20, 30, 40, 50, 60, 70, 80, 90 and 100 m. Similarly, in order to understand the effect of Error on hydraulic outputs, The RMSE is calculated then added for the resampled topographical data sets. Root Mean Squared Error (RMSE) is a widely used statistic for measuring the error between actual and estimated values. It is used to report a single global value of error in elevations for the entire DEM (Fisher & Tate, 2006). For this study, RMSE is used to evaluate the difference in accuracy between the reference DEM and its resampled DEMs. It should be noted that the errors could have occurred due to other factors and not limited to resampling error (Saksena, 2014). However, this study aims to quantify the magnitude of error occurring in different resample DEMs and understand how these errors affect the outputs of hydraulic modeling mapping.

The RMSE is calculated as the square root of the sum of squares of elevation difference between the resampled DEM and the reference DEM for each point divided by the total number of points (Z. Li, 1988). This analysis illustrates the variation of RMSE against grid size. The RMSE values are calculated using the following equation:

$$RMSE_r = \left[\frac{1}{n}\sum_{i=1}^{n}\left(Z_{ir} - Z_{ir_e}\right)^2\right]^{\frac{1}{2}} \qquad (4.2)$$

Where:

Z_{ir} =elevation value for the ith point extracted from Reference DEM,

Z_{ir_e} =elevation value for the ith point extracted from a resampled DEM,

n =total number of Cells for which elevation values are extracted and

$RMSE_r$ is the root mean squared error or a resampled DEM when compared to a reference DEM.

To analyze these DEMs, most studies use a random distributed point shape file which overlay on the reference dataset and then elevation values are extracted to each point in the shape file using the base-reference DEM. This process is carried out for the same points representing elevations corresponding to different resolution resampled datasets. While in this study, since the topographical datasets have the identical extend, it is possible to calculate the RMSE error for each cell. Firstly, the resampled DEM resampled again for 10 meter resolution as the reference DEM, using Nearest Neighbor the values that go into the grid stay exactly the same. Secondly, subtract the resample DEM from the reference DEM. Thirdly use zonal statistics to calculate the mean for each group according to resample DEM, which will produce the RMSE Raster. Then resample again the produced raster to be as the same coarse resolution you start with using the same Nearest Neighbor. Finally add RMSE Raster to the resampled raster to obtain raster with error. The following (Figure 4.2) describes the flow chart of obtaining RMSE as example for 50 m-resampled DEM.

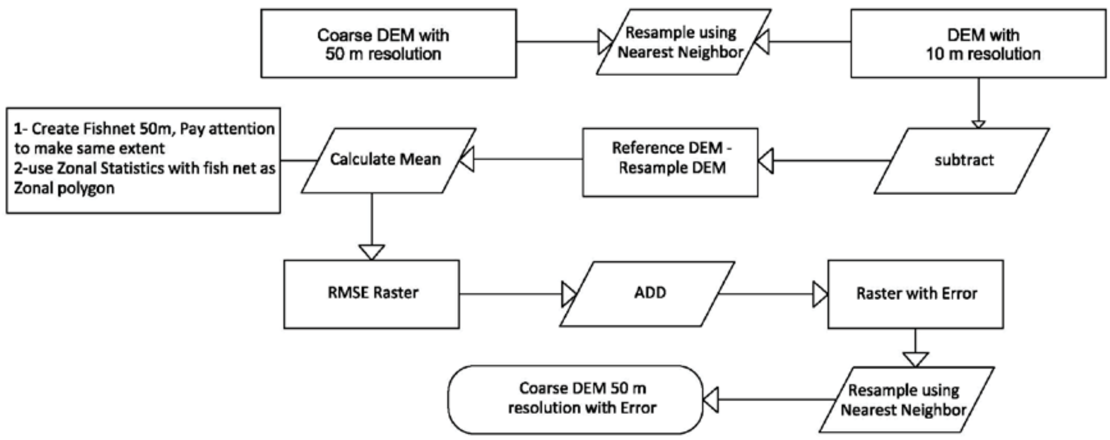

Figure 4.2 Flow chart of obtaining RMSE

4.2 River Network Extraction

Hydrology module from the spatial analysis tool set within ArcGIS 10.2 was used to extract river networks from different DEMs. Same procedures (Figure 4.3) are used on all DEMs of different resolution.

Flow direction and sinks were first identified in each DEM. If sinks existed, they were filled and flow direction was revised. With corrected flow direction, the procedure identified grid cells representing streams based upon a flow accumulation threshold, which affected the density of a drainage network and size of a catchment area (Tarboton, Bras, & Rodriguez-Iturbe, 1992).

A larger threshold reduces the number of extracted streams, avoiding redundant or artificial streams, whereas applying a smaller threshold creates more stream features, some of which may not actually exist. Such a statistical strategy suggested by (Tarboton, Bras, & Rodriguez-Iturbe, 1991; Tarboton et al., 1992) and using the Tau-DEM tool, a threshold value of approximately 0.36 km2 was determined to be the most appropriate for the network extraction procedure based upon the corresponding t-statistic. However, in this study the threshold value was set up as 10% from the basin area, the same threshold was applied to all topographical datasets to facilitate comparison. With grid cells representing streams and the flow direction information, the final step was to create line features representing the river network see (Figure 4.4).

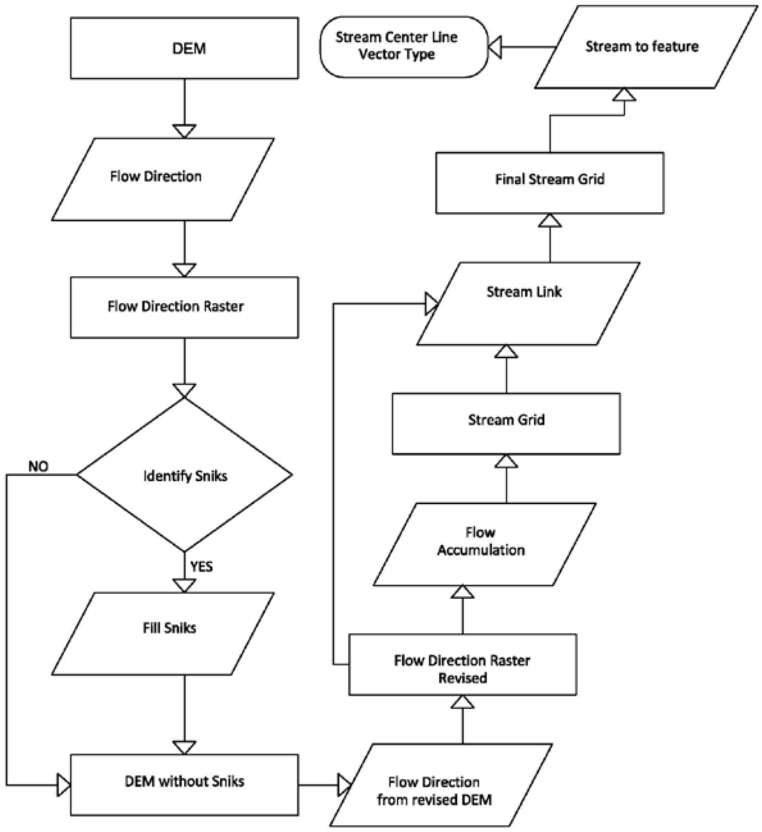

Figure 4.3 Flow chart describing the river extraction

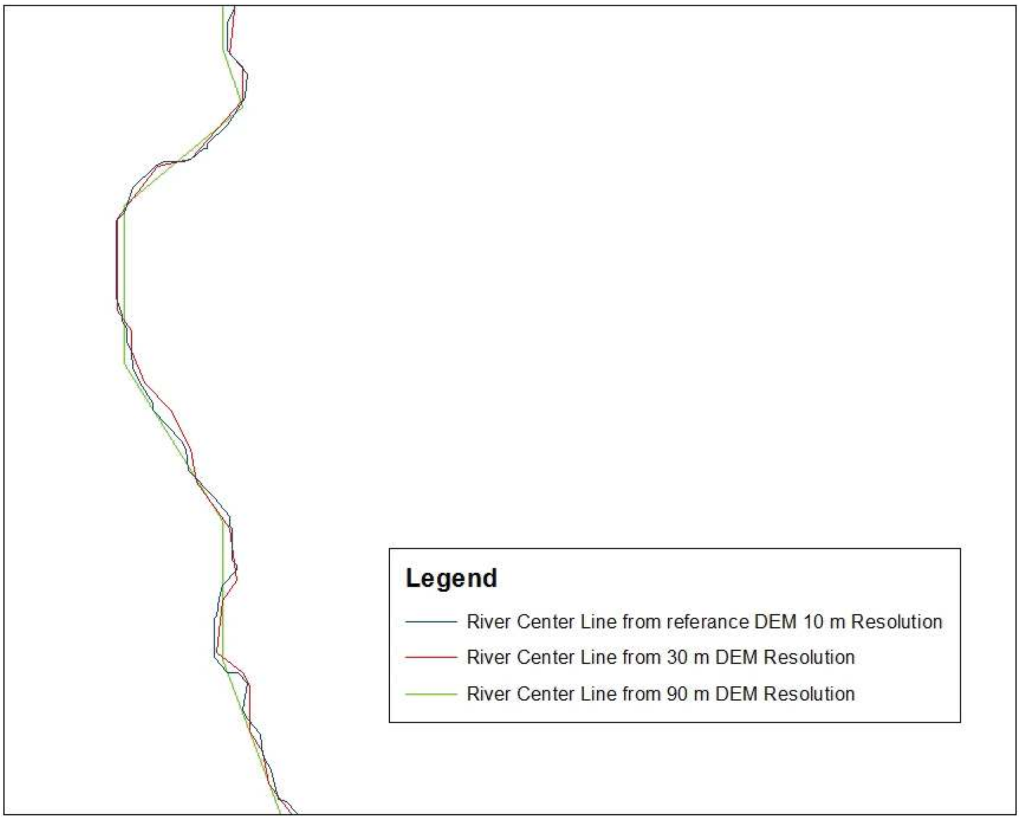

Figure 4.4 River center lines comparison

4.3 Pre-processing of Geometric Data

For efficient use of multiple software packages, a very rigorous data preparation procedure is implemented in the study.

4.3.1 Creating Geometric Data Layers

Before preparing the data for a hydraulic model a new ArcMap project should start and be saved in a specific directory, and then appropriate coordinate system should be assigned in the ArcMap for the Iyidere Basin, the projected WGS_1984_UTM_Zone_37N coordinate system was used.

Creating the geometry data file consider the main part of the pre-processing task. The geometry file data is prepared to be used by HEC-RAS. The geometry data file consists of essential information describing cross-sections, hydraulic structures, river bank points and other physical attributes of river channels (Merwade, 2012). In order to do the pre-processing task the HEC-GeoRAS extinction in ArcMap was use for creating the physical attribute, once the geometry files were ready, they could exported to the HEC_RAS geometry file. In pre-processing task, a geo-database automatically created then each attribute is stored in a separate feature class referred to as a RAS Layer (Merwade, 2012). This Geo-Database is saved under the same name and at the same location as the ArcMap project. An empty GIS layer using the RAS Geometry menu was created before start digitizing the river streams and the cross sections. It can create all the RAS layers in one step and those layers will be directly saved in the geo-database with already created. The following RAS layers are used in this study: river, flow paths, XsCutLines. The following sections explain how each individual RAS layer created or digitized is.

Creating river center line: consider the most important layer; due to the river center-line present the river network for HEC-RAS. The sketch tool from the Editor Toolbar was used to digitize the river center line. During the digitizing process it is essential to notice that digitization proceeds in the direction of river flow and the process begins at the uppermost end of the stream (defined by the project extent), and ends at the outlet (the outlet on the black sea). In this study, beside DEMs, the digitizing process used the rivers which extract using the procedure explained in section 4.2.

Once all of the river reaches were digitize, the reaches were named. Each river in HEC-RAS, as well as each reaches within a river. In order to assign a unique name for each reaches “Assign River Code and Reach Code” menu item was used.

To be sure that all the created reaches are connected in order to be able to then populate the remaining attributes of the river layer, “Topology” order from “Stream Centerline Attributes” in the geometry list from the HEC-GoeRAS menu was used. This function is populated by the FromNode and ToNode attribute of the River layer. To populated The Length/Stations fields a similar procedure was used. (Figure 4.5) shows an attribute table for river GIS layer (Iyidere River). The meaning of each attribute is explained below.

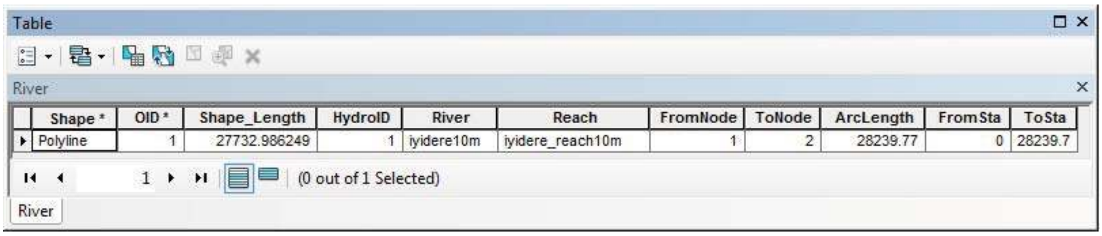

	Shape *	OID *	Shape_Length	HydroID	River	Reach	FromNode	ToNode	ArcLength	FromSta	ToSta
▸	Polyline	1	27732.986249	1	iyidere10m	iyidere_reach10m	1	2	28239.77	0	28239.7

Figure 4.5 Attributes of the river (river centerline) layer

HydroID is a unique number for a given feature in a geodatabase this number cannot repeated in whole Geo-Database. The River and Reach attributes contain names for rivers and reaches, respectively and those names should be unique for each river and reach. The FromNode and ToNode attributes define the connectivity between reaches. The actual length of the reach in the map units is presented in the ArcLength column, and is equal to Shape_Length.

In HEC-RAS, distances are represented using station numbers measured from downstream to upstream (USACE, 2010a). For instance, each river has a station number of zero at the downstream end, and it is equal to the length of the river at the upstream end. Since the Figure 6 shows only one reach for the iyidere river, the FromSta attribute is zero and the ToSta attribute is equal to the Arc-Length.

Creating Flow paths: The flow-path layer is a set of lines that follows the center of mass of the water flowing down the river, during the flood event (Meyer & Olivera, 2007). Three type lines could be found in the flow-path layer: centerline, right over-bank, and left overbank. In the case of main channel, the flow-path centerline is defined to be the same as the stream centerline.

To label the Flow-path as Right, Channel, and Right looking in downstream direction “select flow path and line type attributes” assign button was used.

Creating Cross-sections: Cross-sections consider one of the most important inputs to HEC-RAS. The main use of the Cross section cut-lines is to extract the elevation data from the terrain in order to create a ground profile across the flow. HEC-RAS attributes such as bank stations (locations that separate main channel from the floodplain), and downstream reach lengths (distance between cross- sections) can be computed using the intersection of cross section cut-lines with other RAS layers such as centerline and flow path.

Following the principle which emphasized by Wonkovich (2007) those cross-sections of equal width and similar spacing should be digitized across the channel to reduce the effects of sudden width changes.

- Based on USACE (2009) & Meyer and Olivera (2007) the following roles should follow in the process of creating cross section cut lines:
- Cut lines are drawn perpendicular to the direction of flow. At some locations, "S" shape of cross-section is used.
- Cross section cut lines are drawn directionally from left to right bank, looking at downstream direction.
- The width of the cross sections cut lines is extended far enough on either side of the channel to contain the entire portion of the floodplain.
- The cross sections cut lines do not intersect each other.
- Cut lines should intersect the centerline, each bank line and flow path line only once, and
- Cut lines must not extend beyond the boundary of the DEM.

Figure 4.6 shows Terrain Pre-processing for Iyidere River

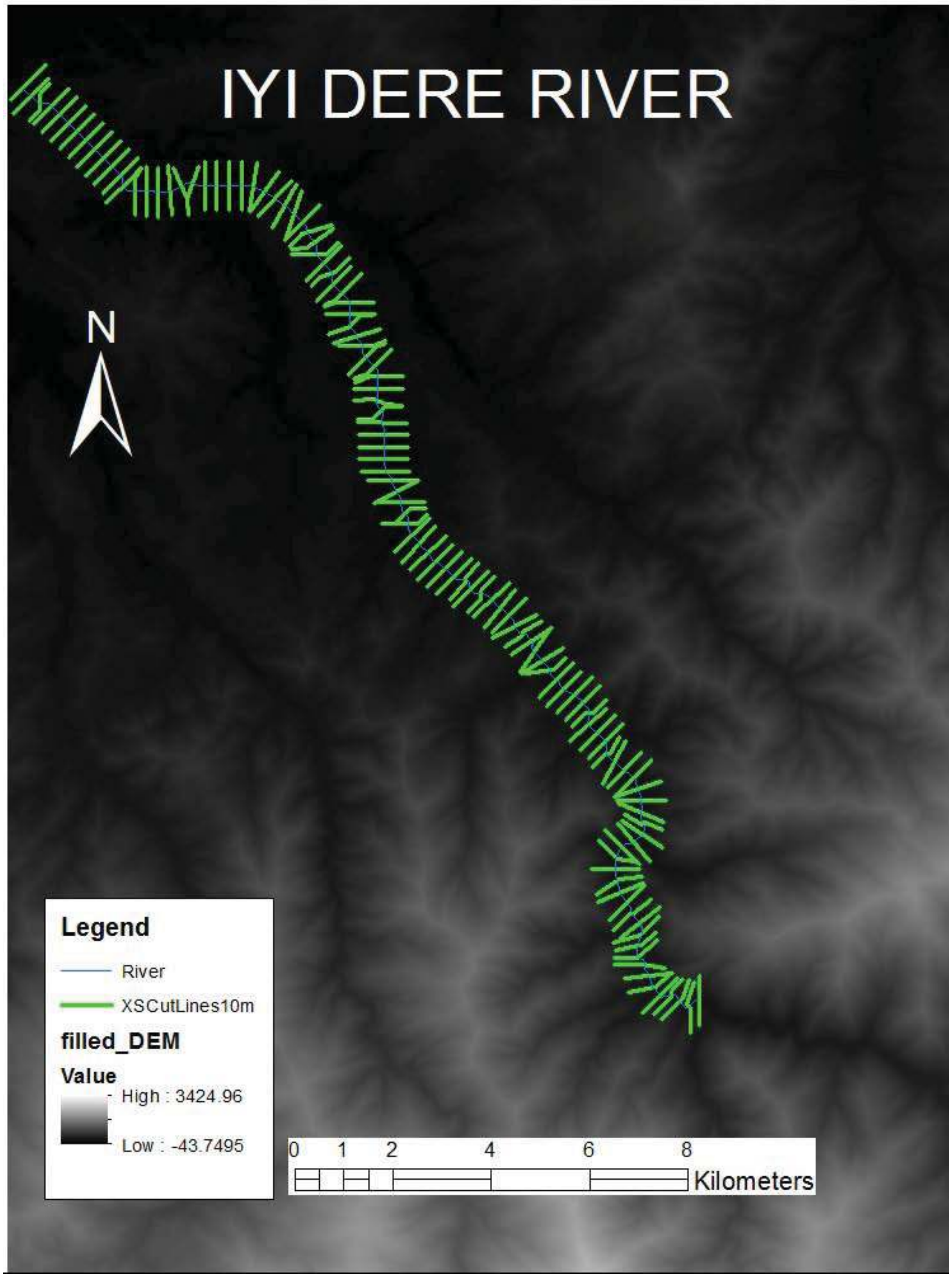

Figure 4.6 Terrain pre-processing for İyidere river

Populating the attribute table of the digitized XSCutLines feature class constitutes one of the important steps. From the HEC-Geo RAS toolbar, "RAS Geometry" then "XS Cut Line Attributes" then "All" is selected. By the intersection between the two dimension feature class XSCutLines and the Digital Elevation Model XS Cut Lines

Profiles (3D) was created. After that, the attribute table and cross-sections are examined in order to check their correctness. Figure 4.7 and Figure 4.8 shows examples of an adequately populated attribute table of XSCutLines and of an adequate definition of cross-section, respectively.

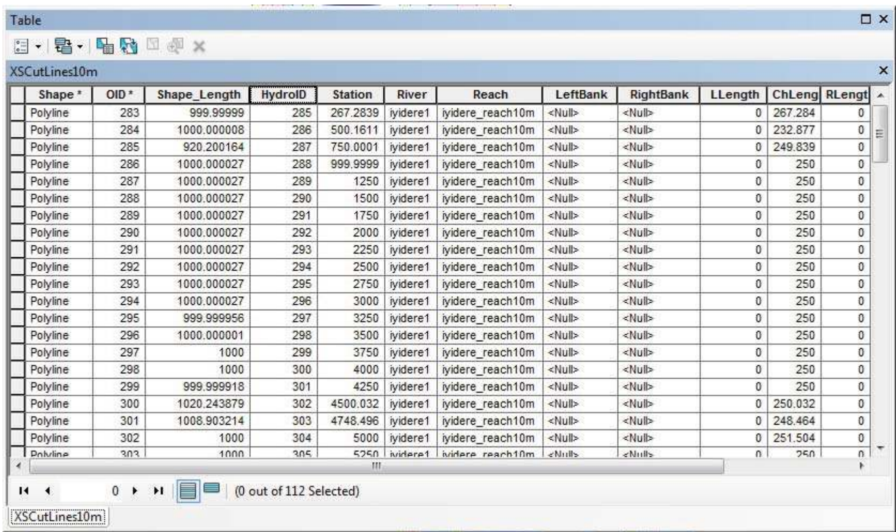
Table

XSCutLines10m

Shape *	OID *	Shape_Length	HydroID	Station	River	Reach	LeftBank	RightBank	LLength	ChLeng	RLengt
Polyline	283	999.99999	285	267.2839	iyidere1	iyidere_reach10m	<Null>	<Null>	0	267.284	0
Polyline	284	1000.000008	286	500.1611	iyidere1	iyidere_reach10m	<Null>	<Null>	0	232.877	0
Polyline	285	920.200164	287	750.0001	iyidere1	iyidere_reach10m	<Null>	<Null>	0	249.839	0
Polyline	286	1000.000027	288	999.9999	iyidere1	iyidere_reach10m	<Null>	<Null>	0	250	0
Polyline	287	1000.000027	289	1250	iyidere1	iyidere_reach10m	<Null>	<Null>	0	250	0
Polyline	288	1000.000027	290	1500	iyidere1	iyidere_reach10m	<Null>	<Null>	0	250	0
Polyline	289	1000.000027	291	1750	iyidere1	iyidere_reach10m	<Null>	<Null>	0	250	0
Polyline	290	1000.000027	292	2000	iyidere1	iyidere_reach10m	<Null>	<Null>	0	250	0
Polyline	291	1000.000027	293	2250	iyidere1	iyidere_reach10m	<Null>	<Null>	0	250	0
Polyline	292	1000.000027	294	2500	iyidere1	iyidere_reach10m	<Null>	<Null>	0	250	0
Polyline	293	1000.000027	295	2750	iyidere1	iyidere_reach10m	<Null>	<Null>	0	250	0
Polyline	294	1000.000027	296	3000	iyidere1	iyidere_reach10m	<Null>	<Null>	0	250	0
Polyline	295	999.999956	297	3250	iyidere1	iyidere_reach10m	<Null>	<Null>	0	250	0
Polyline	296	1000.000001	298	3500	iyidere1	iyidere_reach10m	<Null>	<Null>	0	250	0
Polyline	297	1000	299	3750	iyidere1	iyidere_reach10m	<Null>	<Null>	0	250	0
Polyline	298	1000	300	4000	iyidere1	iyidere_reach10m	<Null>	<Null>	0	250	0
Polyline	299	999.999918	301	4250	iyidere1	iyidere_reach10m	<Null>	<Null>	0	250	0
Polyline	300	1020.243879	302	4500.032	iyidere1	iyidere_reach10m	<Null>	<Null>	0	250.032	0
Polyline	301	1008.903214	303	4748.496	iyidere1	iyidere_reach10m	<Null>	<Null>	0	248.464	0
Polyline	302	1000	304	5000	iyidere1	iyidere_reach10m	<Null>	<Null>	0	251.504	0
Polyline	303	1000	305	5250	iyidere1	iyidere_reach10m	<Null>	<Null>	0	250	0

(0 out of 112 Selected)

XSCutLines10m

Figure 4.7 Example of populated attribute table of XSCutLines

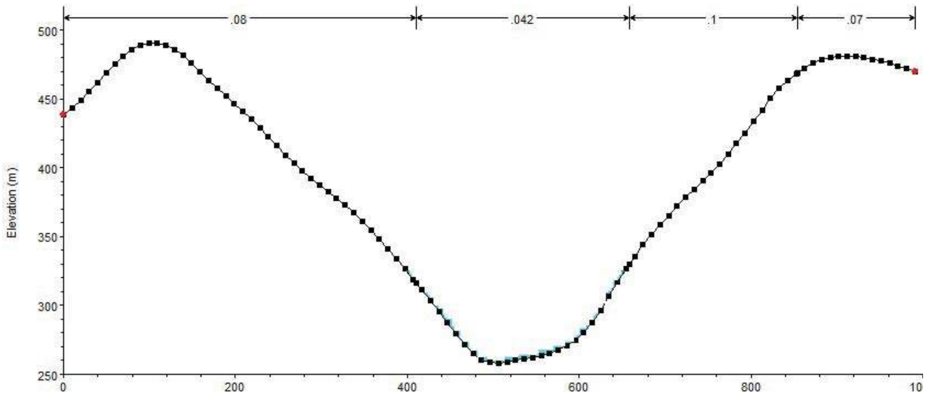

Figure 4.8 Example of definition of cross-sections

4.3.2 Assigning Manning's n Roughness Values

After digitizing these features, Manning's n values are assigned to the cross-sections. Selecting the appropriate Manning's n value is very important for accurate computation of water surface profiles. The energy losses due to the roughness of the river bed are usually evaluated in terms of Manning's Equation:

$$Q = KS_f^{\frac{1}{2}} \tag{4.2}$$

$$K = \frac{1}{n}AR^{\frac{2}{3}} \tag{4.3}$$

Where:

K = conveyance of subdivision [L^3T^{-1}],

n = Manning's roughness coefficient for subdivision [$L^{-1/3}$ T],

R = hydraulic radius of subdivision (Area/wetted parameter) [L],

A = flow area for subdivision [L^2] and

S_f = the slope the energy grade line [L/L].

The value of Manning's n is highly variable and depends upon a number of factors including: surface roughness, channel irregularities, channel alignment, size and shape of channel, scour and deposition, vegetation, obstructions, stage and discharge, seasonal change, temperature, suspended materials and bed load (USACE, 2010a). The n value decreases with increases in stage and discharge. When the water depth is shallow, irregularities of the channel bottom are exposed and their effect may become pronounced. However, the n value may be large at high stages if the banks are rough and grassy (Chow, 1959).

In the floodplain inundation mapping, the manning roughness coefficient should assign to the main channel of the stream as well as to overbank flow area. The general approach for estimating n values consists of the selection of a base roughness value for a straight, uniform, smooth channel in the materials involved, then, through a consideration of various factors, modifying values are added to the base n value to obtain the n value for the channel under consideration (Chow, 1959; Cowan, 1956).

The n value for a given depth of flow may be calculated by the general equation (Cowan, 1956)

$$n = (n_0+n_1+n_2+n_3+n_4)m \quad (4.4)$$

Where:

n_0 = the base value for a straight uniform channel;

n_1 = the additive value due to the effect of cross-section irregularity;

n_2 = the additive value due to variations of the channel;

n_3 = the additive value due to the relative effect of obstructions;

n_4 = the additive value due to the type and density of vegetation; and

m is represent a value for the degree of meandering used to multiply the sum of the previous values.

In this study, for the Iyidere river the values $n_0, n_1, n_2, n_3 and\ n_4$ were assigned as 0.026, 0.006, 0.00, 0.002 and 0.001 respectively.

The degree of meandering, m, depends on the ratio of the total length of the meandering channel in the reach being considered to the straight length of the channel reach (Figure 4.9). The meandering is considered minor for ratios of 1.0 to 1.2, appreciable for ratios of 1.2 to 1.5, and severe for ratios of 1.5 and greater, According to Cowan (1956) the following table (Table 4.1) reveals the degree of meandering and manning value for all the river streams which extracted from the reference DEM and other coarse DEMs, see section 4.2.

Table 4.1 Degree of meandering and manning values for the river streams

Resolution	Total length (M)	Straight Length	Meandering	Manning Value
10	28239.770	23512.495	1.201	0.042036881
20	28143.806	23521.400	1.197	0.041878171
30	28093.502	23466.059	1.197	0.041901905
40	27637.316	23470.045	1.178	0.041214495
50	27860.042	23510.412	1.185	0.041475304
60	27579.320	23483.132	1.174	0.041105087
70	27805.846	23484.957	1.184	0.041439489
80	27626.692	23469.897	1.177	0.041198913
90	27612.827	23520.385	1.174	0.041089845
100	27230.628	23543.495	1.157	0.040481329

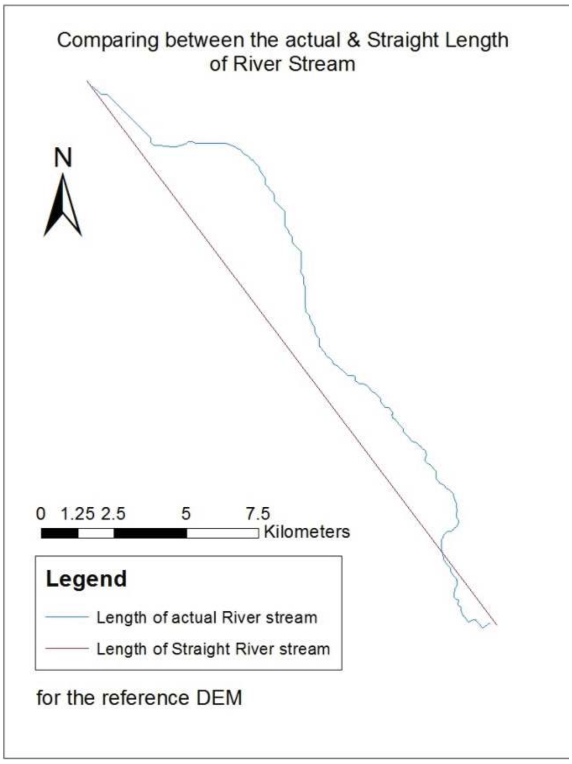

Figure 4.9 Comparing between the actual & Euclidean line distances

The manning roughness coefficient of the over-bank flow area assigned based on the study carried out by Mills & Badcock, (2001). This study used the same land use classification type Corine land cover 2006 - Version 17 (12/2013) - published by the

European Commission programme to Coordinate information on the Environment (Corine), the value of manning roughness coefficient was assign according to each category as shown in the following table.

Table 4.2 Corine land use survey classifications (2000) and assigned manning's 'n' floodplain roughness values (Mills & Badcock, 2011)

CORINE Land Use Classifications			Final Assigned Manning's 'n'
Level 1	Level 2	Level 3	
Artificial Surfaces	Urban Fabric	1.1.1 Continuous Urban Fabric	0.2
		1.1.2 Discontinuous Urban Fabric	0.1
	Industrial, Commercial and Transport Units	1.2.1 Industrial or Commercial Units	0.2
		1.2.2 Road and Rail Networks and Associated Land	0.05
		1.2.3 Seaports	0.05
		1.2.4 Airports	0.03
	Construction Areas	1.3.3 Construction Sites	0.03
		1.4.1 Green Urban Areas	0.02
		1.4.2 Sport and Leisure Facilities	0.02
	Arable Land	2.1.1 Non-Irrigated Arable Land	0.07
	Pastures	2.3.1 Pastures	0.06

Table 4.2 Corine land use survey classifications (2000) and assigned manning's 'n' floodplain roughness values (Mills & Badcock, 2011) (continue)

Agricultural Areas	Heterogeneous Agricultural Areas	2.4.2 Complex Cultivation Patterns	0.07
		2.4.3 Land Principally Occupied by Agriculture with	0.08
	Forests	3.1.1 Broad-leaved Forest	0.1
		3.1.2 Coniferous Forest	0.25
		3.1.3 Mixed Forest	0.1
	Scrub / Herbaceous Vegetation Associations	3.2.1 Natural Grassland	0.05
Forest and Semi-Natural Areas		3.2.2 Moors and Heaths	0.05
		3.2.4 Transitional Woodland Scrub	0.06
	Open Spaces with Little or No Vegetation	3.3.2 Bare Rocks	0.03
		3.3.3 Sparsely Vegetated	0.04
	Inland Wetlands	4.1.1 Inland Marshes	0.09
Wetlands		4.1.2 Peat Bogs	0.04

After the formation of these layers, different topographic datasets are used to extract elevations and the files are exported into HEC-RAS.

4.3.3 Exporting GIS Data to HEC-RAS

The last step is to create a GIS import file for HEC-RAS so that it could import the GIS data to create the geometry file. Firstly, it is necessary to define which layers would be exported to HEC-RAS. The tabs “RAS Geometry” then “Layer Setup” are selected from the HEC-GeoRAS toolbar. Four tabs: Required Surface, Required Layers, Optional Layers and Optional Tables are available in the Layer Setup window. The Required Surface option is used for choosing DEM for export. The Required Layers option is used for entering the River Layer, XSCutLines Layer and XSCutLines 3D Layer. Other RAS layers can be entered by using the Optional Layers option. (Figure 4.10) Shows a typical RAS Layers definition at required Layers tab. Other RAS Layers, which are not used in this study, show a Null value. Export of GIS Data is performed in the following way: The menu item “RAS Geometry” then “export RAS data” is selected from the HECGeoRas toolbar.

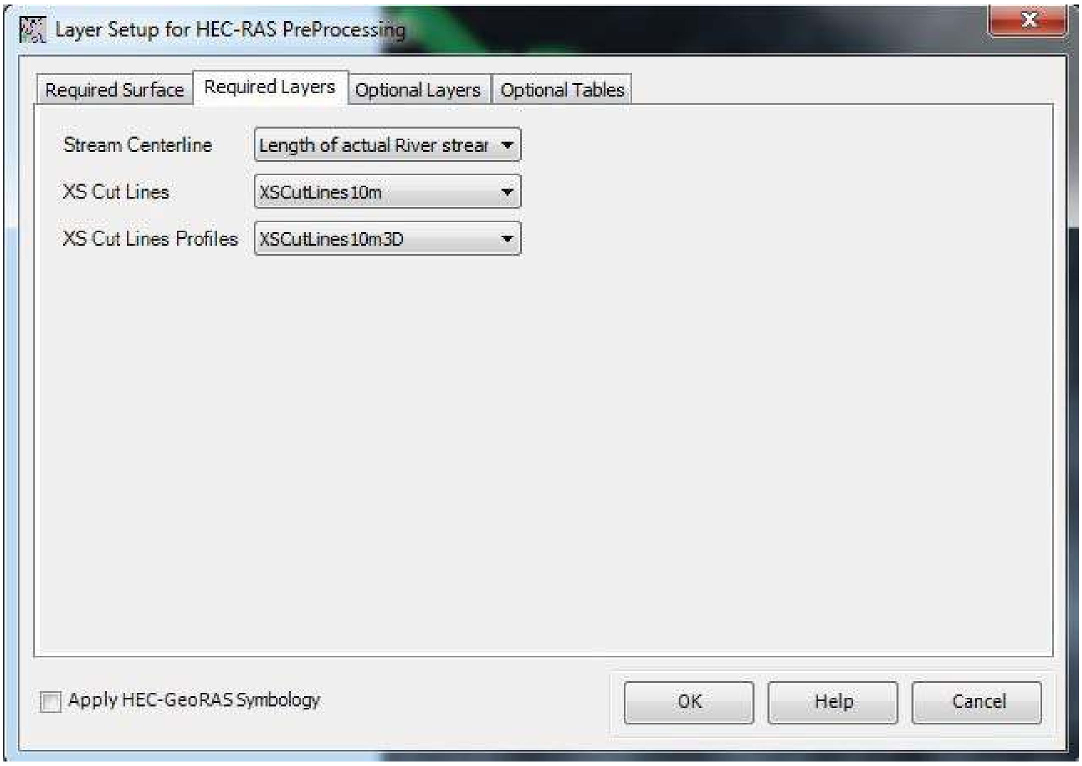

Figure 4.10 Required layers definition

4.4 Hydraulic Modeling

The Hydrologic Engineering Centre River Analysis System, shorter HEC-RAS, is an integrated software system designed to perform one-dimensional water surface calculations. HEC-RAS system is comprised of a graphical user interface, separate hydraulic analysis components, data storage and management capabilities, and graphing and reporting facilities. The HEC-RAS model can perform three types of calculations: (1) steady flow, (2) unsteady flow, and (3) movable boundary flow (USACE, 2010a). The steady flow component uses the standard step method for the solution of steady gradually varied flow. The unsteady flow component uses a numerical solution of the complete equations of gradually varied unsteady flow, commonly referred to as the dynamic wave. The movable boundary component uses the sediment continuity and one of several sediment transport equations to calculate river bed aggradation and/or degradation (Ponce, 2011).

Computation engine of HEC-RAS is based on the solution of the one-dimensional energy equation. Energy losses are evaluated by friction (Manning's formula), contraction, and expansion (USACE, 2010a). In the cases where the water surface profile is rapidly varied the use of momentum equitation is required. These cases include: mixed flow regime calculations, bridge hydraulic calculations and evaluation of profiles at river confluence. The effects of bridges, culverts, dam's weirs, and other structures in the river and floodplain can be calculated by HEC-RAS. The brief introduction of main concept and equations follows.

Steady and Unsteady Flow. The channel flow is steady if each depth, discharge, and average velocity of flow at a certain station does not change with time, or if it can be assumed constant during the time period under consideration. While if the above three factor does change with time at the same location, the flow then is unsteady: it can neglect time factors during the steady flow calculation, but a time factor is taken into account explicitly in the case of unsteady flow analysis.

Uniform and Non Uniform Flow: the channel flow is uniform if the depth, the discharge and the mean velocity do not change in space. Which mean the energy grade line; water surface elevation and channel bottom are all parallel for uniform flow. This type of flow rarely occurs in reality. While Non-Uniform Flow occur when depth, the discharge and the mean velocity do change in space. Non-Uniform

Flow are sometimes designated as varied flow even can be further classified as gradually varied and rapidly varied.

Subcritical and Supercritical Flow: Froude number to disperse between the Subcritical and Supercritical Flow, subcritical flow happens when Froude number is less than one and the inertial forces are less than the gravitational forces, and the flow depth in subcritical flow is greater than the flow depth in critical flow. While if the flow is supercritical, the Froude number is greater than one and the inertial forces are greater than gravitational forces. The flow depth in supercritical flow is less than the flow depth in critical flow.

$$F_r = \frac{V}{\sqrt{gL}} \tag{4.6}$$

Where:

F_r = Froude number (dimensionless)

V = Mean channel flow velocity [L/T]

g = Acceleration due to gravity (L/T^2) and

L = Hydraulic depth [L].

Continuity Equation: In the case of the steady channel flow analysis, the continuity equation states that flow remain constant between adjacent cross-sections.

$$Q = A_1V_1 = A_2V_2 = constant \tag{4.7}$$

Q = flow rate/discharge [L^3/T]

V = mean flow velocity [L/T] and

A = cross-sectional flow area [L^2].

Water section profiles are computed from one section to next by solving the energy equation, while the water surface elevations are interpolated between the two cross sections to generate an entire surface (USACE, 2010a).

Energy Equation: Gradually varied water surface profiles are based on the principle of the conservation of energy, which states that the sum of the kinetic energy and potential energy at a particular cross section is equal to the sum of the potential and kinetic energy at any other cross section plus or minus energy loss or gains between the sections (Figure 4.11). Water surface is calculated from one cross section to the next by solving the energy equation written as:

$$Z_2 + Y_2 + \frac{\alpha V_2^2}{2g} = Z_1 + Y_1 + \frac{\alpha V_1^2}{2g} + h_e \tag{4.8}$$

Where:

Z_1, Z_2 = elevation of the main channel invert [L].

Y_1, Y_2 = depth of water at cross section [L].

V_1, V_2 = average velocities (Total discharge/Total flow area)[LT^{-1}].

α = velocity weighted coefficient.

g = gravitational acceleration [LT^{-2}].

h_e = energy head loss [L].

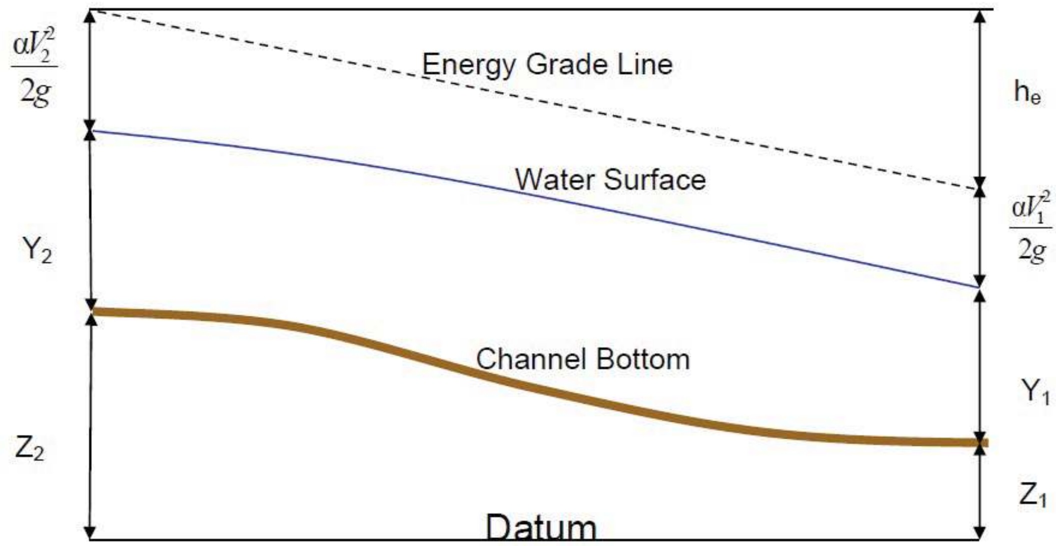

Figure 4.11 Presentation of the terms of energy equation (USACE, 2010a)

The conveyance from the main channel, right overbank and left overbank are calculated separately and then added to yield the total conveyance (Saksena, 2014). Incremental conveyance values are obtained using Equation 4.9

$$Q = \frac{1}{n} A R^{\frac{2}{3}} S_f^{\frac{1}{2}} \tag{4.9}$$

Where:

Q = total conveyance [L^3T],

n = manning's roughness coefficient for subdivision [$L^{-1/3}$ T],

R = hydraulic radius of subdivision (Area/wetted parameter) [L],

A = flow area for subdivision [L^2] and

S_f = the slope the energy grade line [L/L].

4.4.1 Model Execution

The following section presents brief manual for use of HEC-RAS program for computation of water surface profiles. Contour based DEMs including the reference DEM resulted in 10 different geometry files Iyidere river, twenty additional; ten of geometry files were created to by adding RMSE for produced DEMs while the other ten where created by using bilinear technique algorithm. Thus 30 geometry file were created to measure the effect of grid size and errors on hydraulic outputs.

4.4.1.1 Creating HEC-RAS Project and Importing Geometry

The initial step for using the program involves opening of the main HEC-RAS interface window and entering the title and file name.

The Geometric Data Window opens from the main HEC-RAS user window. To enter the geometry select "File" then select "GIS Format" from "Import Geometry Data" then "Browse for Desired RAS GIS Import File (GIS2RAS.RASImpor.sdf)". Firstly, from the Import Options window, SI (metric) unit was selected. Then, "River and Reach Stream Lines" was selected. The Geometry Data are saved in the Geometric Data window. Figure 4.12 shows the Geometric Data window with the geo-referenced river system.

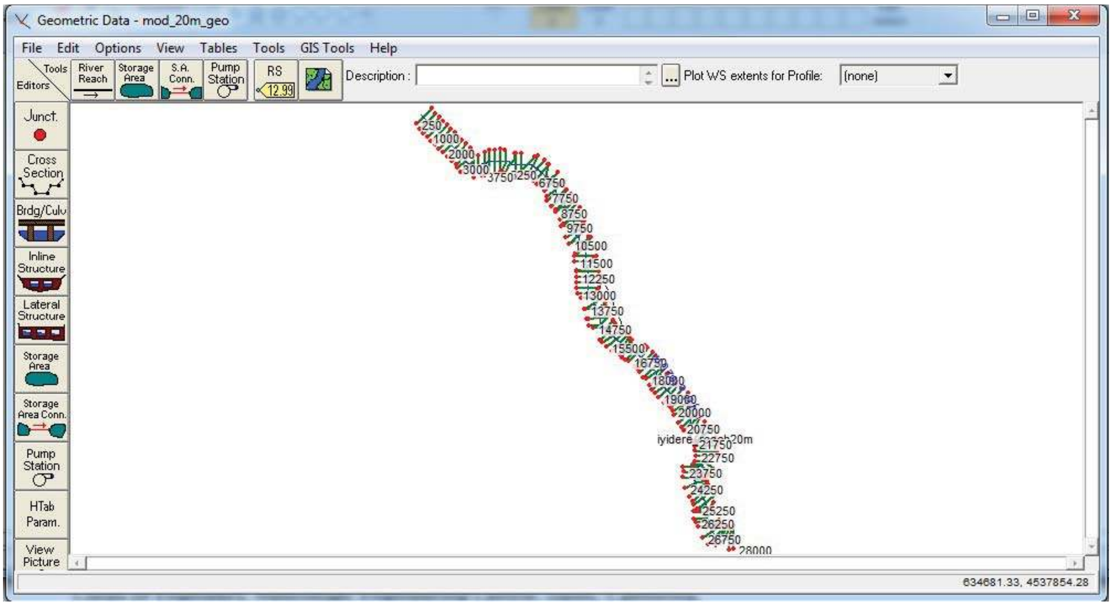

Figure 4.12 Geometric data window

4.4.1.2 *Flow Data and Boundary Conditions*

In order to understand the effect of changing hydraulic flow on the flood inundation mapping results, a six return period "recurrence interval" 2-year, 5-year, 10-year, 25-year, 50-year and 100-year flow value we used as unsteady-flow input in to HEC-RAS. In the unsteady flow it is required to enter boundary condition at all of the external boundaries of the systems (USACE, 2010b).

Boundary conditions are first entered by selecting the boundary condition tab from the unsteady flow data editor. River, reach and river station locations of the external bounds of the system will automatically be entered in to the table. There are several different types of boundary conditions. However, for this study the flow hydrograph was used as an upstream boundary condition. Iyidere River is an open-end reach to the black sea. The Normal Depth can used as a downstream boundary condition, to use the Normal Depth condition it's required to enter a friction slope for reach in the vicinity of boundary condition (USACE, 2010b), Which used as 0.001.

4.4.1.3 HEC-RAS Computation and Data Export

Once all geometry and unsteady flow data have been entered, it can begin performing the unsteady flow calculation, to execute the model, the unsteady flow analysis was selected from the run menu list from the HEC-RAS main menu; (Figure 4.13) show the unsteady flow analysis window.

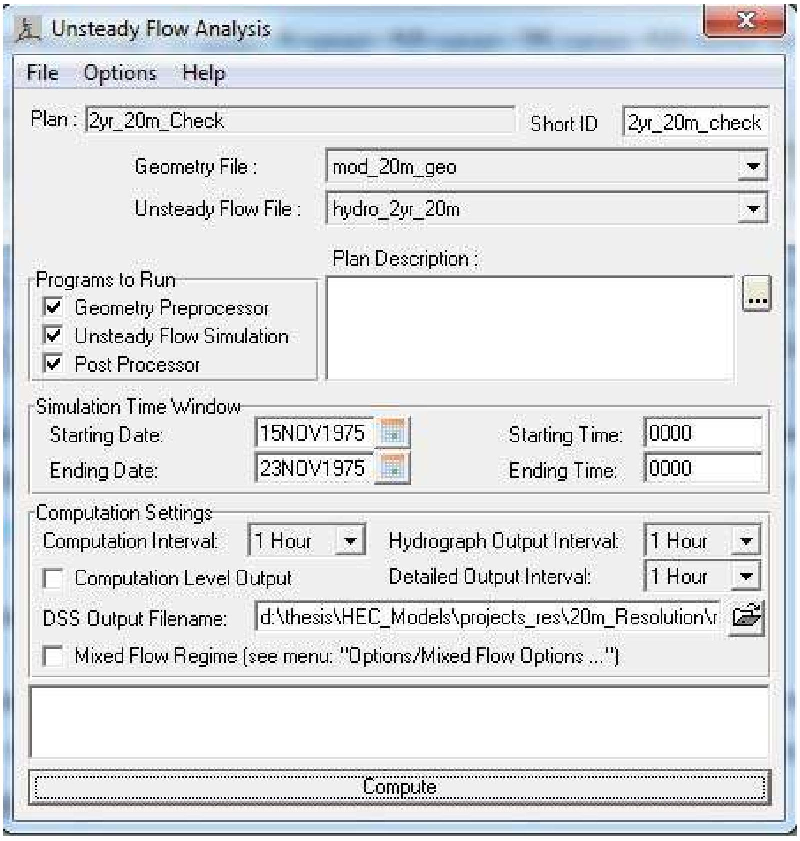

Figure 4.13 The unsteady flow analysis window

The final step involves export of the computation results (water surface elevation) back to GIS. The following computational steps are used from the main HEC-RAS window: “File” then “Export GIS Data”. In the GIS export window, the max water surface profile results are selected and exported using the default format “RASexport.sdf”. Figure 4.14 shows the GIS Export window and the selected profiles used for export.

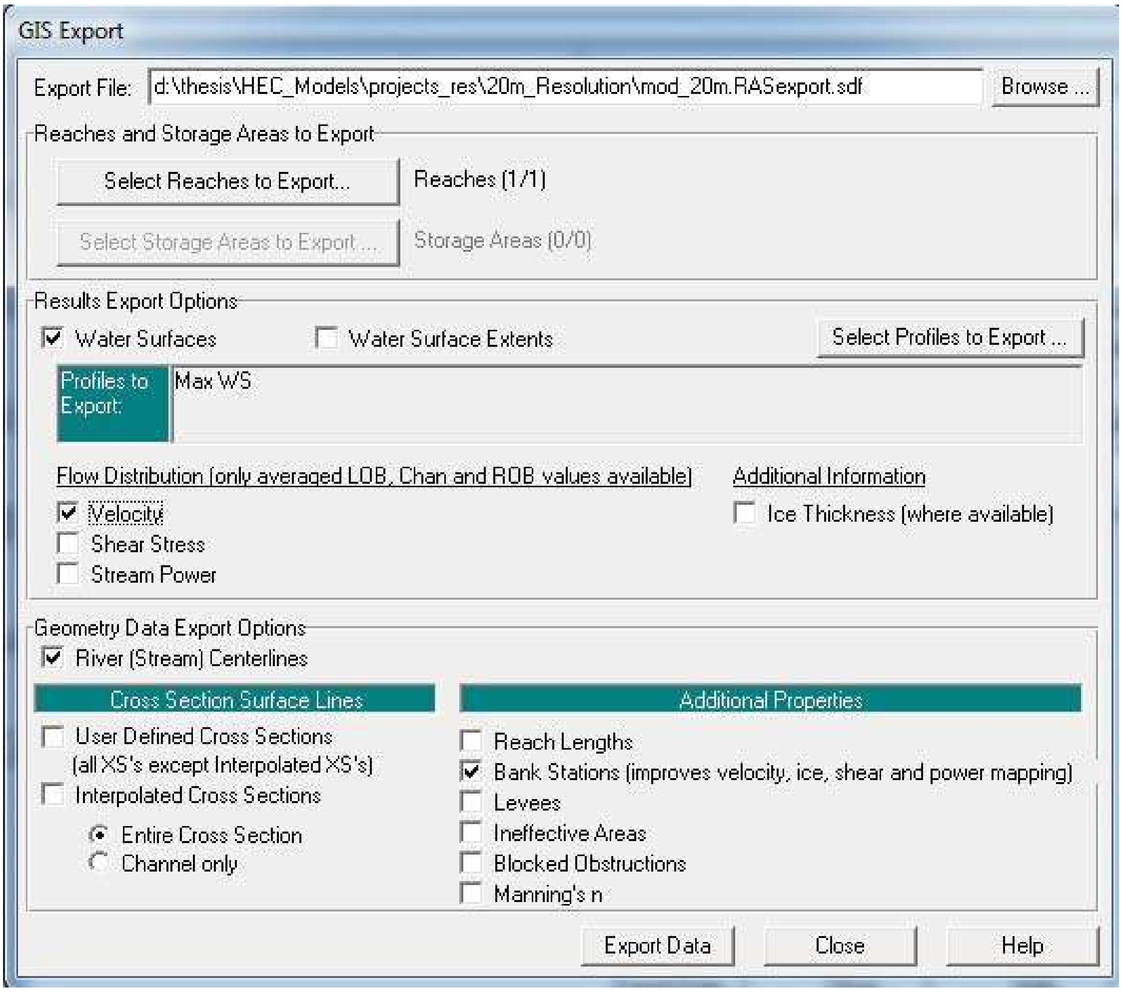

Figure 4.14 The GIS export window and the selected profiles used for export

4.5 Post-Processing of Hydraulic Results and Floodplain Mapping

The post-processing of computation results are performed using the same ArcGIS maps which are used for the pre-processing of geometry data. The only additions to these maps are new map layers.

4.5.1 Import the Data to GIS from HEC-RAS

Formatting, the process starts with opening a desired ArcMap for post-processing. Since the HEC-GeoRAS cannot read the proprietary spatial data format (.RASExport.sdf) file created in the HEC-RAS, it is necessary to convert it into the

XML file format, supported by HECGeoRAS. This is achieved by selecting the "Import RAS SDF File" option from the HEC-Geo RAS Toolbar.

Generation of Digital Terrain Model, The first step in the post-processing stage was to create a Digital Terrain Model of the river system in a Triangulated Irregular Network format. In order to proceed with accurate analyses the TIN must be constructed with a special care. Elevation data for each cross section is extracted from the TIN. Another function for the TIN is to determine floodplain boundaries and calculate the inundation depths.

The Digital Terrain Model is a representation of the topographical surface in terms of regularly spaced x, y, z, coordinates. Ground survey, photogrammetry, surface sensing and cartography are the alternatives which The DTM can be generated though. In the TIN model, each point has defined x, y, and z coordinates. The height is representing by z coordination. These points are connected by their edges to form a network of overlapping triangles (finite surfaces) that represent the terrain surface (Lo & Yeung, 2007).

The contour based DEMs with different resolutions in grid format are used in TIN development. Raster to TIN tool was performed from 3 D analyst conversion toolset to create TINs.

Layer setup, establishing the Layer Setup is a necessary step for processing the HEC-RAS results. In the Layer Setup window, the type of analysis and the input and output data are identified. (Figure 4.15) Shows a typical Layer Setup window from the data post-processing, for the post-processing analyses, the rasterization cell size is set as same as TIN resolution in each map.

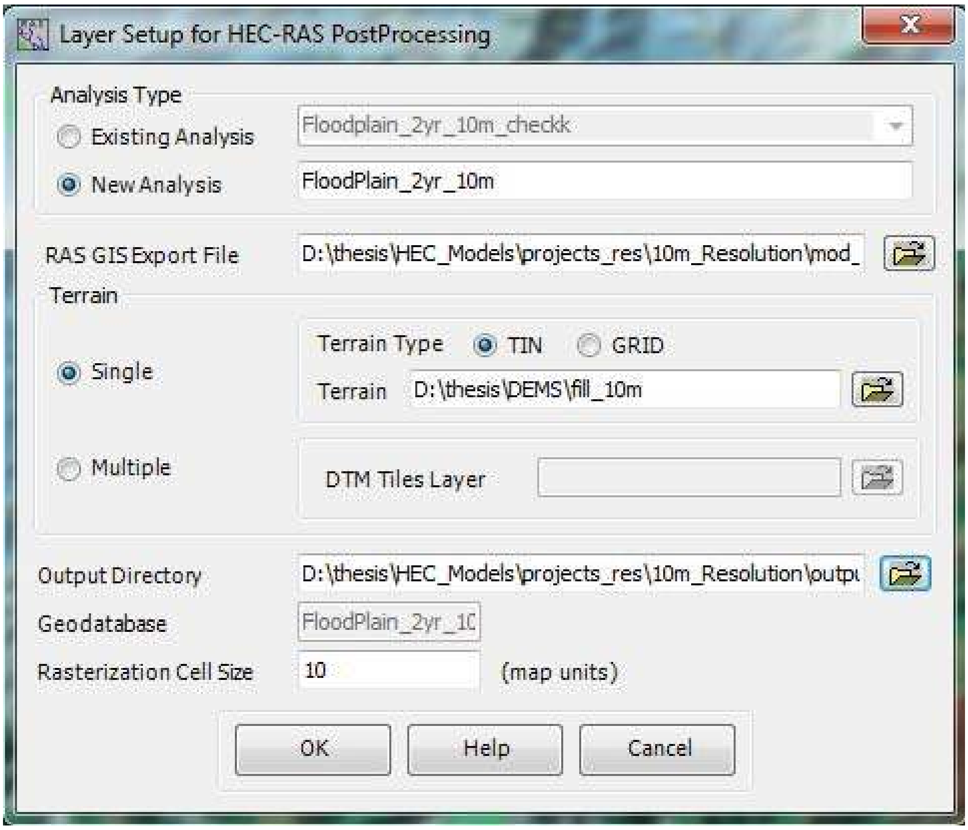

Figure 4.15 Typical layer setup window from the data post-processing

Reading RAS GIS export file, after input data is entered in the layer setup, the HEC-RAS results have to be imported into the GIS in order to continue with the post-processing. The following computational steps are selected from the HEC-GeoRAS toolbar: "RAS Mapping" then "import RAS data". This selection introduces a new data frame with the following feature classes: River2D, XS Cut Lines, and Bounding Polygon.

4.5.2 Floodplain Mapping

Floodplain mapping is performed using the water surface elevations on the XS cut lines, within the limits of the bounding polygon. Floodplain mapping is completed in two steps, which are explained in following paragraphs.

Water surface TIN, in order to delineate the flood inundation area, the first step is to create a water surface TIN from the cross section water surface elevations. The following computational steps are selected from the HEC-GeoRAS toolbar "RAS Mapping" then "Inundation Mapping" then "Water Surface Generation". The maximum water surface was selected. For maximum water surface profile, a water surface TIN was created without consideration of the terrain model. The TIN is created using the ArcGIS triangulation method. This allowed for the creation of a surface using cut lines as hard break lines with constant elevation. (Figure 4.16) shows the water surface TIN.

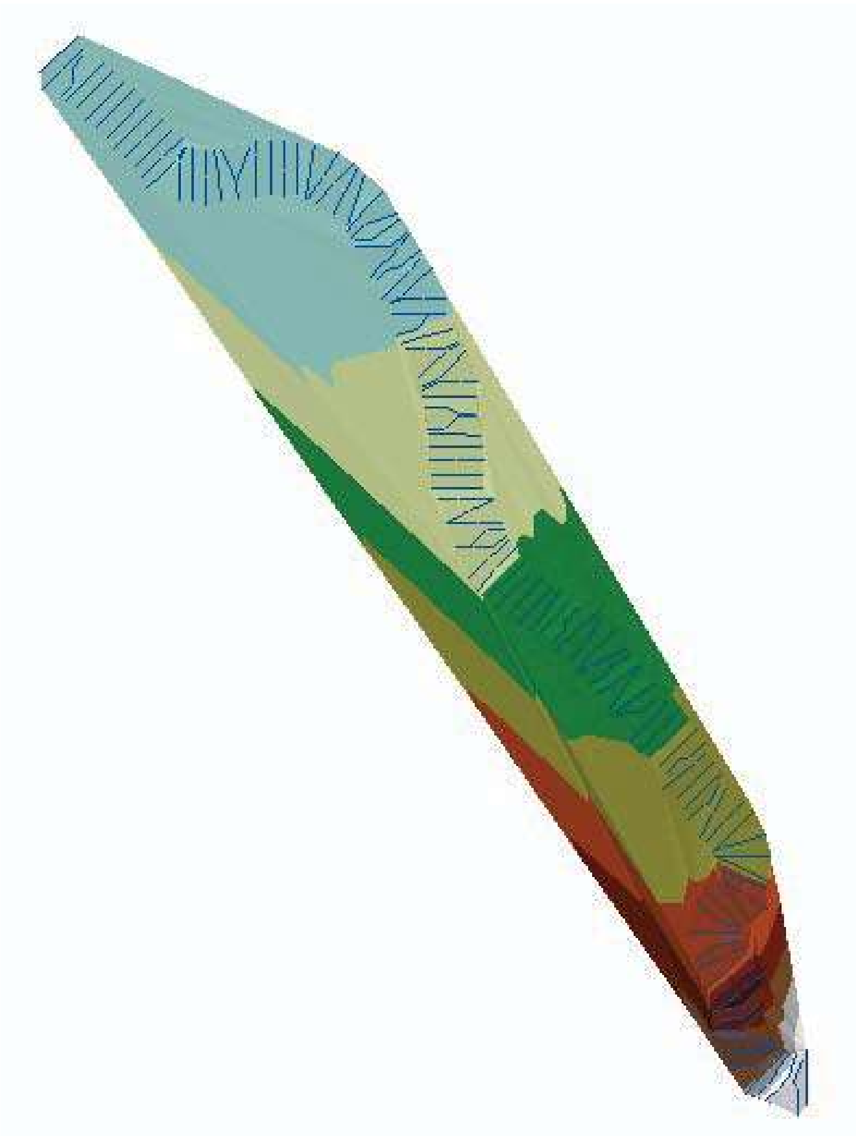

Figure 4.16 The water surface TIN model

Floodplain delineation, after water surface TIN was generated, the floodplain may then be delineated for maximum water surface profile. Floodplain Delineation using Rasters was performed from Inundation Mapping at RAS Menu list.

A floodplain polygon will be created based on the water surface profile TIN that was created previously. The floodplain polygons result from intersecting the water surface and terrain surface. The water surface TIN is converted to grid and compared with terrain grid, a depth grid is then created with values where the water surface grid is higher than terrain grid. The depth grid is then clipped with the bounding polygon to remove are not included in the river hydraulic model (USACE, 2011).

Figure 4.17 presents an example of a floodplain boundary feature class

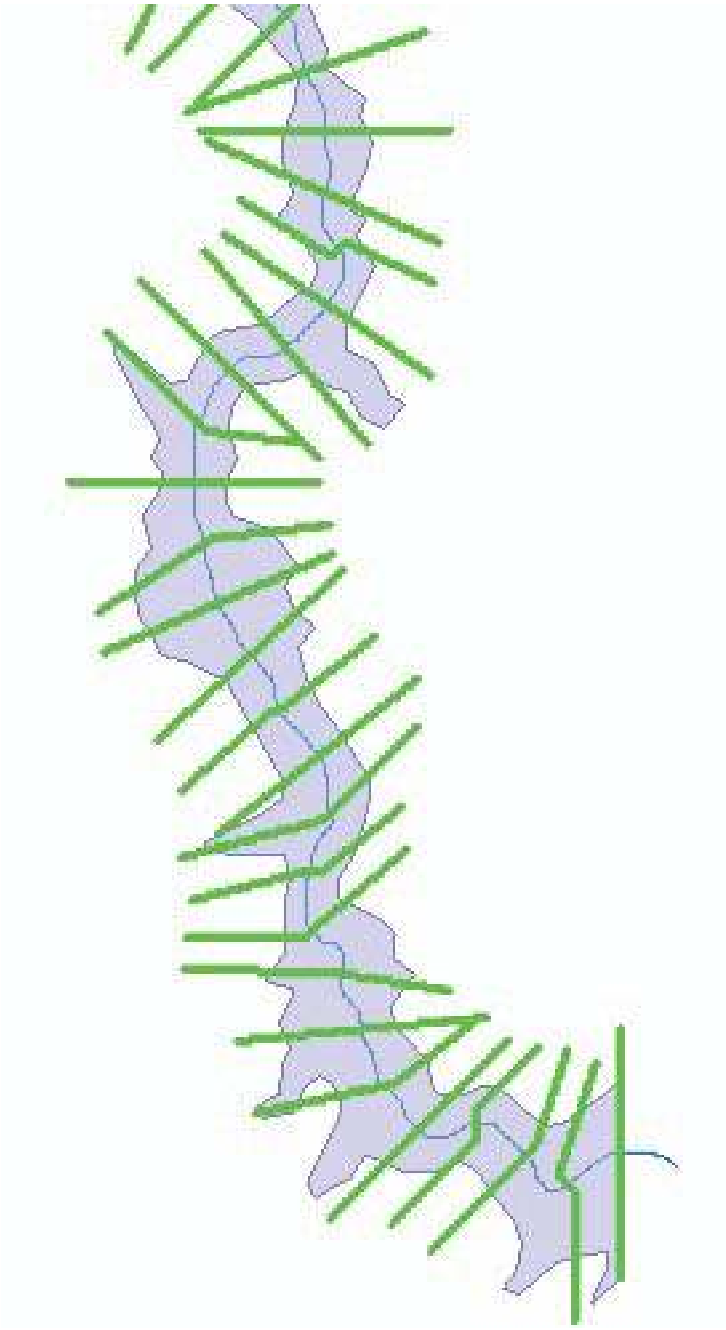

Figure 4.17 Floodplain boundary feature class

CHAPTER FIVE
RESULTS

In this chapter, the results which obtained from the Hydraulic model using HEC-RAS and the flood inundation map using HEC-GeoRAS are presented. With the intention of understanding the impact of added value of DEM. The varying between hydraulic output and grid size, average water surface elevations, flood inundation extends and recurrence interval of the flood are presented. In this study the average water surface elevation calculated as an average for continues surface of flood extend. Inundation area refers to the maximum area which is expected to cover with water. The percentage change in inundation area is obtainable using reference DEM (10 m) generated results as base value. In addition of that the value of 9 topographic datasets containing error also presented to analyze the effect of DEM errors on average water surface elevation and inundation area.

5.1 Effect of DEM Resolution on Hydraulic Model Outputs

The objective of this study is to investigate the effect of DEM resolution changing in flood inundation mapping.

The water surface elevations, flood inundation maps and percentage change in inundation areas for all the topographic data sets are evaluated by referred to the reference 10 m DEM.

For each DEM resolution, hydraulic model execute with varying recurrence interval of the flood – return period–, the return periods which used in this study is 2-yr, 5-yr, 10-yr,25-yr, 50-yr and 100-yr.

The following tables (Table5.1 to Table 5.6) shows the water surface elevations, median surface elevations, inundations areas and percentage change in inundated area for DEMs of increasing grid size or in other words decreasing resolution for the Iyidere

Table 5.1 Hydraulic output for Iyidere with 2-yr return period flood

2yr				
Grid Size (m)	Mean WS (m)	Median WS (m)	Inundation Areas (km^2)	Change %
10.00	17.91	3.00	5.37	0.00
20.00	10.11	2.00	4.87	-10.32
30.00	22.28	2.00	5.63	4.86
40.00	12.04	3.00	5.07	-5.57
50.00	13.07	1.00	4.40	-18.09
60.00	10.12	2.00	4.24	-21.09
70.00	12.09	3.00	4.85	-9.67
80.00	9.55	3.00	4.93	-8.13
90.00	8.86	4.00	5.20	-3.18
100.00	11.80	4.00	5.40	0.61

The table shows that oscillate with the hydraulic results when 2yr recurrence interval of the flood was used, The reference 10 m DEM has a water surface elevation of 17.91 m while the 100 m grid size DEM has a water surface elevation of 11.8 m thus a difference of about 6 m is observed. The inundation areas for both the reference 10 m DEM and the 100 m DEM were so similar with a difference less than 1%, 5.37 km2 and 5.4 km2 respectively. In addition the its was shown that 30m, 100m DEMs resolution recorded over estimation relative to the reference 10 m DEM and the other DEM recorded under estimations for the inundation areas.

Table 5.2 Hydraulic output for Iyidere with 5-yr return period flood

5yr				
Grid Size (m)	**Mean WS (m)**	**Median WS (m)**	**Inundation Areas (km2)**	**Change %**
10.00	11.57	2.00	5.19	0.00
20.00	**27.56**	**3.00**	**5.99**	**15.55**
30.00	17.54	3.00	5.93	14.39
40.00	**15.85**	**4.00**	**5.21**	**0.49**
50.00	14.21	2.00	4.92	-5.04
60.00	**15.80**	**2.00**	**4.37**	**-15.81**
70.00	13.51	3.00	4.78	-7.80
80.00	**15.57**	**4.00**	**5.86**	**12.96**
90.00	11.25	4.00	5.45	5.08
100.00	**12.28**	**4.00**	**5.55**	**7.06**

The result of the table reveals that the water surface elevations and the inundation areas were also varying with increasing grid size when 5yr recurrence interval of the flood was used as input for the model, The reference 10 m DEM predicts a water surface elevation of 11.57 m while the 100 m resolution DEM has a water surface elevation of 12.28 m with difference of about 0.71 m. for the 5yr return period it was notice that the small gird size resolutions (20m, 30m and 40m) and the largest grid resolutions (80m, 90m, and 100m) had over estimations for inundation areas, while the middle grid size resolutions (50m, 60m, and 70m) had recorded under estimation for the inundation areas.

Table 5.3 Hydraulic output for Iyidere with 10yr return period flood

10yr				
Grid Size (m)	Mean WS (m)	Median WS (m)	Inundation Areas (km^2)	Change%
10.00	20.28	3.00	6.02	0.00
20.00	27.52	3.00	6.02	0.01
30.00	15.81	2.00	5.42	-10.05
40.00	16.39	4.00	5.72	-4.96
50.00	14.22	2.00	4.74	-27.17
60.00	17.77	2.00	4.37	-27.43
70.00	17.24	3.00	5.39	-10.46
80.00	21.52	3.00	5.44	-9.74
90.00	22.29	4.00	5.92	-1.69
100.00	19.38	4.00	5.72	-5.06

The same trend continuing with 10yr recurrence intervals of the flood was used as input for the model. The reference 10 m DEM has a water surface elevation of 20.28 m while the 100 m grid size DEM has a water surface elevation of 19.38 m. Despite 20 m gird size DEM recorded a significant rise of water surface elevation 7 m increase of level more than the water level recorded for the reference 10 m reference DEM the inundation areas for both the 10 m reference DEM and 20 m grid size DEM almost identical. It's also notice that the all coarse DEM predicted under estimation inundation areas relative to 10 m reference DEM.

Table 5.4 Hydraulic output for Iyidere with 25yr return period flood

25yr				
Grid Size (m)	Mean WS (m)	Median WS (m)	Inundation Areas (km2)	Change %
10.00	21.85	4.00	6.31	0.00
20.00	27.72	5.00	6.43	1.93
30.00	42.11	4.00	7.61	20.53
40.00	17.60	4.00	5.72	-9.33
50.00	21.51	2.00	4.89	-22.42
60.00	29.97	8.00	6.08	-3.71
70.00	26.43	6.00	6.76	7.08
80.00	23.52	5.00	6.72	6.55
90.00	19.02	5.00	6.96	10.33
100.00	19.90	5.00	6.92	9.65

The 25yr recurrence interval of the flood table result shows varying in the water surface elevations and inundation areas with some different trend from the previous results, the 30 m grid size DEM showed a noteworthy rise in water surface elevation to reach the peak with 42.11 m, the water surface elevations for 10 m reference DEM and 100 m grid size DEM were 21.85 m and 19.90 m correspondingly. The percentage change in inundation area is not significant with increasing the gird size but a change in inundation area of about 9.65 % occurs for a 100 m resolution DEM.

Table 5.5 Hydraulic output for Iyidere with 50yr return period flood

50yr				
Grid Size (m)	Mean WS (m)	Median WD (m)	Inundation Areas (km^2)	Change %
10.00	45.16	9.00	7.98	0.00
20.00	16.61	2.00	5.83	-26.98
30.00	32.50	4.00	6.85	-14.21
40.00	17.60	4.00	5.72	-28.35
50.00	35.17	5.00	6.20	-22.30
60.00	27.79	3.00	5.15	-35.55
70.00	35.40	7.00	7.20	-9.85
80.00	21.33	4.00	6.02	-24.58
90.00	25.16	7.00	7.20	-9.84
100.00	25.98	4.00	6.33	-20.68

According to the results in the 50yr return period table the water surface for 10 m reference DEM is 45.16 m while the water surface for 100 m grid size DEM is 25.98 thus a difference of about 20 m is observed. In addition of that all the coarse DEMs had under estimation inundation areas comparative with 10 m reference DEM. And the highest change in inundation areas recorded for 60 m grid size with 35.55 %.

Table 5.6 Hydraulic output for Iyidere with 100yr return period flood

100yr				
Grid Size (m)	Mean WS (m)	Median WS (m)	Inundation Areas (km^2)	Changing %
10.00	22.20	4.00	6.70	0.00
20.00	28.39	5.00	6.94	3.52
30.00	17.70	3.00	5.42	-19.08
40.00	27.06	6.00	7.51	12.07
50.00	19.35	3.00	5.52	-17.63
60.00	24.76	3.00	5.28	-21.18
70.00	23.91	4.00	5.57	-16.92
80.00	39.26	20.00	8.82	31.51
90.00	45.27	5.00	7.01	4.59
100.00	21.71	5.00	6.53	-2.60

The result from the hydraulic modeling for the Iyidere river show that there is a difference of 0.49 m between the water surface elevations generated from 10 m reference DEM and 100 m gird size DEM. The percentages in change in the inundation areas are not significant with increasing grid size for DEMs, however the change in inundation area of about 2.60 % occur for a 100 m resolution DEM. In addition of that its was shown that all coarse DEMs had under estimation inundation areas with one exception of 20 m resolution as over estimation.

Figure 5.1 shows the cross-sections for the reference 10 m DEM versus the 30m, 90, and 100m DEM cross-sections for Iyidere River

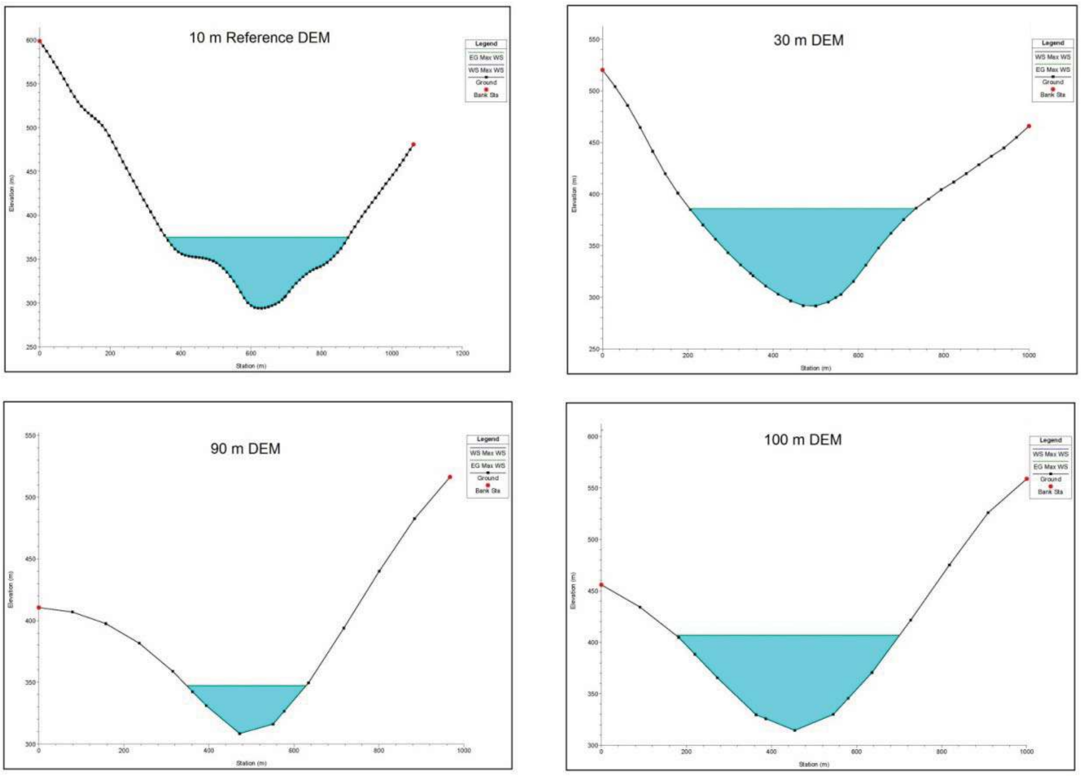

Figure 5.1 Cross-section for the station 26250 across Iyidere for (a) 10m reference DEM; (b) 30m DEM; (c) 90m DEM and (d) 100m DEM

The cross-section evaluation for the Iyidere River shows the effect of reducing the DEM resolution as significant amount of the topographic features are lost after increasing the grid size of DEM. The river channel is be more smooth as the gird size of DEM increase, due to this smoothing in the river channel, the DEM do not represent the channel cross section accurately. The overall channel bed elevation increased also when reducing the resolution of DEM or raising the grid size, which considers one reason for the over estimation in inundation areas when the grid size of DEMs is increased.

Figure 5.2 shows the comparison between flood inundation map for Iyidere River created (a) 10 m reference DEM; (b) 30 m DEM; (c) 60 m DEM; and (d) 100 m DEM

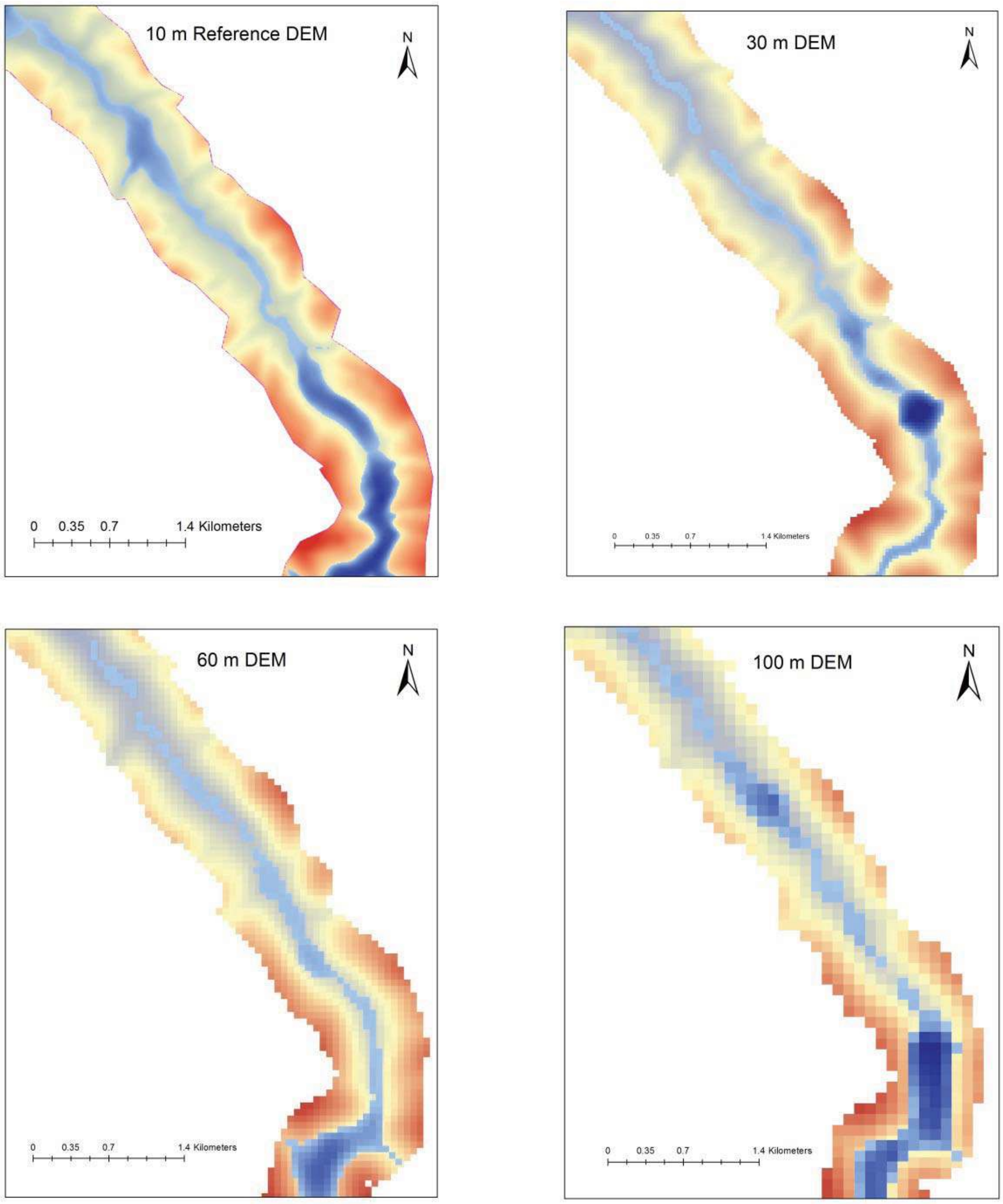

Figure 5.2 Inundation map generated from different resolutions; 10m, 30m, 60m, and 100m

It was shown that the quality of floodplain inundation mapping decreases as the resolution is reduced. In order to understand how the spatial resolution affects the hydraulic result it’s important to know that the 10 m DEM means that each 100m2 area has a single elevation value, while for the 100 m resolution DEM has a single elevation value for 10000m^2 area.

The predicted inundation extends for the Iyidere River do change significantly, in some cases the changes in the inundation areas can reach for 35% like the case when the 60 m grid size DEM with 50yr return period of flood was used.

A 100 m resolution DEM results in loss for river attribute as shown by the flood inundation maps. As a comparison between the 10 m reference DEM and 100 m DEM, the 100 m DEM flood map consider as a scattered set of cells showing inundation while for 10 m reference DEM represent the extent of flooding across river channel with better manner.

For the Iyidere basin, it was found that there is significant variation between the flood inundation mapping generated from the 10 m reference DEM and the 30 m, 60m, and 100m resolution DEMs.

The comparison shows significant changes in the overall quality of flood maps and extents on using coarser resolutions DEMs, the 30 m, 60 m, and 100 m resolution DEMs predicted inundated areas which not similar for the inundated area predicted from the 10 m reference DEM, however, there is a difference of about 2.21 km2 in the inundation areas obtained from the 10 m reference DEM and 80 m grid size DEM which is an over estimation with an overall change in inundation areas around 30% relative to 10 m DEM.

In general for Iyidere basin, the flood inundated areas which obtained from the DEMs coarser than 60 m resolution start to loss the topography attribute and do not given an appropriate description of river and flood plain morphology.

5.2 Effect of Resample Algorithm on Hydraulic Outputs

The topo to raster algorithm was used to produce contour lines based DEMs, however in order to investigate if changing the resample algorithm plays role and affect the hydraulic output, a 9 topographical data sets were produces using the bilinear resample technique see Section (4.1).

Table 5.7 present the results obtained from the hydraulic modelling using the DEMs produced by the bilinear resample method with 100yr return flow as hydraulic flow input.

Table 5.7 Hydraulic output for Iyidere with 100yr return period flood, bilinear resample algorithm was used

100yr			
Grid Size (m)	Mean WD (m)	Inundation Areas (km^2)	Change %
10.00	22.20	6.70	0
20.00	35.54	6.13	-8.48
30.00	25.93	6.19	-7.54
40.00	23.61	5.19	-22.53
50.00	49.87	10.24	52.83
60.00	32.82	5.55	-17.21
70.00	54.19	5.44	-18.82
80.00	26.16	4.63	-30.86
90.00	39.72	6.68	-0.34
100.00	72.21	6.81	1.63

The results show that there is a significant change in water elevation surface between 10 m reference DEM and 100 m resample DEM, the variation in result is around 3 times more even though the percentage changes in inundation areas not large 1.63% over estimation.

The highest change in inundation area obtained for 50 m gird size resolution DEM with water surface elevation and inundated area 49.87 m and 10.24 km2 respectively.

The results were obtained from the bilinear resample method has a remarkable difference from the result obtained by using topo to raster contour line base DEM technique. Due to the overall trend for the predicted areas from the bilinear algorithm has an under estimation inundated areas with two exceptions at 50 m and 100 m grid size DEMs, while as its shown in table (5.6) the overall trend is so oscillates between over-estimation and under estimation.

Figure 5.3 shows the comparison between 10 m reference DEM, 30 m, 60 m, and 100 m grid size resolution DEMs in one cross-section across Iyidere River.

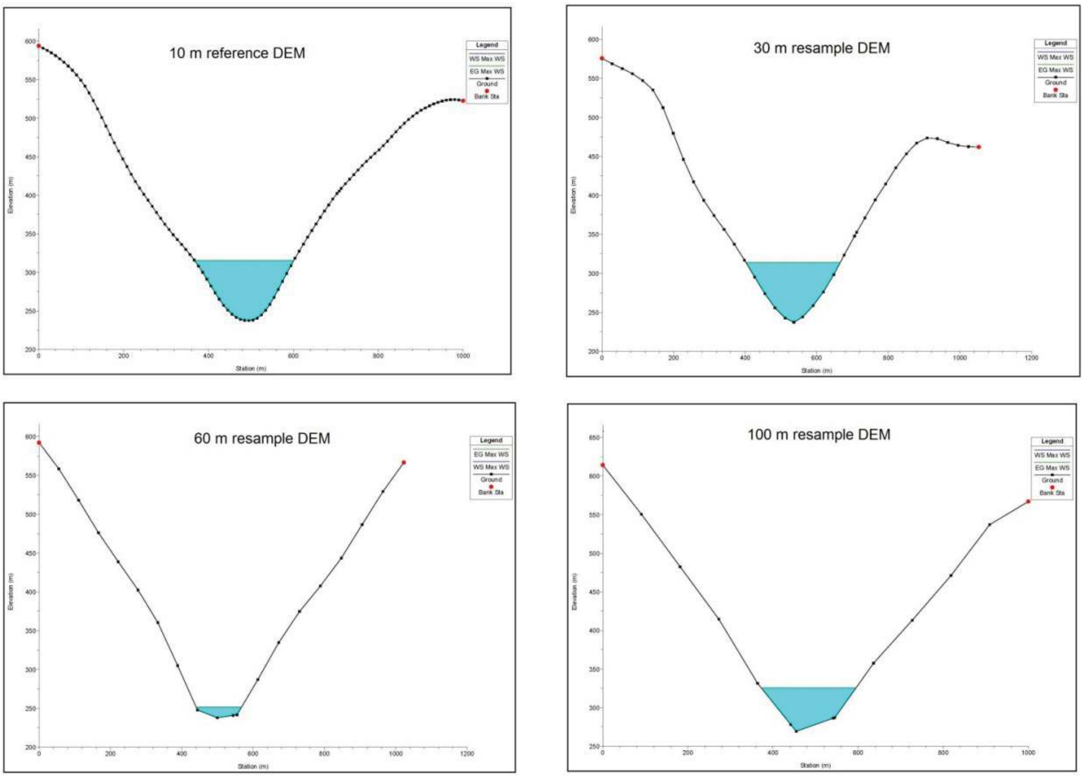

Figure 5.3 Cross-section for the station 23500 across Iyidere river for (a) 10 m reference DEM; (b) 30 m; (c) 60 m; (d) 100 m resample DEMs

It was clearly seen that as increase of the grid size as loss of the attribute of the cross sections attributes topographic details. In addition, the bed elevation of the 100 m resample DEM is increased which the lowest point in the bed almost start at 275 m above sea level, while for 10 m reference DEM the lowest point recorded as 230m above sea level. Due to Channel River smoothing, the coarse resample DEMs do not represent the river cross sections details accurately.

5.3 The Effect of DEM Error on Hydraulic Outputs

5.3.1 RMSE of Elevations Versus Grid Size

With the aim of measure the amount of error present in the produced DEMs with respect to the 10 m reference DEM, RMSE for different grid sizes of DEMs was calculated see Section (4.1), the results for RMSE versus grid size are represented in Table (5.8).

Table 5.8 RMSE against the grid size

100yr	
Grid Size (m)	RMSE (m)
10.00	
20.00	2.98
30.00	5.10
40.00	7.26
50.00	9.87
60.00	12.90
70.00	14.63
80.00	19.02
90.00	20.44
100.00	21.94

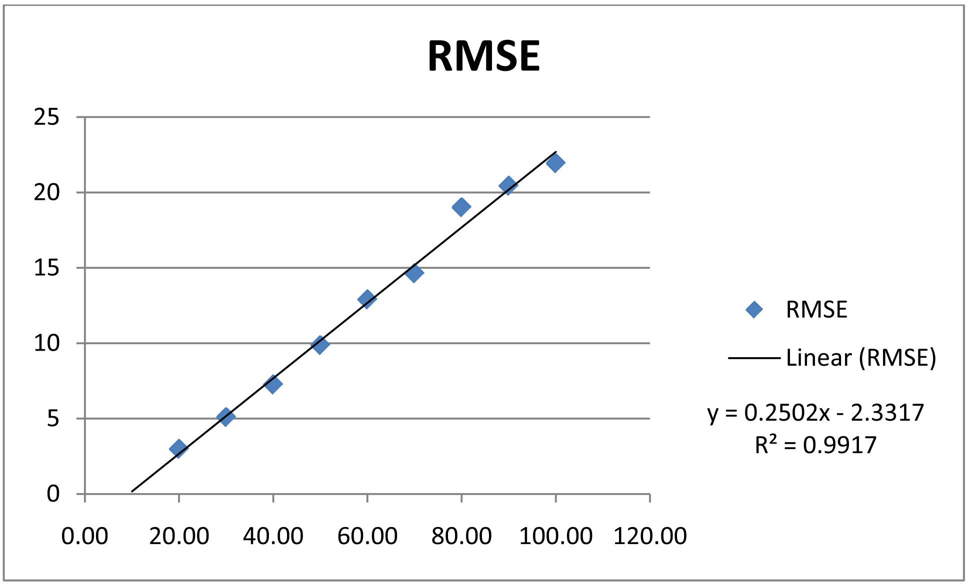

Figure 5.4 Graphic representation of RMSE against the grid size

The result clearly shows that the RMSE have a linear relationship with grid size. The predicted linear equation between RMSE and grid size have an R^2 greater than 99%. The high R2 values suggest a very good linear fit between the Errors and DEMs resolution.

The significant change of the RMSE values, which start from around 3 m for the 20 m grid size DEM up to almost 22 m for 100 m grid size DEM, this can be explained because of the shape and slope for the Iyidere valley due to Iyidere River had a high slope for the bank sides.

The graph also suggests that amount of error rises linearly with increasing the grid size for the topographical datasets, which means that the accuracy of DEM declines with decreasing the resolution or increasing the grid size.

5.3.2 *Effect of Error Existing in DEMs on Hydraulic Modeling Outputs*

With the intention of test the relation between hydraulic model output and DEM accuracy, 9 more topographic datasets were created for Iyidere River which errors were added see Section (4.1), the result obtained from the hydraulic analysis using digital elevation models containing errors are presented in Table (5.9).

Table 5.9 Hydraulic output for DEMs with errors, 100-yr return period was used as hydro-flow input

100yr				
Grid Size (m)	Mean WD (m)	Median WD (m)	Inundation Areas (km2)	Change %
10.00	22.20	4.00	6.70	0
20.00	30.02	3.00	6.33	-5.58
30.00	30.25	5.00	6.13	-8.52
40.00	40.08	14.00	7.57	12.94
50.00	33.02	6.00	6.31	-5.93
60.00	43.15	24.00	6.56	-2.14
70.00	30.07	5.00	5.79	-13.58
80.00	23.74	7.00	5.67	-15.41
90.00	46.00	15.00	9.43	40.66
100.00	17.00	6.00	5.81	-13.39

The result in the table obviously shows that the existence of errors has a significant impact on the predicated hydraulic outputs; average water surface elevations and flood inundation mapping. There is a dramatically increase in the average water surface elevations up to 40 m gird size DEM with obtained water surface elevation around double the water surface elevation obtained from the 10 m reference DEM, followed by varying in the water surface elevations outputs for the other topographic datasets. The inundation areas have also affected from adding the errors to the topographic data sets, the predicted area in using the 10 m reference

DEM is 6.7 km^2, while this value decrease up to 0.7 km^2 for a 100 m grid size DEM which is decrease of about 13.5% as an under estimation. The percentage change of inundated areas is observed to be negative for almost of DEMs; seventh of them. The 90 m gird size DEM recorded unexpected either water surface elevation or inundated area which is more than 2 time as water surface elevation (46.00m) while the inundated area increase up to 3 km2 for a 90 m grid size DEM which is raised of about 40% as an over estimation.

The RMSE for the 20 m grid size DEM was 2.98 m as compared to 21.94 m for an 100 m DEM Table (5.8), this suggest that DEM errors can have a significant impact on hydraulic predictions such a basin like Iyidere valley due to the decrease od accursing resulting from increased the grid size for DEMs.

By reason of those errors being random in nature, the addition of those errors can cause significant change for hydraulic outputs thus creating a large a unexpected result as spike in the hydraulic output such what happen in 90 m grid size DEM hydraulic model. However, those spikes have a significant change for cells with smaller size which is not fit with this research case study.

Even though the mean of the errors added to DEMs up to 50 m grid size is small, the small grid size accounts to a larger spatial variability between the cells thus reducing the inundation extent. But for larger grid sizes; more than 50 m grid size, the amount of error is very high and results in high estimation of water surface elevations and oscillatory for inundation extents.

Figure 5.5 shows the cross-sections for station 21750.00 obtained from topographic datasets of different resolution and amount of error.

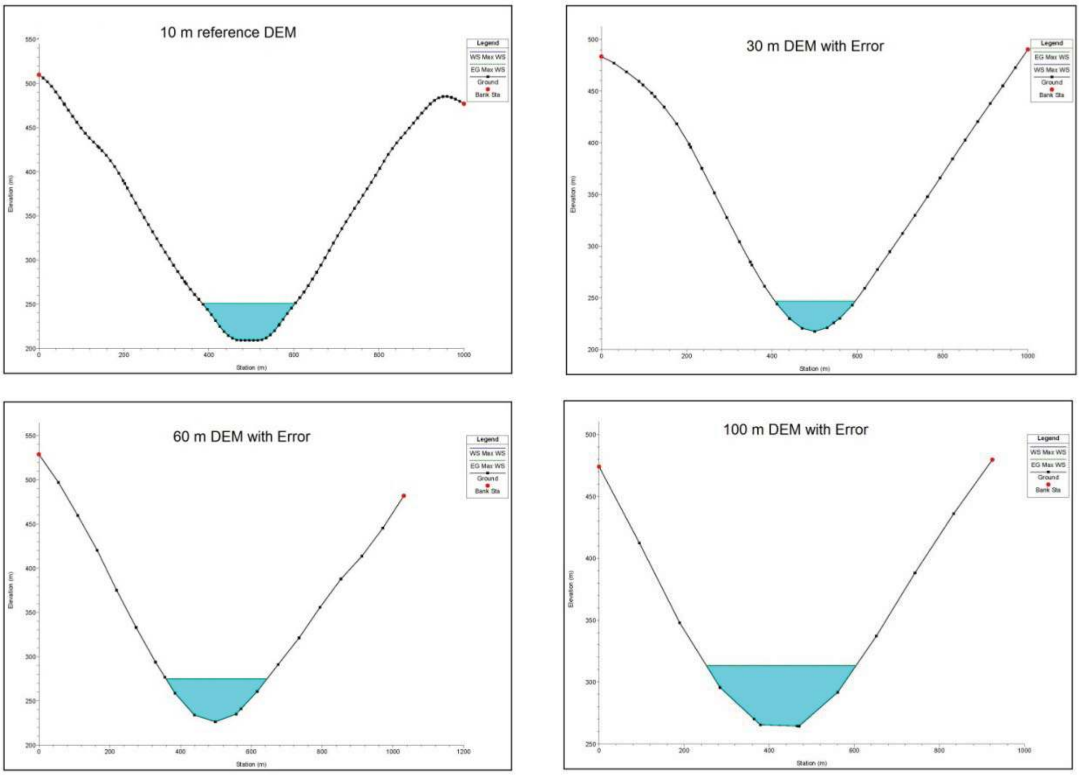

Figure 5.5 Cross-section station 6512.8 for (a) 10 m reference DEM; (b) 30 m DEM with error; (c) 60 m DEM with error; and (d) 100 m DEM with error

The figure shows that there is some loss in the cross sections profile particularly at the edges, also its clear that there main channel for the river becomes wider as the resolution of the DEMs goes coarser. The 100 m grid size DEM obtained the wider bed main channel from all the other cross section profiles, therefore as increase the grid size of DEM as misrepresent the cross section profile. This is by reason of existing errors with a high amount thought overall the topography dataset.

Figure 5.6 shows the comparison of the flood maps generated using topographical data containing different amount errors and resolutions for the Iyidere River.

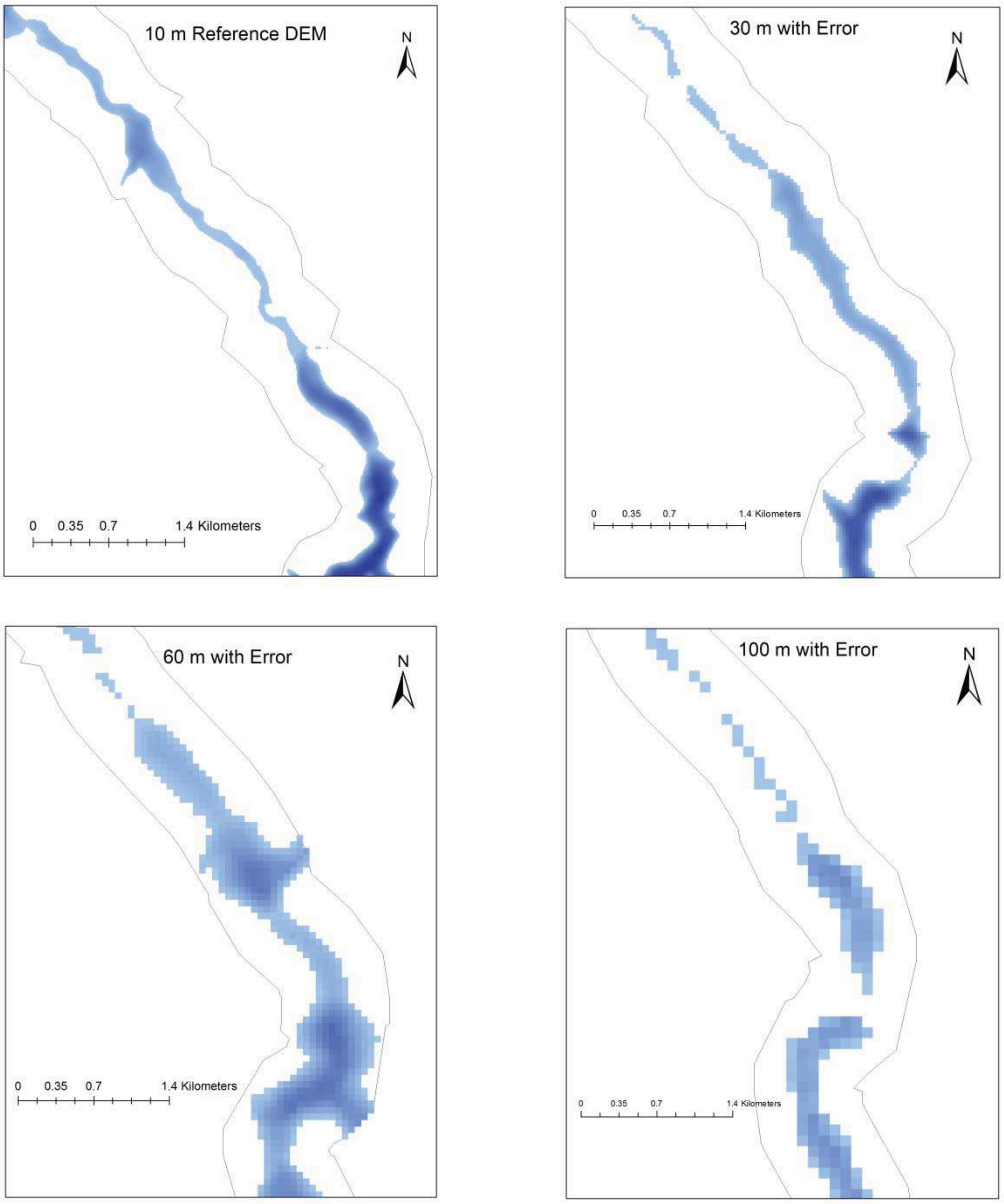

Figure 5.6 Inundation maps generated from (a) 10 m reference DEM; (b) 30 DEM with error; (c) 30 m DEM with error; and (d) 100 m DEM with error

The flood maps show that an addition of errors in general results in an increase in flood extents. The 10 m reference DEM is inundated mostly around the main channel while the 60 m and 100 m resolution DEM with error predicts inundation for a larger area in the floodplain. The magnitude of error added to the 100 m resolution DEM results in large variations in elevations which show higher depth of inundation for some parts of the river channel while no inundation for certain parts of the main channel itself.

In order to understand the changing in hydraulic modelling results, the bias in the results for the coarser DEMs with the respect to 10 m reference DEM was calculated. The formula was used to calculate the bias is

$$bias = \left[\frac{Di - D_{10m}}{D_{10m}}\right] \times 100 \quad (5.1)$$

Where:

Di =the average water depth which obtain from the coarser DEMs.

D_{10m} =the average water depth obtained from the 10 m reference DEM.

The same formula was used to calculate the bias in the floodplain inundation areas.

Table 5.10 compares the bias for the average water depth in meter which existing relative to the 10 m reference DEM for each coarse resolution and recurrence interval for flood plain.

Table 5.10 Bias for the average water depth, return period against grid size

Return Period	Gird size resolution For DEMs								
	20 m	30 m	40 m	50 m	60 m	70 m	80 m	90 m	100 m
2yr	43.56	24.43	32.76	27.01	43.48	32.47	46.70	50.50	34.09
5yr	138.13	51.59	36.99	22.76	36.54	16.69	34.57	2.80	6.08
10yr	35.70	22.04	19.17	29.88	12.38	15.00	6.13	9.92	4.43
25yr	26.89	92.73	19.46	1.53	37.17	20.95	7.67	12.93	8.91
50yr	63.22	28.03	61.03	22.12	38.46	21.60	52.76	44.29	42.47
100yr	27.90	20.26	21.89	12.84	11.53	7.72	76.84	103.94	2.19

According to the result in the table, the smallest bias obtained from 50 m grid size DEM with 25 year recurrence interval for flood, for 20 m grid size the minimum bias in the average water depth obtained for the 25 year return value, with overall range of bias around 27%. For 100 m grid size the result for bias quit dissimilar, the overall range is better than the 20 m grid size, which 9% overall range was observed with the same recurrence interval for flood.

In order to interpret the two main factors (grid size vs. recurrence interval) investigated in this study, a box and whisker plot (sometimes called a boxplot) was used. A box and whisker plot presents information from a five-number summary minimum, first quartile, median, third quartile and maximum. Box and whisker plots are very useful when two or more data sets are being compared.

The box and whisker plot compare the bias for the average water depth in the hydraulic modelling results were obtained from the coarser DEMs with respect to the 10 m reference DEM.

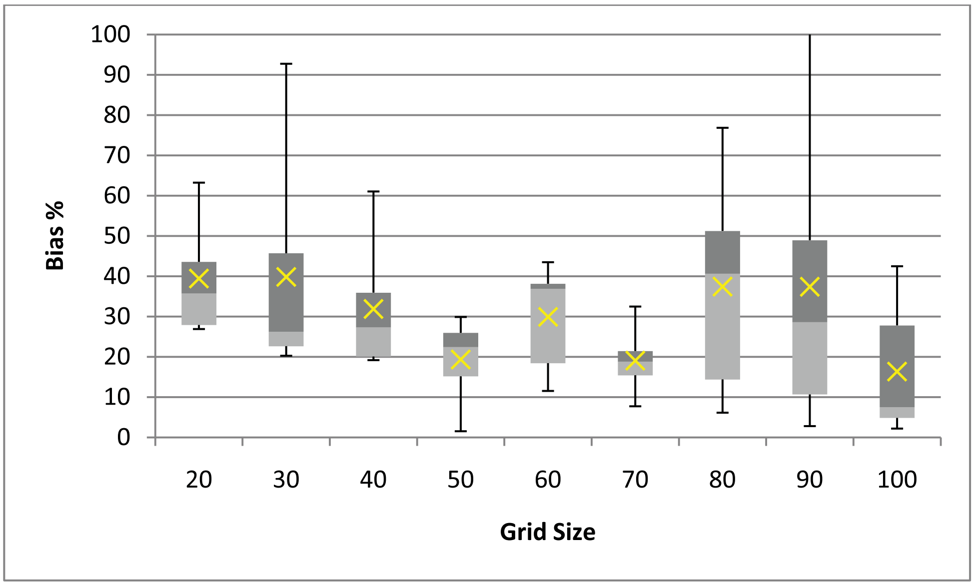

Figure 5.7 Bias for the average water depth, return period against grid size

As it clearly shown in Figure 5.7, the Interquartile range box for the 20 m grid size DEM was observed as 15 % bias, no Skewed data was observed, while the Interquartile range box for the 30 m grid size DEM was detected as 22.5%, a clear Skewed data was observed too. Due to half of data Squeezed between the biases 22.5% and 25% while the other half of the bias distributed with bias range more than 15%. Similarity for the 60 m gird size DEM the Skewed in bias data so notable. The IQR for bias was around 20 % and half of bias data located within less than 0.5 % bias and the other half occupied the 19.5 % bias left. The 100 m grid size follows the same trend in bias distribution as 20 m grid size, while 80 m grid size showed another trend in distribution, which the overall range of bias was 72 % and the IQR was around 35%, also a small Skewed in bias data was observed for the 80 m gird size DEM. In addition the figure suggest that for the 50 m, and 100 m grid size DEM the varying of the recurrence interval of flood as input for the hydraulic model does not play a significant role in changing the result due to the bias for all return period of flood used so closed to each other.

Table 5.11 Bias obtained from floodplain inundation areas, return period against grid size

Return Period	Gird size resolution For DEMs								
	20 m	30 m	40 m	50 m	60 m	70 m	80 m	90 m	100 m
2yr	9.35	4.86	5.57	18.09	21.09	9.67	8.13	3.18	0.61
5yr	15.55	14.39	0.49	5.04	15.81	7.80	12.96	5.08	7.06
10yr	0.01	10.05	4.96	21.36	27.43	10.46	9.74	1.69	5.06
25yr	1.93	20.53	9.33	22.42	3.71	7.08	6.55	10.33	9.65
50yr	26.98	14.21	28.35	22.30	35.55	9.85	24.58	9.84	20.68
100yr	3.52	19.08	12.07	17.63	21.18	16.92	31.51	4.59	2.60

Table 5.11 shows a significant change in the bias obtained from floodplain inundation areas (km^2). For the 20 m grid size the smallest bias or the best result obtained when 10-year return period of flood was used. While the closest best result of bias or the smallest bias was obtained for the 40 m grid size DEM when 5-year return period was used, followed by the bias obtained for the 100 m grid size DEM when 2-year return period was used as input flow chart for the hydraulic model.

The box plot compare the Bias obtained from floodplain inundation areas (km^2) in the hydraulic modelling results were obtained from the coarser DEMs with respect to the 10 m reference DEM.

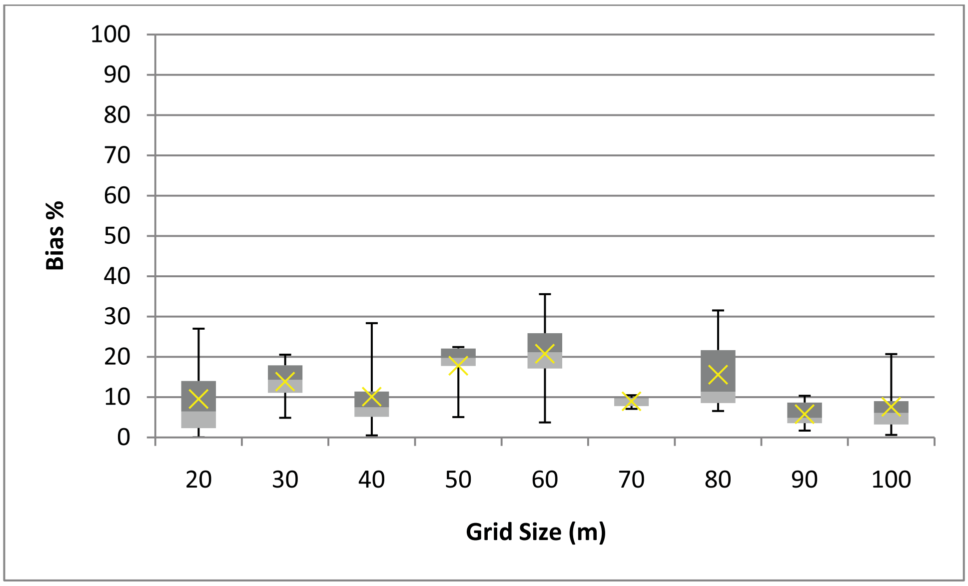

Figure 5.8 Bias obtained from floodplain inundation areas (km^2), return period against the grid size

The 20 m grid size DEM consider the closet resolution for the 10 m reference DEM, however the figure suggest that the bias in Extent index obtained from the 20 m resolution is higher than most of the bias which obtained from in the topographical data sets and the varying in the flood recurrence interval does play a slight role changing the result of the hydraulic model this is clear to observed from the relative wide range for the Interquartile range box which is around 10%. The figure also suggest that for the DEMs with resolution 70 m and 90 m has the similar bias value which is so a little, in the case of 70 m grid size the changing in recurrence interval of flood as input for the hydraulic modeling does not play any role in changing the results, while for the 20 m, 60 m, and 80m grid size DEMs the varying in return period does play a significant role in changing the hydraulics results. In the case of 60 m grid size DEM the bias reach around 35% in 50yr return period of flood as input.

5.3.3 Vulnerability Weighted Indices

With the aim of introducing a better understanding of flood plain mapping, the horizontal Euclidian extent of the floodplain was evaluated. In order to do so, the floodplain areas were divided to 10 rings from the right and left side of river stream center line (buffer zone); each ring has 50 m width, those rings are in the left and right side of the stream center line.

Figure 5.9 shows the horizontal rings produced for 10 m resolution stream line.

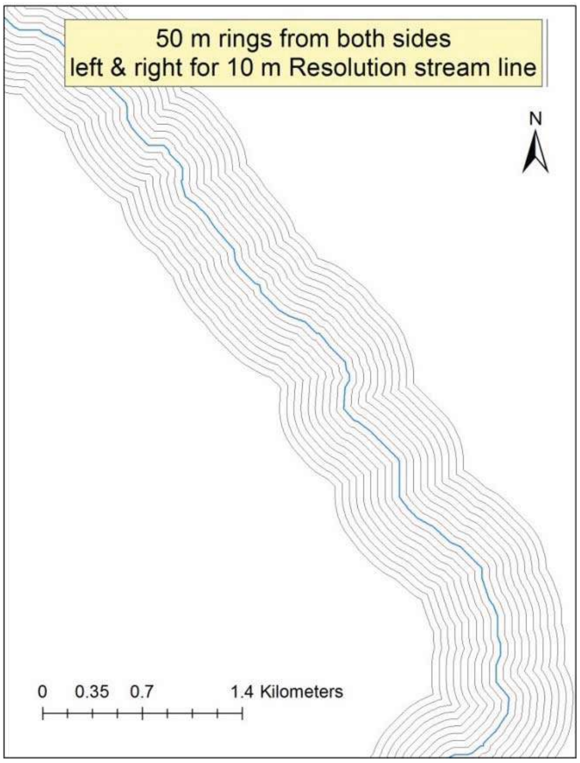

Figure 5.9 50 m buffer areas, 10 m resolution stream line

New module was established using a model builder tool in order to investigate the horizontal Euclidian extent of floodplain. Same procedures (Fig.5.10) are used on all DEMs of different resolution.

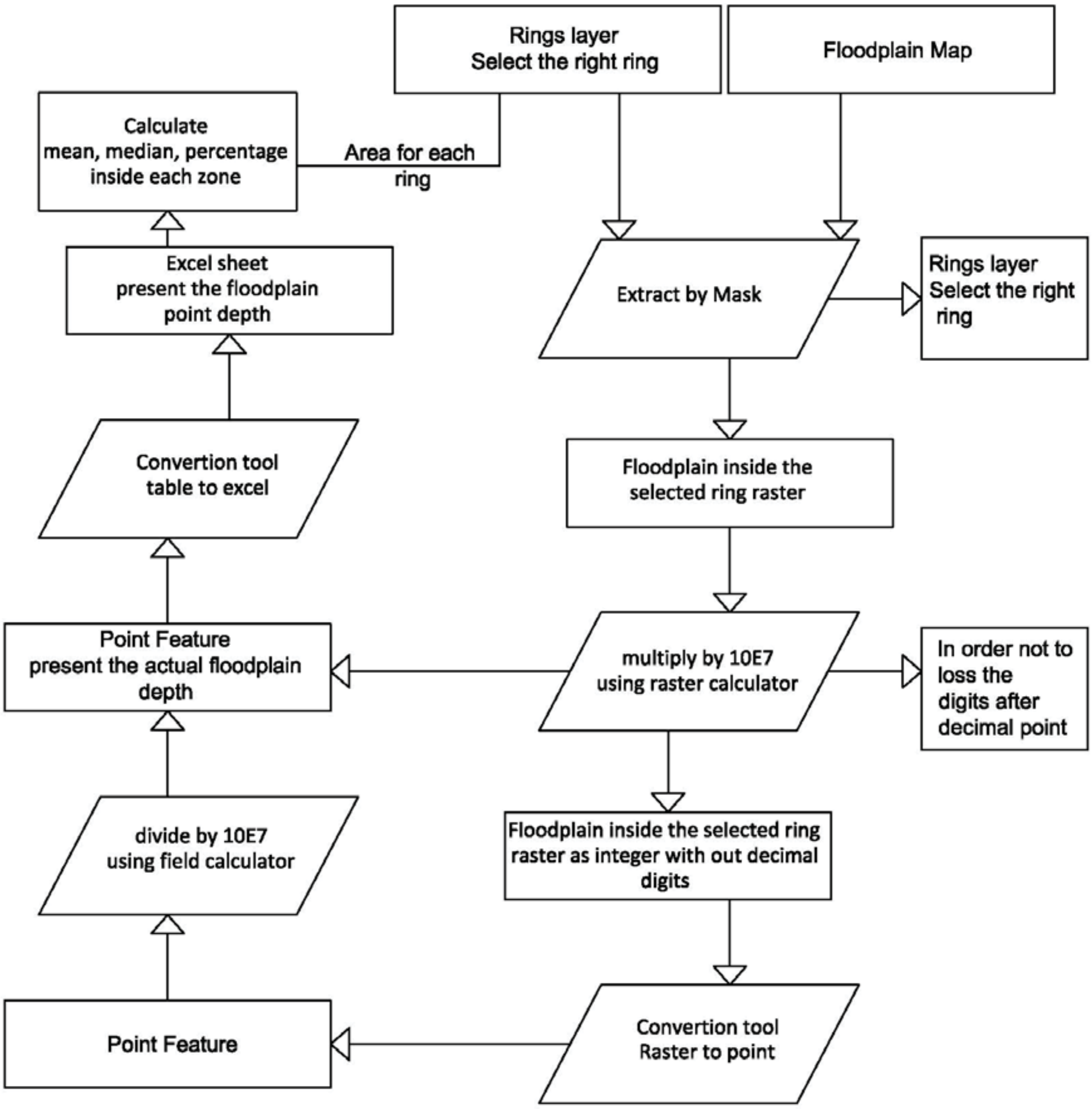

Figure 5.10 Statistical analysis procedures

Once the rings layer was generated, the extract by mask tool was used, putting in consideration selecting the right ring to proceed with the analysis, in order to be able to calculate the statistics parameter such as mean and median, convert the extract floodplain inside each ring become essential, from conversion toolset raster to point was used, with consideration that the raster to point tool work only and only if the input raster type is integer. After generating the point feature and exporting the attribute data as an excel sheet, it can be easy to calculate mean, median and percentage of flood inside each ring.

To calculate the percentage of flood inside each ring, this formula was used

$$percentage(\%) = \frac{area\ of\ flood}{area\ of\ the\ ring} \times 100 \quad (5.2)$$

To cover the entire 6 period flood recurrence interval with different 10 resolution DEMs start from 10 m reference DEM up to the coarsest DEM with 100 m grid size DEM, the above mention analysis was performed 600 times.

With the purpose of generalize the impact of horizontal Euclidian extent of floodplain mapping, order ranking was produced, ten numbers was used from 1 to 10, which the most close ring for the centerline stream has order one followed with rank 2 for the adjacent ring up to rank 10 for most far ring. This order rank numbers used to give weight of the importance – risk – for each ring, by other words; for the first 2 rings which the most closet for the stream center line it was expected that floodplain will reach them, In contrast, it was unexpected for the flood to reach the far rings, therefor the weight of impotence for those rings will magnified respect to the first ring.

Two indices were produced in this study; (1) the depth index: which gives an indicator number in meter for the weighted average water surface level after applying the weighted order ranking; and (2) The extent index: which gives another indicator in percentage for the weighed extend for the floodplain.

The formula was used to calculate the depth index is

$$depth\ index(m) = \frac{\sum_{i=1}^{10}(D_i \times i)}{\sum_{i=1}^{10} i} \quad (5.3)$$

Where:

D =The average depth in each ring, and

i = is the number of ring (weighted order rank) ascending from 1 to 10.

By the same concept, this formula was used to calculate the extent index

$$extent\ index(m) = \frac{\sum_{i=1}^{10}(P_i \times i)}{\sum_{i=1}^{10} i} \quad (5.4)$$

Where:

P : The percentage of floodplain inside each ring with respect to the area of each ring, see equation (5.2), and

i : is the number of ring (weighted order rank) ascending from 1 to 10.

Table 5.12 show the result was obtained from the previous analysis explained in Figure 5.10.

Table 5.12 The depth and extent indices obtained from the Euclidean buffer distances for 2-yr, 5-yr, 10-yr, 25-yr, 50-yr and 100-yr return period of flood

Return Period	**2yr**		**5yr**		**10yr**	
grid Size	Extend %	Depth (m)	Extend %	Depth (m)	Extend %	Depth (m)
10.00	8.12	21.31	7.12	17.36	9.10	20.67
20.00	7.46	7.31	10.78	27.62	10.54	33.01
30.00	9.21	26.31	8.95	15.69	8.24	12.79
40.00	8.89	10.40	9.85	17.08	10.10	13.61
50.00	6.35	13.84	6.89	12.68	6.74	13.69
60.00	5.85	9.88	6.31	18.58	6.48	25.07
70.00	8.20	14.09	6.91	17.26	7.62	18.64
80.00	6.96	9.04	8.75	19.46	9.05	24.21
90.00	7.44	7.70	7.96	10.55	9.39	34.02
100.00	9.94	10.13	9.96	9.94	11.79	23.05

Table 5.12 The depth and extent indices obtained from the Euclidean buffer distances for 2-yr, 5-yr, 10-yr, 25-yr, 50-yr and 100-yr return period of flood (Continue)

Return Period	25yr		50-yr		100yr	
grid Size	Extend %	Depth (m)	Extend %	Depth (m)	Extend %	Depth (m)
10	9.53	20.2	15.27	45.38	10.04	20.02
20	10.9	23.9	9.47	17.1	12.19	25.15
30	14.35	55.8	12.1	36.97	8.64	15.63
40	10.04	21.14	10.04	21.14	13.42	29.98
50	7.48	23.67	11.3	38.57	8.64	20.38
60	10.14	27.54	8.42	30.2	8.3	34.29
70	10.71	23.97	12.94	36.38	9.38	27.27
80	10.8	30.05	9.84	22.22	17.39	39.69
90	10.83	17.58	12.08	25.87	13.34	62.3
100	13.52	16.16	13.82	25.54	13.17	19.6

This table clearly shows that the weighted ranking analysis obtained more generalize average water surface elevation than the average water elevation obtained from the ordinary hydraulic analysis Tables (5.1-5.6).

It was found that there is significant variation in the results between those two analysis, the hydraulic analysis performed with 30 m grid size and 2 year return hydrograph chart as input, the average water elevation obtained from the ordinary analysis was 22.28 m, while the average water elevation obtained from the weighted order rank analysis was 9.21 m with variation more than 10 m.

All the result values obtained from the weighed order rank analysis was observed to be less than the results obtained from the ordinary hydraulic analysis which make more sense in the real life.

The bias was calculated in order to understand the variation in result between the produced coarser DEMs and 10 m reference DEM, for the both depth and extend indices the bias was calculated with respect to the 10 m reference DEM. The formula was used to calculate the bias in depth index is

$$bias\ in\ depth\ index = \left[\frac{Di - D_{10m}}{D_{10m}}\right] \times 100 \qquad (5.5)$$

Where:

Di =the depth index which obtain from the coarser DEMs.

D_{10m} =the depth index obtained from the 10 m reference DEM.

By following the same principle the bias in extent index was calculated.

Table (5.13 compares the bias for the depth index which exist relative to the 10 m reference DEM for each coarse resolution and recurrence interval for floodplain.

Table 5.13 Bias for the Depth index, return period against grid size

return period	**Gird size resolution For DEMs**								
	20 m	30 m	40 m	50 m	60 m	70 m	80 m	90 m	100 m
2yr	8.11	13.37	9.39	21.81	27.93	0.94	14.32	8.45	22.38
5yr	51.42	25.75	38.46	3.16	11.32	2.84	22.93	11.86	39.94
10yr	15.81	9.51	10.95	25.99	28.85	16.24	0.54	3.15	29.58
25yr	14.45	50.65	5.39	21.47	6.42	12.42	13.35	13.74	41.98
50yr	38.02	20.79	34.27	26.03	44.88	15.31	35.57	20.91	9.51
100yr	21.44	13.95	33.67	13.91	17.33	6.55	73.21	32.90	31.12

The table compare the changing in the bias occur due to varying the grid size of DEMs and recurrence interval of flood plain. For the 20 m grid size DEM the lowest bias recorded when 2yr return period of flood was used while the highest bias was observed for 5yr return period with variation more than 40%. The 100 m grid size has a different trend where the lowest bias was 9.51% for the 50yr return period and had been raised by almost 30% to reach the height bias when 25yr return period was used.

The best result or the most close to the 10 m reference DEM in the table was obtained when 70 m grid size was used and 2yr return period of flood data was entered as input for the hydraulic model, while the worst result had been documented at 70 m grid size with 100yr recurrence interval of flood.

Figure 5.11 compares the bias in the Depth index which occurs as result of increase the gird size and varying the return period as input for the hydraulic model.

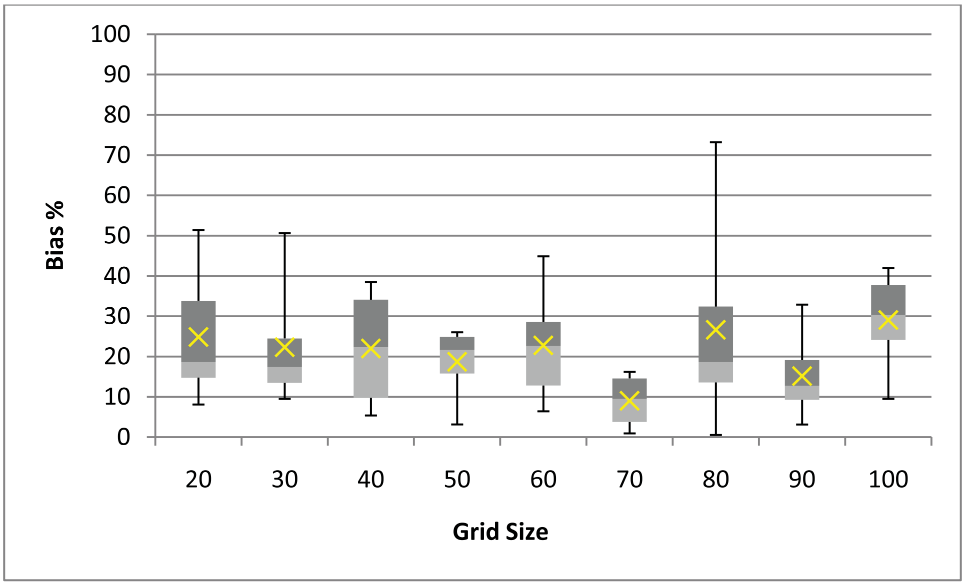

Figure 5.11 Depth index Biases Euclidean Buffers, return period against the grid size

The figure shows the distribution of bias of depth index for each DEM grid size, knowing that the y-axis represent the bias was obtained from the varying of recurrence interval as input. For the 20 m grid size DEM the range of the bias in the depth index is around 40 and more than the half of bias more than 18%. While for 70 m grid size DEM the bias for the depth index much less and present the most close result for the 10 m reference DEM; which the range of the bias is less than 15 and just half of bias more than 10%. The bias for 80 m grid size shows the worst result, where the range of bias around 80% and around half of bias more than 20 %.

As overall view the figure suggest that for all the data set the median bias is about 20 % with some exception in 80 m gird size and 100 m grid size. This might be happen as a reasonable Couse for using the weight order ranking analysis.

Table 5.14 compares the bias for the extent index which exist relative to the 10 m reference DEM for each coarse resolution and recurrence interval for flood plain.

Table 5.14 Bias in extent index, return period against grid size

Return priod	Gird size resoultion For DEMs								
	20 m	30 m	40 m	50 m	60 m	70 m	80 m	90 m	100 m
2yr	8.11	13.37	9.39	21.81	27.93	0.94	14.32	8.45	22.38
5yr	51.42	25.75	38.46	3.16	11.32	2.84	22.93	11.86	39.94
10yr	15.81	9.51	10.95	25.99	28.85	16.24	0.54	3.15	29.58
25yr	14.45	50.65	5.39	21.47	6.42	12.42	13.35	13.74	41.98
50yr	38.02	20.79	34.27	26.03	44.88	15.31	35.57	20.91	9.51
100yr	21.44	13.95	33.67	13.91	17.33	6.55	73.21	32.90	31.12

The table shows a significant change in the bias for the extent index. For the 20 m grid size the smallest bias or the best result obtained when 2-year return period of flood was used, while the best result of bias - or the smallest bias - was obtained for the 70 m grid size DEM when 2-year return period was used, followed by the bias obtained for the 80 m grid size DEM when 5-year return period was used as input flow chart for the hydraulic model.

Figure 5.12 compare the bias in the extend index which occurs as result of increase the gird size and varying the return period as input for the hydraulic model.

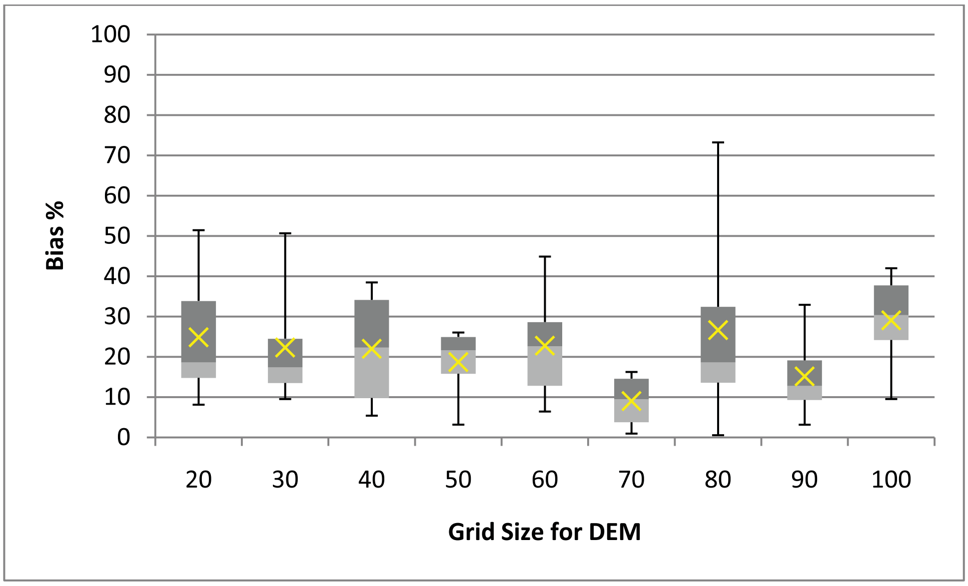

Figure 5.12 Extent index Biases Euclidean Buffers, return period against the grid size

The figure reveals that the median of the bias is around 20% for the produced DEMs up to 60 m resolution. For the 20 m grid size resolution, the range of the bias is 40% and has of bias more than 18%. The worst bias obtained for 80 m grid size DEM which the bias range more than 70 % and almost the bias more than 18%, while the best result obtained for the 70 m grid size DEM with bias range less than 17% and half of this bias less than 10%. The figure suggests that there is a significant varying in bias regarding the DEMs resolution and recurrence interval of flood. In addition the figure suggests that the return period of flood or the recurrence interval does play a role in changing the result of the hydraulic outputs results.

The weighted order rank analysis does not reflect the reality of the topography of the surface and contains some theoretical error due to variation in the actual surface and Euclidean buffer analysis, however, this was a theoretical approach and the horizontal Euclidian buffer analysis is widely used in the regional risk assessment management.

More advance analysis was performed; this analysis put in consideration the actual topography of the surface. Form the distance toolset, path distance was used to calculate the actual topographical surface which the floodplain covers.

The procedure which explained in figure 5.13 was followed, another 600 analysis was performed to obtained the depth and extent indices shows in Table (5.15).

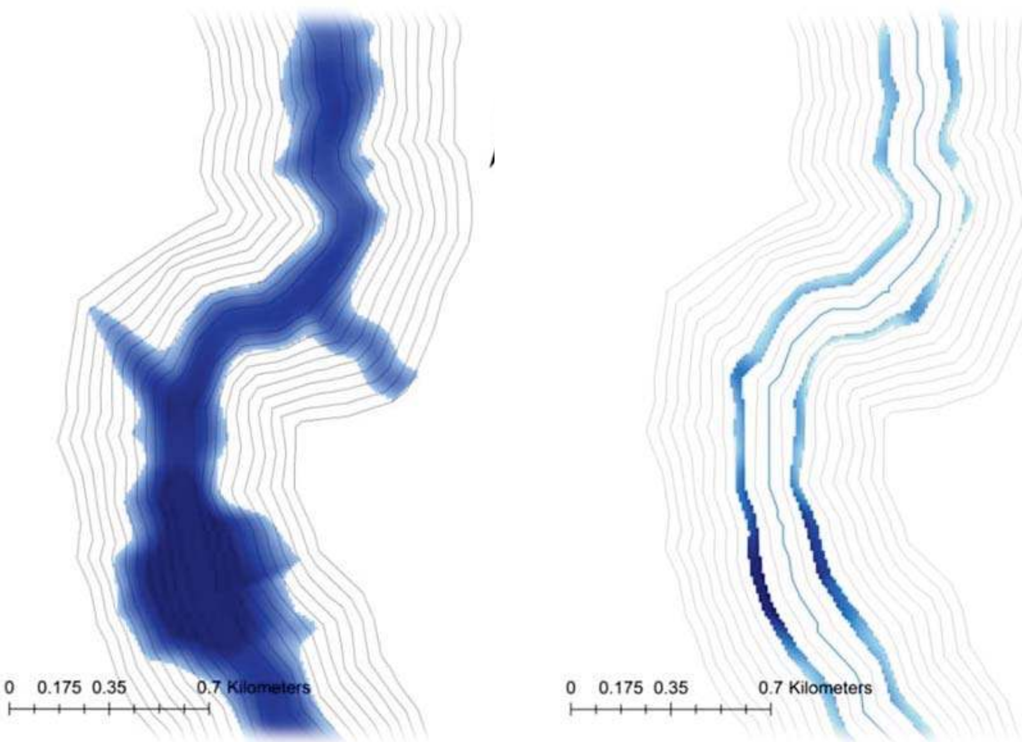

Figure 5.13 (a)Sample sketch of the changes in the depth and extent index when the actual surface rings construct (b) The percentage of flood which located inside the third ring 150m

Table 5.15 The depth and extent indices obtained from the actual topographical surface buffers for 2-yr, 5-yr, 10-yr, 25-yr, 50-yr and 100-yr return period of flood

Return Period	**2yr**		**5yr**		**10yr**	
grid Size	Extend %	Depth (m)	Extend %	Depth (m)	Extend %	Depth (m)
10.00	9.20	22.30	7.92	17.63	10.30	21.27
20.00	8.09	7.55	12.10	28.73	11.91	35.17
30.00	10.09	27.40	9.60	15.97	8.82	12.89
40.00	8.82	11.19	9.77	17.35	10.08	13.68
50.00	7.25	14.35	7.78	13.08	7.61	14.35
60.00	6.08	10.16	6.79	20.35	6.83	25.87
70.00	7.18	14.84	7.15	17.24	8.12	19.05
80.00	6.51	8.92	8.24	19.11	9.28	25.21
90.00	6.61	7.67	7.31	10.66	9.26	32.69
100.00	6.41	10.78	6.17	10.88	7.92	21.53
Return Period	25yr		50yr		100yr	
grid Size	Extend %	Depth (m)	Extend %	Depth (m)	Extend %	Depth (m)
10.00	10.88	20.61	17.81	46.01	11.88	15.52
20.00	12.35	24.34	10.36	17.94	13.26	25.60
30.00	15.74	58.24	13.39	38.59	9.29	15.95
40.00	9.96	21.81	11.63	30.10	14.08	32.14
50.00	8.63	24.30	13.00	39.33	9.26	20.59
60.00	11.04	27.67	9.14	30.95	8.74	34.25
70.00	11.66	24.62	13.78	37.41	9.75	27.98
80.00	10.66	29.89	10.04	22.55	18.29	40.30
90.00	10.22	17.11	11.56	25.32	13.89	64.07
100.00	10.22	17.75	10.58	26.89	9.30	20.71

Bu using the weighted order rank method with actual topographic surface to calculate the depth and extent indices yielded results with no significant variation in the result from the indices which obtained using the straight horizontal analysis. However, almost one unit shift more in the indices obtained from the analysis using the actual surface rings was observed.

The bias was calculated for each depth index obtained from a coarser DEMs with respect to the depth index obtained from the 10 m reference DEM. Table (5.16) compares the result of the depth index for each DEM resolutions and recurrence interval for floodplain

Table 5.16 Depth index obtained from actual surface, Grid Size against Return Period

return period	Grid Size resolution for DEMs								
	20 m	30 m	40 m	50 m	60 m	70 m	80 m	90 m	100 m
2yr	66.14	22.87	49.84	35.65	54.46	33.47	60.01	65.61	51.65
5yr	63.02	9.38	1.57	25.77	15.42	2.17	8.41	39.51	38.26
10yr	65.35	39.38	35.70	32.54	21.64	10.42	18.54	53.70	1.24
25yr	18.11	182.57	5.84	17.91	34.27	19.45	45.02	16.99	13.86
50yr	61.01	16.12	34.57	14.51	32.74	18.69	50.99	44.97	41.55
100yr	64.95	2.76	107.08	32.69	120.70	80.27	159.6	312.8	33.44

The table shows that the bias which obtained is higher for the finest resolution. For the 20 m grid size resolution the minimum bias in the depth index was 18% for the 25-year return period of flood, while the smallest bias or the best result with the closet for the result obtained from the 10 m reference DEM was obtained from 100 m grid size resolution which consider the coarsest resolution in the entire topographical datasets.

In order to present two parameters together, a box and whisker plot was used. (Figure 5.15) presents the bias in depth index obtained using actual topographic surface as a comparison between gird size of DEMs and return period of flood.

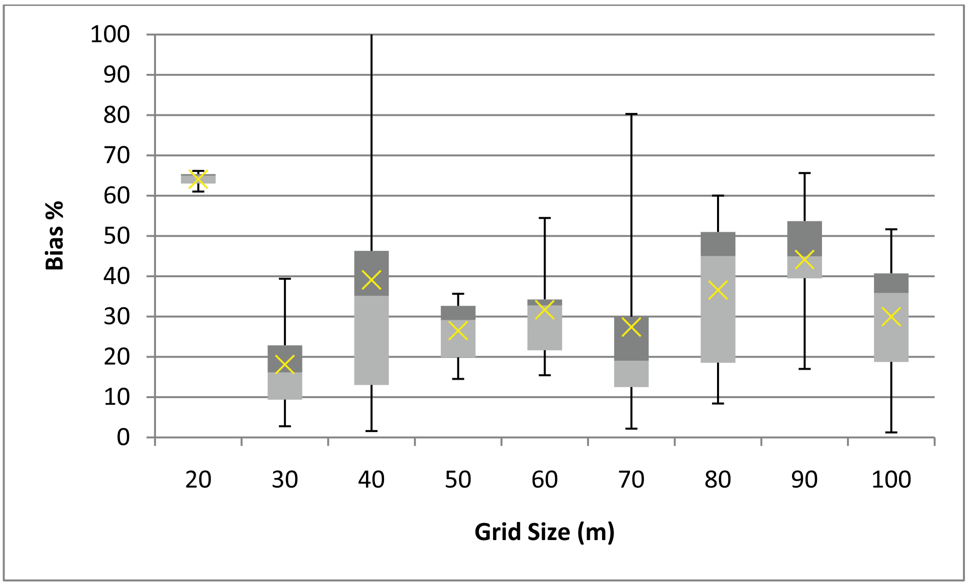

Figure 5.14 Depth index Biases actual surface buffers, return period against grid size, return period against grid size

The 20 m grid size DEM consider the closet resolution for the 10 m reference DEM, however the figure suggest that the bias in depth index obtained from the 20 m resolution is the highest from in the topographical data sets and the varying in the flood recurrence interval does not play a role changing the result of the hydraulic model this is clear to observed from the close range for the Interquartile range box (IQR) which is less than 5%. The figure also suggest that for the DEMs with resolution 40 m and 70 m has the some bias value which is so high, in the case of 40 m grid size with 100 year return period the bias reach around 100%, while for the 70 m grid size DEM the bias observed around 80%.

I addition of that, the figure divide the DEMs for 3 categories, the first category with the finest resolutions have a significant change in bias median, for the second category with have a moderate gird size (50m, 60m, and 70m) have a median bias oscillates around 30%, and for the third category with coarsest resolution have median variation around 10% with respect to the moderate resolution median bias, which is fluctuate around 40%.

Table 5.17 compare the bias for the extent index obtained from the analysis consider the actual topographical surface, which exist relative to the 10 m reference DEM for each coarse resolution and recurrence interval for flood plain.

Table 5.17 Extent index obtained from actual surface, Grid Size against Return Period

Return Priod	Gird size resoultion For DEMs								
	20 m	30 m	40 m	50 m	60 m	70 m	80 m	90 m	100 m
2yr	12.03	9.75	4.07	21.18	33.84	21.97	29.26	28.12	30.25
5yr	52.76	21.24	23.42	1.68	14.29	9.75	4.02	7.63	22.04
10yr	15.61	14.37	2.18	26.13	33.69	21.16	9.89	10.07	23.11
25yr	13.50	44.61	8.50	20.66	1.42	7.17	2.04	6.05	6.07
50yr	41.83	24.79	34.71	27.01	48.67	22.62	43.65	35.06	40.58
100yr	11.67	21.81	18.56	22.02	26.45	17.93	54.01	16.92	21.70

According to the result in the table, the smallest bias obtained from 50 m grid size DEM with 5 year recurrence interval for flood, for 20 m grid size the minimum bias in the extend index obtained for the 2 year return value, with overall range of bias around 40%. For 100 m grid size the result for bias quit deferent, the overall range is better than the 20 m grid size, which 40 % overall range was observed.

The following box plot graph present the relationship between the grid size and recurrence interval for the flood for the extent index which obtained using the analysis reflect the actual topographic surface of the areas which covered by water.

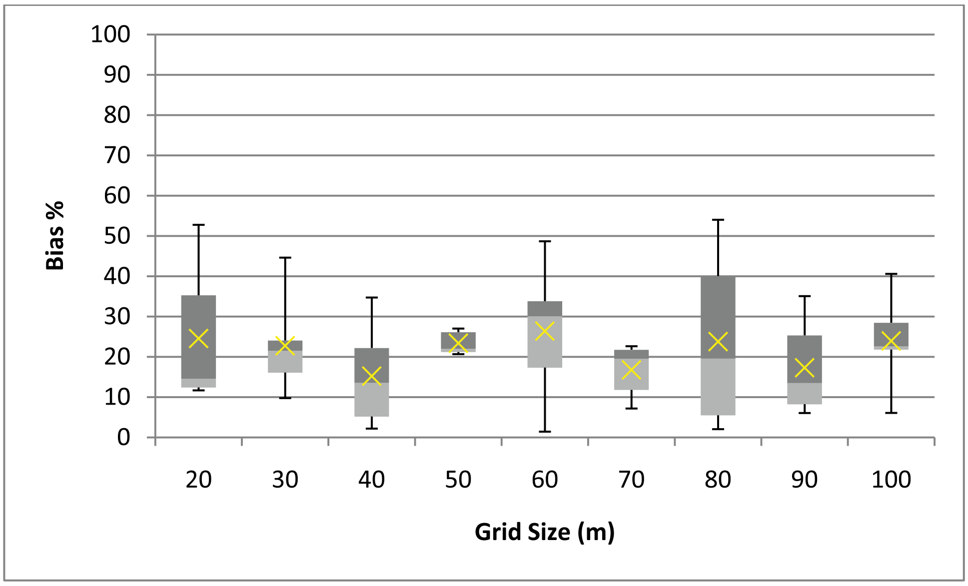

Figure 5.15 Extent index Biases actual surface buffers, return period against grid size, return period against grid size

The Interquartile range box for the 20 m grid size DEM was observed as 23 % bias, a clear Skewed in data was observed too, due to the IQR is 20% but half of data was located between bias of 15% and bias of 35% and the other have of data located between the bias of 12.5% and 15%. Similarity for the 50 m gird size DEM the Skewed in data so notable. The IQR for bias was around 5 % and half of bias data located within less than 0.5 % bias and the other half occupied the 4 % bias left. The 100 m grid size follows the same trend in bias distribution as 50 m grid size, while 80 m grid size showed another trend in distribution, which the overall range of bias was 50 % and the IQR was around 35%, also no Skewed in bias data was observed for the 80 m gird size DEM. In addition the figure suggest that for the 30 m, 50 m, and 100 m grid size DEM the varying of the recurrence interval of flood as input for the hydraulic model does not play a significant role in changing the result due to the bias for all return period of flood used so closed to each other.

CHAPTER SIX
CONCLUSION AND DISCUSSION

In the presented study, impacts of DEM resolution (as variably used in different modeling implementations) on flood maps generated from hydraulic modeling operations were principally analyzed. 10 m resolution which was produced based on 20 m contour lines was selected as the reference DEM for providing comparisons in relation to decreased grid resolutions while representing the topography. Coarser grid representations varying from 10 to 100 m were generated in the study through resampling of the 10 m reference DEM.

Among the different resolution DEMs assessed in this study, the highest DEM resolution data are normally expected to be the most accurate and thus provide a better representation/extraction for the river network while reduced resolutions in forms of coarser DEM data are expected to result in corresponding decrease in the accuracy, precision and thus the reliability of the results, on the contrary.

The RMSE analysis clearly shows that the RMSE have a linear relationship with grid size. The predicted linear equation between RMSE and grid size have an R^2 greater than 99%. The high R^2 values suggest a very good linear fit between the Errors and DEMs resolution.

The significant change of the RMSE values, which start from around 3 m for the 20 m grid size DEM up to almost 22 m for 100 m grid size DEM, this can be explained because of the shape and slope for the Iyidere valley due to Iyidere River had a high slope for the bank sides.

The Graphic representation of RMSE also suggests that amount of error rises linearly with increasing the grid size for the topographical datasets, which means that the accuracy of DEM declines with decreasing the resolution or increasing the grid size.

In order to give better understanding over the outputs from the hydraulic model, two indices were basically produced; depth index and floodplain extent index. Bias was calculated to present potential disparities between the results obtained from the reference 10 m DEM and those repeated by using the coarser topography representations.

In respect to model implementations without considering any vulnerability zoning scheme structured in different distances from the stream centerlines, decreasing the DEM resolution seems to have a remarkable impact on the hydraulics model output, even though the study area has relatively flat terrain characteristics. For further expanding and generalizing the results through some other relevant flood indices, Euclidean buffer vulnerability analysis was additionally performed. The impact of changing resolution of DEMs on the depth index varied significantly from the highest resolution to the lowest. Yet, it is not fully expressed in the study that the first higher resolution provides the best estimation of the floodplain analysis over the hydraulic model as it is only based on a selection within the available data sets. When Euclidean buffer vulnerability analysis was performed, generalization of the error inclusion in the analysis was observed, while by considering actual surface buffers that followed the sloped terrain surfaces, the results produced no distinguishable trend in the index values displayed against the changing topography grid resolutions. Here, the ambiguity in the first better resolution (20 m DEM), where the bias was obtained much higher than the biases obtained for the other coarser DEMs resolutions, appeared explicitly. This might be caused by two reasons: (1) while significant declines in the resolution were applied by providing the reduction in 10 m resolution intervals in assigning the coarser DEM resolutions, in contrast to some other studies that declined the resolution by comparably smaller reduction amounts in 1 m to reach the worst case to 15 m or 30 m grid sizes, in this presented study, the sudden difference between 20 m and 30 m grid sizes of the DEMs remained remarkably high; and also (2) the limitations accompanied in modeling performance through the use of one-dimensional HEC-RAS model. However for the floodplain extent index, using the actual surface buffer somehow generalizes the error to have the horizontal shape instead of the hill shape in the original analysis.

The study also revealed that the flood recurrence interval does not play a significant role with the highest resolution as it is clear in the bias obtained for the depth index from the actual surface analysis where the IQR is so small, while as the resolution becomes much smaller the flood recurrence interval start playing remarkable role which is more explicit in the wide range of IQR. However, for the flood plain extent index it was observed that the flood recurrence interval needs more consideration and this makes sense because the amount of precipitations will increase with increased recurrence intervals as well. Since the bias obtained from the 50 m grid size DEM is smaller than the Bias obtained from 30 m grid size DEM for this specific study case, it may be preferable to use 50 m-sized DEM grid instead of a 30 m resolution to perform the hydraulic analysis, even though the higher resolution is normally expected to give better accuracy.

As the adapted resolution change on the depth and floodplain indices normally has some variable impacts on the parameter, it cannot be easy to produce generic inferences from the comparison due to the known limitations with the hydraulic modeling capacity.

The buffer zone vulnerability analysis still proves to be a helpful approach for assisting the decision-making process with regards to the flood risk issues despite its associated limited capacity in unfolding the needs towards the selection of the best preferable grid resolution in conducting the analyses. Indeed, the approach provides sufficient indications about the extent up to the flood water will reach and the average water depth in the floodplain while additionally covering the buffer zones that serve to address the vulnerability concerns as well.

REFERENCES

Disaster and Emergency Management Presidency (AFAD), (2012). *Strategic Plan 2013 - 2017*. Retrieved 19 August,2015, from https://www.afad.gov.tr/UserFiles/File/STRATEJI/Afad%20Strtjk%20web_en%20son.pdf

Aguilar, F. J., Aguilar, M. A., Agüera, F., & Sánchez, J. (2006). The accuracy of grid digital elevation models linearly constructed from scattered sample data. *International Journal of Geographical Information Science, 20*(2), 169-192.

Aguilar, F. J., Mills, J. P., Delgado, J., Aguilar, M. A., Negreiros, J. G., & Pérez, J. L. (2010). Modelling vertical error in Lidar-derived digital elevation models. *ISPRS Journal of Photogrammetry and Remote Sensing*, *65*(1), 103-110.

Andersson, L., Samuelsson, P., & Kjellström, E. (2011). Assessment of climate change impact on water resources in the pungwe river basin. *Tellus A*, *63*(1), 138-157.

Brandt, S. A. (2005). Resolution issues of elevation data during inundation modeling of river floods. *Paper presented at the XXXI International Association of Hydraulic Engineering and Research Congress, Water Engineering for the Future: Choices and Challenges.,* Seoul, Korea.

Casas, A., Benito, G., Thorndycraft, V. R., & Rico, M. (2006). The topographic data source of digital terrain models as a key element in the accuracy of hydraulic flood modelling. *Earth Surface Processes and Landforms*, *31*(4), 444-456.

Chaplot, V., Darboux, F., Bourennane, H., Leguédois, S., Silvera, N., & Phachomphon, K. (2006). Accuracy of interpolation techniques for the derivation of digital elevation models in relation to landform types and data density. *Geomorphology*, *77*(1–2), 126-141.

Charlton, M. E., Large, A. R. G., & Fuller, I. C. (2003). Application of airborne lidar in river environments: the river coquet, Northumberland, UK. *Earth Surface Processes and Landforms*, *28*(3), 299-306.

Chow, V. T. (1959). *Open-channel hydraulics*. Tokyo; London: McGraw-Hill.

Chu, H.-J., Chen, R.-A., Tseng, Y.-H., & Wang, C.-K. (2014). Identifying Lidar sample uncertainty on terrain features from Dem simulation. *Geomorphology*, *204*(0), 325-333.

Cowan, W. L. (1956). Estimating hydraulic roughness coefficient. *Agricultural Engineering*, *37*(7), 473-475.

Darnell, A. R., Tate, N. J., & Brunsdon, C. (2008). Improving user assessment of error implications in digital elevation models. *Computers, Environment and Urban Systems*, *32*(4), 268-277.

Erdoğan, S. (2010). Modelling the spatial distribution of DEM error with geographically weighted regression: an experimental study. *Computers & Geosciences*, *36*(1), 34-43.

Environmental Systems Research Institute (ESRI), (2014a). *ArcGIS 10.1 Help-Cell size of raster data*.

Environmental Systems Research Institute (ESRI), (2014b). *ArcGIS 10.1 Help-Managing Elevation Data, Part 1: About Elevation Data*.

European Environment Agency, (2012). *Implementation and achievements of clc2006*. Retrieved 18 August,2015, from http://www.eea.europa.eu/data-and-maps/data/clc-2006-vector-data-version-2/clc-final-report/clc-final-report/at_download/file

Fisher, P. F., & Tate, N. J. (2006). Causes and consequences of error in digital elevation models. *Progress in Physical Geography*, *30*(4), 467-489.

Gesch, D., Oimoen, M., Greenlee, S., Nelson, C., Steuck, M., & Tyler, D. (2002). The national elevation dataset. *Journal of the American Society for Photogrammetry And Remote Sensing*, *68*(1).

Gonga-Saholiariliva, N., Gunnell, Y., Petit, C., & Mering, C. (2011). Techniques for quantifying the accuracy of gridded elevation models and for mapping uncertainty in digital terrain analysis. *Progress in Physical Geography*, *35*(6), 739-764.

Haile, A. T., & Rientjes, T. H. M. (2005). Effects of LIDAR DEM resolution in flood modelling: a model sensitivity study for the city of tegucigalpa, honduras. *Paper presented at the ISPRS WG III/3, III/4, V/3 Workshop "Laser scanning 2005"*, Enschede, the Netherlands.

Heritage, G. L., Milan, D. J., Large, A. R. G., & Fuller, I. C. (2009). Influence of survey strategy and interpolation model on dem quality. *Geomorphology*, *112*(3–4), 334-344.

Li, J., & Wong, D. W. S. (2010). Effects of DEM sources on hydrologic applications. *Computers, Environment and Urban Systems*, *34*(3), 251-261.

Li, Z. (1988). On the measure of digital terrain model accuracy. *The Photogrammetric Record*, *12*(72), 873-877.

Lo, C. P., & Yeung, A. K. W. (2007). *Concepts and techniques of geographic information systems*. Upper Saddle River, NJ: Pearson Prentice Hall.

Merwade, V. (2012). *Tutorial on using HEC-GeoRAS with arcgis 10 and HEC-RAS modeling*. Indiana, USA: Purdue University Retrieved 18 August,2015, from https://web.ics.purdue.edu/~vmerwade/education/georastutorial.pdf.

Meyer, S., & Olivera, F. (2007). *Floodplain mapping & hydraulic analysis with HEC-GeoRAS 4.1.1 and ArcGIS 9.1*. Texas A&M University Retrieved 18 August,2015, from http://www.irfanakar.com/gis_remote_sensing_files/hecras/Floodplain%20Mapping%20&%20Hydraulic%20Analysis%20with%20HEC-GeoRAS%204.1.1%20and%20ArcGIS%209.1.pdf.

Mills, P., & Badcock, A. (2011). *Preliminary flood risk assessment fluvial flood hazard mapping- normal depth method.* Retrieved 18 August,2015, from http://www.cfram.ie/pdfs-downloads/TechDocs/Fluvial%20Normal-Depth%20Report%20-%20Final.pdf

Moore, I. D., Grayson, R. B., & Ladson, A. R. (1991). Digital terrain modelling: a review of hydrological, geomorphological, and biological applications. *Hydrological Processes*, *5*(1), 3-30.

Omer, C. R., Nelson, E. J., & Zundel, A. K. (2003). Impact of varied data resolution on hydraulic modeling and floodplain delineation. *JAWRA Journal of the American Water Resources Association*, *39*(2), 467-475.

Ousluel Gul G., Gul A., Asikoglu Ö.L., Akay O., Dalkilic Y., Arbaros F., & Ergul H.E., L. Y. (2013). *Assessing flood frequency estimation methods under environmental changes*. Final Report from the TUBITAK COST

Parker, J. A., Kenyon, R. V., & Troxel, D. (1983). Comparison of interpolating methods for image resampling. *Medical Imaging, IEEE Transactions on*, *2*(1), 31-39.

Ponce, V. M. (2011). *When to use unsteady flow with Hec-Ras*. Retrieved 18 April, 2015, from http://ponce.sdsu.edu/unsteady_flow_with_hec_ras.html

Rayburg, S., Thoms, M., & Neave, M. (2009). A comparison of digital elevation models generated from different data sources. *Geomorphology*, *106*(3–4), 261-270.

Saksena, S. (2014). *Investigating the role of DEM resolution and accuracy on flood inundation mapping*. M.Sc. Thesis, Purdue University, Indiana, Retrieved 18 August, 2015, from https://web.ics.purdue.edu/~vmerwade/reports/2014_02.pdf

Sanders, B. F. (2007). Evaluation of On-Line DEMs for flood Inundation Modeling. *Advances in Water Resources*, *30*(8), 1831-1843.

Schumann, G., Matgen, P., Cutler, M. E. J., Black, A., Hoffmann, L., & Pfister, L. (2008). Comparison of remotely sensed water stages from LIDAR, topographic contours and SRTM. *ISPRS Journal of Photogrammetry and Remote Sensing*, *63*(3), 283-296.

Tarboton, D. G., Bras, R. L., & Rodriguez-Iturbe, I. (1991). On the extraction of channel networks from digital elevation data. *Hydrological Processes*, *5*(1), 81-100.

Tarboton, D. G., Bras, R. L., & Rodriguez-Iturbe, I. (1992). A physical basis for drainage density. *Geomorphology*, *5*(1–2), 59-76.

Tate, E., & Maidment, D. (1999). *Floodplain mapping using HEC-RAS and Arcview GIS.* Retrieved 18 August, 2015, from http://www.ce.utexas.edu/prof/maidment/grad/tate/research/Floodmap/webfiles/floodmap.html

Tate, E., Maidment, D. R., Olivera, F., & Anderson, D. J. (2002). Creating a terrain model for floodplain mapping. *Journal of Hydrologic Engineering*, *7*(2), 100-108.

United States Army Corps of Engineers (USACE), (2009). *HEC-RAS, river analysis system aplication guides*. United States Army Corps of Engineers, Hydrologic Engineering Centre, Davis, California, UAS Retrieved 18 August, 2015, from http://www.hec.usace.army.mil/software/hec-ras/documentation/HEC-RAS_4.1_Applications_Guide.pdf.

United States Army Corps of Engineers (USACE), (2010a). *HEC-RAS, river analysis system hydraulic reference manual*. United States Army Corps of Engineers, Hydrologic Engineering Centre, Davis, California, UAS Retrieved 18 August, 2015, from http://www.hec.usace.army.mil/software/hec-ras/documentation/HEC-RAS_4.1_Reference_Manual.pdf.

United States Army Corps of Engineers (USACE), (2010b). *HEC-RAS, river analysis system user's manual version 4.1*. United States Army Corps of Engineers, Hydrologic Engineering Centre, Davis, California, UAS Retrieved 18 August, 2015, from http://www.hec.usace.army.mil/software/hec-ras/documentation/HEC-RAS_4.1_Users_Manual.pdf.

United States Army Corps of Engineers (USACE), (2011). *HEC-GeoRAS, GIS tools for support of Hec-Ras using ArcGIS, users manual*. United States Army Corps of Engineers, Hydrologic Engineering Centre, Davis, California, UAS Retrieved 18 August, 2015, from http://www.hec.usace.army.mil/software/hec-georas/documentation/HEC-GeoRAS_43_Users_Manual.pdf.

Vaze, J., Teng, J., & Spencer, G. (2010). Impact of DEM accuracy and resolution on topographic indices. *Environmental Modelling & Software*, *25*(10), 1086-1098.

Werner, M. G. F. (2001). Impact of grid size in GIS based flood extent mapping using a 1D flow model. *Physics and Chemistry of the Earth, Part B: Hydrology, Oceans and Atmosphere*, *26*(7–8), 517-522.

Wonkovich, M. (2007). *Evaluation of high-resolution digital elevation models for creating inundation maps* M.Sc. Thesis Bowling Green State University, Ohio, Retrieved 18 August, 2015, from https://etd.ohiolink.edu/!etd.send_file?accession=bgsu1167945221&disposition=inline

Zandbergen, P. A. (2006). The effect of cell resolution on depressions in digital elevation models. *Applied GIS*.

APPENDICES

Appendix A

Input Hydrographs Iyidere River 2-Year Return Period of Flood

Date	Time	Inflow (m3/s)	Outflow (m3/s)
15-Nov-75	0:00	11	11
15-Nov-75	1:00	10.9	10.9
15-Nov-75	2:00	10.9	10.9
15-Nov-75	3:00	10.8	10.8
15-Nov-75	4:00	10.8	10.8
15-Nov-75	5:00	11.2	11.2
15-Nov-75	6:00	12.8	12.8
15-Nov-75	7:00	18.5	18.5
15-Nov-75	8:00	57.8	57.8
15-Nov-75	9:00	210.2	210.2
15-Nov-75	10:00	387.6	387.6
15-Nov-75	11:00	444.3	444.3
15-Nov-75	12:00	461	461
15-Nov-75	13:00	467.1	467.1
15-Nov-75	14:00	469.4	469.4
15-Nov-75	15:00	468.7	468.7
15-Nov-75	16:00	467.5	467.5
15-Nov-75	17:00	463.4	463.4

15-Nov-75	18:00	456.9	456.9
15-Nov-75	19:00	450.2	450.2
15-Nov-75	20:00	440.7	440.7
15-Nov-75	21:00	429	429
15-Nov-75	22:00	418	418
15-Nov-75	23:00	407.7	407.7
16-Nov-75	0:00	398	398
16-Nov-75	1:00	387.5	387.5
16-Nov-75	2:00	371	371
16-Nov-75	3:00	349.8	349.8
16-Nov-75	4:00	329.7	329.7
16-Nov-75	5:00	310.8	310.8
16-Nov-75	6:00	293	293
16-Nov-75	7:00	276.3	276.3
16-Nov-75	8:00	260.5	260.5
16-Nov-75	9:00	245.7	245.7
16-Nov-75	10:00	231.8	231.8
16-Nov-75	11:00	218.6	218.6
16-Nov-75	12:00	206.2	206.2
16-Nov-75	13:00	194.6	194.6
16-Nov-75	14:00	183.6	183.6
16-Nov-75	15:00	173.3	173.3
16-Nov-75	16:00	163.6	163.6

16-Nov-75	17:00	154.4	154.4
16-Nov-75	18:00	145.8	145.8
16-Nov-75	19:00	137.7	137.7
16-Nov-75	20:00	130.1	130.1
16-Nov-75	21:00	122.9	122.9
16-Nov-75	22:00	116.1	116.1
16-Nov-75	23:00	109.8	109.8
17-Nov-75	0:00	103.8	103.8
17-Nov-75	1:00	98.1	98.1
17-Nov-75	2:00	92.8	92.8
17-Nov-75	3:00	87.8	87.8
17-Nov-75	4:00	83.1	83.1
17-Nov-75	5:00	78.6	78.6
17-Nov-75	6:00	74.5	74.5
17-Nov-75	7:00	70.5	70.5
17-Nov-75	8:00	66.8	66.8
17-Nov-75	9:00	63.3	63.3
17-Nov-75	10:00	61.8	61.8
17-Nov-75	11:00	61.5	61.5
17-Nov-75	12:00	61.1	61.1
17-Nov-75	13:00	60.8	60.8
17-Nov-75	14:00	60.5	60.5
17-Nov-75	15:00	60.2	60.2

17-Nov-75	16:00	59.9	59.9
17-Nov-75	17:00	59.5	59.5
17-Nov-75	18:00	59.2	59.2
17-Nov-75	19:00	58.9	58.9
17-Nov-75	20:00	58.6	58.6
17-Nov-75	21:00	58.3	58.3
17-Nov-75	22:00	58	58
17-Nov-75	23:00	57.7	57.7
18-Nov-75	0:00	57.4	57.4
18-Nov-75	1:00	57.1	57.1
18-Nov-75	2:00	56.8	56.8
18-Nov-75	3:00	56.5	56.5
18-Nov-75	4:00	56.2	56.2
18-Nov-75	5:00	55.9	55.9
18-Nov-75	6:00	55.6	55.6
18-Nov-75	7:00	55.3	55.3
18-Nov-75	8:00	55	55
18-Nov-75	9:00	54.7	54.7
18-Nov-75	10:00	54.4	54.4
18-Nov-75	11:00	54.1	54.1
18-Nov-75	12:00	53.8	53.8
18-Nov-75	13:00	53.5	53.5
18-Nov-75	14:00	53.2	53.2

18-Nov-75	15:00	53	53
18-Nov-75	16:00	52.7	52.7
18-Nov-75	17:00	52.4	52.4
18-Nov-75	18:00	52.1	52.1
18-Nov-75	19:00	51.8	51.8
18-Nov-75	20:00	51.6	51.6
18-Nov-75	21:00	51.3	51.3
18-Nov-75	22:00	51	51
18-Nov-75	23:00	50.7	50.7
19-Nov-75	0:00	50.5	50.5
19-Nov-75	1:00	50.2	50.2
19-Nov-75	2:00	49.9	49.9
19-Nov-75	3:00	49.7	49.7
19-Nov-75	4:00	49.4	49.4
19-Nov-75	5:00	49.2	49.2
19-Nov-75	6:00	48.9	48.9
19-Nov-75	7:00	48.6	48.6
19-Nov-75	8:00	48.4	48.4
19-Nov-75	9:00	48.1	48.1
19-Nov-75	10:00	47.9	47.9
19-Nov-75	11:00	47.6	47.6
19-Nov-75	12:00	47.4	47.4
19-Nov-75	13:00	47.1	47.1

19-Nov-75	14:00	46.9	46.9
19-Nov-75	15:00	46.6	46.6
19-Nov-75	16:00	46.4	46.4
19-Nov-75	17:00	46.1	46.1
19-Nov-75	18:00	45.9	45.9
19-Nov-75	19:00	45.6	45.6
19-Nov-75	20:00	45.4	45.4
19-Nov-75	21:00	45.1	45.1
19-Nov-75	22:00	44.9	44.9
19-Nov-75	23:00	44.7	44.7
20-Nov-75	0:00	44.4	44.4
20-Nov-75	1:00	44.2	44.2
20-Nov-75	2:00	43.9	43.9
20-Nov-75	3:00	43.7	43.7
20-Nov-75	4:00	43.5	43.5
20-Nov-75	5:00	43.3	43.3
20-Nov-75	6:00	43	43
20-Nov-75	7:00	42.8	42.8
20-Nov-75	8:00	42.6	42.6
20-Nov-75	9:00	42.3	42.3
20-Nov-75	10:00	42.1	42.1
20-Nov-75	11:00	41.9	41.9
20-Nov-75	12:00	41.7	41.7

20-Nov-75	13:00	41.4	41.4
20-Nov-75	14:00	41.2	41.2
20-Nov-75	15:00	41	41
20-Nov-75	16:00	40.8	40.8
20-Nov-75	17:00	40.6	40.6
20-Nov-75	18:00	40.4	40.4
20-Nov-75	19:00	40.1	40.1
20-Nov-75	20:00	39.9	39.9
20-Nov-75	21:00	39.7	39.7
20-Nov-75	22:00	39.5	39.5
20-Nov-75	23:00	39.3	39.3
21-Nov-75	0:00	39.1	39.1
21-Nov-75	1:00	38.9	38.9
21-Nov-75	2:00	38.7	38.7
21-Nov-75	3:00	38.5	38.5
21-Nov-75	4:00	38.3	38.3
21-Nov-75	5:00	38.1	38.1
21-Nov-75	6:00	37.9	37.9
21-Nov-75	7:00	37.7	37.7
21-Nov-75	8:00	37.5	37.5
21-Nov-75	9:00	37.3	37.3
21-Nov-75	10:00	37.1	37.1
21-Nov-75	11:00	36.9	36.9

21-Nov-75	12:00	36.7	36.7
21-Nov-75	13:00	36.5	36.5
21-Nov-75	14:00	36.3	36.3
21-Nov-75	15:00	36.1	36.1
21-Nov-75	16:00	35.9	35.9
21-Nov-75	17:00	35.7	35.7
21-Nov-75	18:00	35.5	35.5
21-Nov-75	19:00	35.3	35.3
21-Nov-75	20:00	35.1	35.1
21-Nov-75	21:00	35	35
21-Nov-75	22:00	34.8	34.8
21-Nov-75	23:00	34.6	34.6
22-Nov-75	0:00	34.4	34.4
22-Nov-75	1:00	34.2	34.2
22-Nov-75	2:00	34	34
22-Nov-75	3:00	33.9	33.9
22-Nov-75	4:00	33.7	33.7
22-Nov-75	5:00	33.5	33.5
22-Nov-75	6:00	33.3	33.3
22-Nov-75	7:00	33.1	33.1
22-Nov-75	8:00	33	33
22-Nov-75	9:00	32.8	32.8
22-Nov-75	10:00	32.6	32.6

22-Nov-75	11:00	32.4	32.4
22-Nov-75	12:00	32.3	32.3
22-Nov-75	13:00	32.1	32.1
22-Nov-75	14:00	31.9	31.9
22-Nov-75	15:00	31.8	31.8
22-Nov-75	16:00	31.6	31.6
22-Nov-75	17:00	31.4	31.4
22-Nov-75	18:00	31.3	31.3
22-Nov-75	19:00	31.1	31.1
22-Nov-75	20:00	30.9	30.9
22-Nov-75	21:00	30.8	30.8
22-Nov-75	22:00	30.6	30.6
22-Nov-75	23:00	30.4	30.4
23-Nov-75	0:00	30.3	30.3

Input Hydrographs Iyidere River 5-Year Return Period of Flood

Date	Time	Inflow (m3/s)	Outflow (m3/s)
15-Nov-75	0:00	11	11
15-Nov-75	1:00	10.9	10.9
15-Nov-75	2:00	10.9	10.9
15-Nov-75	3:00	10.8	10.8
15-Nov-75	4:00	11	11

15-Nov-75	5:00	12.3	12.3
15-Nov-75	6:00	16.9	16.9
15-Nov-75	7:00	29.5	29.5
15-Nov-75	8:00	92.5	92.5
15-Nov-75	9:00	317.4	317.4
15-Nov-75	10:00	566.3	566.3
15-Nov-75	11:00	640.5	640.5
15-Nov-75	12:00	660.5	660.5
15-Nov-75	13:00	666.1	666.1
15-Nov-75	14:00	666.7	666.7
15-Nov-75	15:00	663.5	663.5
15-Nov-75	16:00	659.6	659.6
15-Nov-75	17:00	651.8	651.8
15-Nov-75	18:00	640.8	640.8
15-Nov-75	19:00	629.6	629.6
15-Nov-75	20:00	614.9	614.9
15-Nov-75	21:00	597.3	597.3
15-Nov-75	22:00	580.8	580.8
15-Nov-75	23:00	565.3	565.3
16-Nov-75	0:00	550.7	550.7
16-Nov-75	1:00	535.1	535.1
16-Nov-75	2:00	511.8	511.8
16-Nov-75	3:00	482.3	482.3

16-Nov-75	4:00	454.4	454.4
16-Nov-75	5:00	428.2	428.2
16-Nov-75	6:00	403.5	403.5
16-Nov-75	7:00	380.3	380.3
16-Nov-75	8:00	358.4	358.4
16-Nov-75	9:00	337.8	337.8
16-Nov-75	10:00	318.4	318.4
16-Nov-75	11:00	300.2	300.2
16-Nov-75	12:00	283	283
16-Nov-75	13:00	266.9	266.9
16-Nov-75	14:00	251.6	251.6
16-Nov-75	15:00	237.3	237.3
16-Nov-75	16:00	223.8	223.8
16-Nov-75	17:00	211.1	211.1
16-Nov-75	18:00	199.2	199.2
16-Nov-75	19:00	188	188
16-Nov-75	20:00	177.4	177.4
16-Nov-75	21:00	167.4	167.4
16-Nov-75	22:00	158	158
16-Nov-75	23:00	149.2	149.2
17-Nov-75	0:00	140.9	140.9
17-Nov-75	1:00	133	133
17-Nov-75	2:00	125.7	125.7

17-Nov-75	3:00	118.7	118.7
17-Nov-75	4:00	112.2	112.2
17-Nov-75	5:00	106	106
17-Nov-75	6:00	100.2	100.2
17-Nov-75	7:00	94.8	94.8
17-Nov-75	8:00	89.6	89.6
17-Nov-75	9:00	84.8	84.8
17-Nov-75	10:00	80.3	80.3
17-Nov-75	11:00	76	76
17-Nov-75	12:00	71.9	71.9
17-Nov-75	13:00	68.1	68.1
17-Nov-75	14:00	64.5	64.5
17-Nov-75	15:00	61.9	61.9
17-Nov-75	16:00	61.6	61.6
17-Nov-75	17:00	61.3	61.3
17-Nov-75	18:00	60.9	60.9
17-Nov-75	19:00	60.6	60.6
17-Nov-75	20:00	60.3	60.3
17-Nov-75	21:00	60	60
17-Nov-75	22:00	59.7	59.7
17-Nov-75	23:00	59.3	59.3
18-Nov-75	0:00	59	59
18-Nov-75	1:00	58.7	58.7

18-Nov-75	2:00	58.4	58.4
18-Nov-75	3:00	58.1	58.1
18-Nov-75	4:00	57.8	57.8
18-Nov-75	5:00	57.5	57.5
18-Nov-75	6:00	57.2	57.2
18-Nov-75	7:00	56.9	56.9
18-Nov-75	8:00	56.6	56.6
18-Nov-75	9:00	56.3	56.3
18-Nov-75	10:00	56	56
18-Nov-75	11:00	55.7	55.7
18-Nov-75	12:00	55.4	55.4
18-Nov-75	13:00	55.1	55.1
18-Nov-75	14:00	54.8	54.8
18-Nov-75	15:00	54.5	54.5
18-Nov-75	16:00	54.2	54.2
18-Nov-75	17:00	53.9	53.9
18-Nov-75	18:00	53.6	53.6
18-Nov-75	19:00	53.3	53.3
18-Nov-75	20:00	53.1	53.1
18-Nov-75	21:00	52.8	52.8
18-Nov-75	22:00	52.5	52.5
18-Nov-75	23:00	52.2	52.2
19-Nov-75	0:00	51.9	51.9

19-Nov-75	1:00	51.7	51.7
19-Nov-75	2:00	51.4	51.4
19-Nov-75	3:00	51.1	51.1
19-Nov-75	4:00	50.8	50.8
19-Nov-75	5:00	50.6	50.6
19-Nov-75	6:00	50.3	50.3
19-Nov-75	7:00	50	50
19-Nov-75	8:00	49.8	49.8
19-Nov-75	9:00	49.5	49.5
19-Nov-75	10:00	49.2	49.2
19-Nov-75	11:00	49	49
19-Nov-75	12:00	48.7	48.7
19-Nov-75	13:00	48.5	48.5
19-Nov-75	14:00	48.2	48.2
19-Nov-75	15:00	47.9	47.9
19-Nov-75	16:00	47.7	47.7
19-Nov-75	17:00	47.4	47.4
19-Nov-75	18:00	47.2	47.2
19-Nov-75	19:00	46.9	46.9
19-Nov-75	20:00	46.7	46.7
19-Nov-75	21:00	46.4	46.4
19-Nov-75	22:00	46.2	46.2
19-Nov-75	23:00	45.9	45.9

20-Nov-75	0:00	45.7	45.7
20-Nov-75	1:00	45.5	45.5
20-Nov-75	2:00	45.2	45.2
20-Nov-75	3:00	45	45
20-Nov-75	4:00	44.7	44.7
20-Nov-75	5:00	44.5	44.5
20-Nov-75	6:00	44.3	44.3
20-Nov-75	7:00	44	44
20-Nov-75	8:00	43.8	43.8
20-Nov-75	9:00	43.6	43.6
20-Nov-75	10:00	43.3	43.3
20-Nov-75	11:00	43.1	43.1
20-Nov-75	12:00	42.9	42.9
20-Nov-75	13:00	42.6	42.6
20-Nov-75	14:00	42.4	42.4
20-Nov-75	15:00	42.2	42.2
20-Nov-75	16:00	42	42
20-Nov-75	17:00	41.7	41.7
20-Nov-75	18:00	41.5	41.5
20-Nov-75	19:00	41.3	41.3
20-Nov-75	20:00	41.1	41.1
20-Nov-75	21:00	40.9	40.9
20-Nov-75	22:00	40.7	40.7

20-Nov-75	23:00	40.4	40.4
21-Nov-75	0:00	40.2	40.2
21-Nov-75	1:00	40	40
21-Nov-75	2:00	39.8	39.8
21-Nov-75	3:00	39.6	39.6
21-Nov-75	4:00	39.4	39.4
21-Nov-75	5:00	39.2	39.2
21-Nov-75	6:00	39	39
21-Nov-75	7:00	38.7	38.7
21-Nov-75	8:00	38.5	38.5
21-Nov-75	9:00	38.3	38.3
21-Nov-75	10:00	38.1	38.1
21-Nov-75	11:00	37.9	37.9
21-Nov-75	12:00	37.7	37.7
21-Nov-75	13:00	37.5	37.5
21-Nov-75	14:00	37.3	37.3
21-Nov-75	15:00	37.1	37.1
21-Nov-75	16:00	36.9	36.9
21-Nov-75	17:00	36.7	36.7
21-Nov-75	18:00	36.5	36.5
21-Nov-75	19:00	36.3	36.3
21-Nov-75	20:00	36.2	36.2
21-Nov-75	21:00	36	36

21-Nov-75	22:00	35.8	35.8
21-Nov-75	23:00	35.6	35.6
22-Nov-75	0:00	35.4	35.4
22-Nov-75	1:00	35.2	35.2
22-Nov-75	2:00	35	35
22-Nov-75	3:00	34.8	34.8
22-Nov-75	4:00	34.6	34.6
22-Nov-75	5:00	34.5	34.5
22-Nov-75	6:00	34.3	34.3
22-Nov-75	7:00	34.1	34.1
22-Nov-75	8:00	33.9	33.9
22-Nov-75	9:00	33.7	33.7
22-Nov-75	10:00	33.6	33.6
22-Nov-75	11:00	33.4	33.4
22-Nov-75	12:00	33.2	33.2
22-Nov-75	13:00	33	33
22-Nov-75	14:00	32.9	32.9
22-Nov-75	15:00	32.7	32.7
22-Nov-75	16:00	32.5	32.5
22-Nov-75	17:00	32.3	32.3
22-Nov-75	18:00	32.2	32.2
22-Nov-75	19:00	32	32
22-Nov-75	20:00	31.8	31.8

22-Nov-75	21:00	31.6	31.6
22-Nov-75	22:00	31.5	31.5
22-Nov-75	23:00	31.3	31.3
23-Nov-75	0:00	31.1	31.1

Input Hydrographs Iyidere River 10-Year Return Period of Flood

Date	Time	Inflow (m3/s)	Outflow (m3/s)
15-Nov-75	0:00	11	11
15-Nov-75	1:00	10.9	10.9
15-Nov-75	2:00	10.9	10.9
15-Nov-75	3:00	10.8	10.8
15-Nov-75	4:00	11.2	11.2
15-Nov-75	5:00	13.6	13.6
15-Nov-75	6:00	21.3	21.3
15-Nov-75	7:00	39.4	39.4
15-Nov-75	8:00	119.1	119.1
15-Nov-75	9:00	393.8	393.8
15-Nov-75	10:00	691	691
15-Nov-75	11:00	776.6	776.6
15-Nov-75	12:00	798.3	798.3
15-Nov-75	13:00	803.2	803.2
15-Nov-75	14:00	802.4	802.4
15-Nov-75	15:00	797.1	797.1
15-Nov-75	16:00	791.1	791.1
15-Nov-75	17:00	780.6	780.6
15-Nov-75	18:00	766.6	766.6
15-Nov-75	19:00	752.3	752.3

15-Nov-75	20:00	733.9	733.9
15-Nov-75	21:00	712.3	712.3
15-Nov-75	22:00	692	692
15-Nov-75	23:00	672.9	672.9
16-Nov-75	0:00	654.9	654.9
16-Nov-75	1:00	635.8	635.8
16-Nov-75	2:00	607.7	607.7
16-Nov-75	3:00	572.6	572.6
16-Nov-75	4:00	539.4	539.4
16-Nov-75	5:00	508.2	508.2
16-Nov-75	6:00	478.8	478.8
16-Nov-75	7:00	451.1	451.1
16-Nov-75	8:00	425.1	425.1
16-Nov-75	9:00	400.6	400.6
16-Nov-75	10:00	377.5	377.5
16-Nov-75	11:00	355.8	355.8
16-Nov-75	12:00	335.4	335.4
16-Nov-75	13:00	316.1	316.1
16-Nov-75	14:00	298	298
16-Nov-75	15:00	281	281
16-Nov-75	16:00	264.9	264.9
16-Nov-75	17:00	249.8	249.8
16-Nov-75	18:00	235.6	235.6

16-Nov-75	19:00	222.2	222.2
16-Nov-75	20:00	209.6	209.6
16-Nov-75	21:00	197.7	197.7
16-Nov-75	22:00	186.6	186.6
16-Nov-75	23:00	176.1	176.1
17-Nov-75	0:00	166.2	166.2
17-Nov-75	1:00	156.8	156.8
17-Nov-75	2:00	148.1	148.1
17-Nov-75	3:00	139.8	139.8
17-Nov-75	4:00	132	132
17-Nov-75	5:00	124.7	124.7
17-Nov-75	6:00	117.8	117.8
17-Nov-75	7:00	111.3	111.3
17-Nov-75	8:00	105.2	105.2
17-Nov-75	9:00	99.5	99.5
17-Nov-75	10:00	94	94
17-Nov-75	11:00	88.9	88.9
17-Nov-75	12:00	84.1	84.1
17-Nov-75	13:00	79.6	79.6
17-Nov-75	14:00	75.4	75.4
17-Nov-75	15:00	71.4	71.4
17-Nov-75	16:00	67.6	67.6
17-Nov-75	17:00	64	64

17-Nov-75	18:00	61.9	61.9
17-Nov-75	19:00	61.5	61.5
17-Nov-75	20:00	61.2	61.2
17-Nov-75	21:00	60.9	60.9
17-Nov-75	22:00	60.6	60.6
17-Nov-75	23:00	60.2	60.2
18-Nov-75	0:00	59.9	59.9
18-Nov-75	1:00	59.6	59.6
18-Nov-75	2:00	59.3	59.3
18-Nov-75	3:00	59	59
18-Nov-75	4:00	58.7	58.7
18-Nov-75	5:00	58.3	58.3
18-Nov-75	6:00	58	58
18-Nov-75	7:00	57.7	57.7
18-Nov-75	8:00	57.4	57.4
18-Nov-75	9:00	57.1	57.1
18-Nov-75	10:00	56.8	56.8
18-Nov-75	11:00	56.5	56.5
18-Nov-75	12:00	56.2	56.2
18-Nov-75	13:00	55.9	55.9
18-Nov-75	14:00	55.6	55.6
18-Nov-75	15:00	55.3	55.3
18-Nov-75	16:00	55	55

18-Nov-75	17:00	54.7	54.7
18-Nov-75	18:00	54.4	54.4
18-Nov-75	19:00	54.2	54.2
18-Nov-75	20:00	53.9	53.9
18-Nov-75	21:00	53.6	53.6
18-Nov-75	22:00	53.3	53.3
18-Nov-75	23:00	53	53
19-Nov-75	0:00	52.7	52.7
19-Nov-75	1:00	52.5	52.5
19-Nov-75	2:00	52.2	52.2
19-Nov-75	3:00	51.9	51.9
19-Nov-75	4:00	51.6	51.6
19-Nov-75	5:00	51.3	51.3
19-Nov-75	6:00	51.1	51.1
19-Nov-75	7:00	50.8	50.8
19-Nov-75	8:00	50.5	50.5
19-Nov-75	9:00	50.3	50.3
19-Nov-75	10:00	50	50
19-Nov-75	11:00	49.7	49.7
19-Nov-75	12:00	49.5	49.5
19-Nov-75	13:00	49.2	49.2
19-Nov-75	14:00	48.9	48.9
19-Nov-75	15:00	48.7	48.7

19-Nov-75	16:00	48.4	48.4
19-Nov-75	17:00	48.2	48.2
19-Nov-75	18:00	47.9	47.9
19-Nov-75	19:00	47.7	47.7
19-Nov-75	20:00	47.4	47.4
19-Nov-75	21:00	47.2	47.2
19-Nov-75	22:00	46.9	46.9
19-Nov-75	23:00	46.7	46.7
20-Nov-75	0:00	46.4	46.4
20-Nov-75	1:00	46.2	46.2
20-Nov-75	2:00	45.9	45.9
20-Nov-75	3:00	45.7	45.7
20-Nov-75	4:00	45.4	45.4
20-Nov-75	5:00	45.2	45.2
20-Nov-75	6:00	44.9	44.9
20-Nov-75	7:00	44.7	44.7
20-Nov-75	8:00	44.5	44.5
20-Nov-75	9:00	44.2	44.2
20-Nov-75	10:00	44	44
20-Nov-75	11:00	43.8	43.8
20-Nov-75	12:00	43.5	43.5
20-Nov-75	13:00	43.3	43.3
20-Nov-75	14:00	43.1	43.1

20-Nov-75	15:00	42.8	42.8
20-Nov-75	16:00	42.6	42.6
20-Nov-75	17:00	42.4	42.4
20-Nov-75	18:00	42.2	42.2
20-Nov-75	19:00	41.9	41.9
20-Nov-75	20:00	41.7	41.7
20-Nov-75	21:00	41.5	41.5
20-Nov-75	22:00	41.3	41.3
20-Nov-75	23:00	41.1	41.1
21-Nov-75	0:00	40.8	40.8
21-Nov-75	1:00	40.6	40.6
21-Nov-75	2:00	40.4	40.4
21-Nov-75	3:00	40.2	40.2
21-Nov-75	4:00	40	40
21-Nov-75	5:00	39.8	39.8
21-Nov-75	6:00	39.6	39.6
21-Nov-75	7:00	39.3	39.3
21-Nov-75	8:00	39.1	39.1
21-Nov-75	9:00	38.9	38.9
21-Nov-75	10:00	38.7	38.7
21-Nov-75	11:00	38.5	38.5
21-Nov-75	12:00	38.3	38.3
21-Nov-75	13:00	38.1	38.1

21-Nov-75	14:00	37.9	37.9
21-Nov-75	15:00	37.7	37.7
21-Nov-75	16:00	37.5	37.5
21-Nov-75	17:00	37.3	37.3
21-Nov-75	18:00	37.1	37.1
21-Nov-75	19:00	36.9	36.9
21-Nov-75	20:00	36.7	36.7
21-Nov-75	21:00	36.5	36.5
21-Nov-75	22:00	36.3	36.3
21-Nov-75	23:00	36.1	36.1
22-Nov-75	0:00	35.9	35.9
22-Nov-75	1:00	35.7	35.7
22-Nov-75	2:00	35.6	35.6
22-Nov-75	3:00	35.4	35.4
22-Nov-75	4:00	35.2	35.2
22-Nov-75	5:00	35	35
22-Nov-75	6:00	34.8	34.8
22-Nov-75	7:00	34.6	34.6
22-Nov-75	8:00	34.4	34.4
22-Nov-75	9:00	34.3	34.3
22-Nov-75	10:00	34.1	34.1
22-Nov-75	11:00	33.9	33.9
22-Nov-75	12:00	33.7	33.7

22-Nov-75	13:00	33.5	33.5
22-Nov-75	14:00	33.4	33.4
22-Nov-75	15:00	33.2	33.2
22-Nov-75	16:00	33	33
22-Nov-75	17:00	32.8	32.8
22-Nov-75	18:00	32.7	32.7
22-Nov-75	19:00	32.5	32.5
22-Nov-75	20:00	32.3	32.3
22-Nov-75	21:00	32.1	32.1
22-Nov-75	22:00	32	32
22-Nov-75	23:00	31.8	31.8
23-Nov-75	0:00	31.6	31.6

Input Hydrographs Iyidere River 25-Year Return Period of Flood

date	time	inflow (m3/s)	outflow (m3/s)
15-Nov-75	0:00	11	11
15-Nov-75	1:00	10.9	10.9
15-Nov-75	2:00	10.9	10.9
15-Nov-75	3:00	10.9	10.9
15-Nov-75	4:00	11.8	11.8
15-Nov-75	5:00	16.4	16.4
15-Nov-75	6:00	28.6	28.6

15-Nov-75	7:00	54.5	54.5
15-Nov-75	8:00	156.6	156.6
15-Nov-75	9:00	496.3	496.3
15-Nov-75	10:00	855.4	855.4
15-Nov-75	11:00	955.3	955.3
15-Nov-75	12:00	979	979
15-Nov-75	13:00	982.8	982.8
15-Nov-75	14:00	979.9	979.9
15-Nov-75	15:00	971.7	971.7
15-Nov-75	16:00	962.8	962.8
15-Nov-75	17:00	948.7	948.7
15-Nov-75	18:00	930.5	930.5
15-Nov-75	19:00	912.1	912.1
15-Nov-75	20:00	888.9	888.9
15-Nov-75	21:00	861.9	861.9
15-Nov-75	22:00	836.6	836.6
15-Nov-75	23:00	812.7	812.7
16-Nov-75	0:00	790.3	790.3
16-Nov-75	1:00	766.6	766.6
16-Nov-75	2:00	732.3	732.3
16-Nov-75	3:00	689.9	689.9
16-Nov-75	4:00	649.8	649.8
16-Nov-75	5:00	612.1	612.1

16-Nov-75	6:00	576.6	576.6
16-Nov-75	7:00	543.2	543.2
16-Nov-75	8:00	511.7	511.7
16-Nov-75	9:00	482.1	482.1
16-Nov-75	10:00	454.3	454.3
16-Nov-75	11:00	428	428
16-Nov-75	12:00	403.3	403.3
16-Nov-75	13:00	380.1	380.1
16-Nov-75	14:00	358.2	358.2
16-Nov-75	15:00	337.6	337.6
16-Nov-75	16:00	318.3	318.3
16-Nov-75	17:00	300	300
16-Nov-75	18:00	282.8	282.8
16-Nov-75	19:00	266.7	266.7
16-Nov-75	20:00	251.5	251.5
16-Nov-75	21:00	237.1	237.1
16-Nov-75	22:00	223.6	223.6
16-Nov-75	23:00	210.9	210.9
17-Nov-75	0:00	199	199
17-Nov-75	1:00	187.7	187.7
17-Nov-75	2:00	177.2	177.2
17-Nov-75	3:00	167.2	167.2
17-Nov-75	4:00	157.8	157.8

17-Nov-75	5:00	149	149
17-Nov-75	6:00	140.6	140.6
17-Nov-75	7:00	132.8	132.8
17-Nov-75	8:00	125.4	125.4
17-Nov-75	9:00	118.5	118.5
17-Nov-75	10:00	112	112
17-Nov-75	11:00	105.8	105.8
17-Nov-75	12:00	100	100
17-Nov-75	13:00	94.6	94.6
17-Nov-75	14:00	89.4	89.4
17-Nov-75	15:00	84.6	84.6
17-Nov-75	16:00	80	80
17-Nov-75	17:00	75.7	75.7
17-Nov-75	18:00	71.7	71.7
17-Nov-75	19:00	67.9	67.9
17-Nov-75	20:00	64.3	64.3
17-Nov-75	21:00	61.9	61.9
17-Nov-75	22:00	61.6	61.6
17-Nov-75	23:00	61.2	61.2
18-Nov-75	0:00	60.9	60.9
18-Nov-75	1:00	60.6	60.6
18-Nov-75	2:00	60.3	60.3
18-Nov-75	3:00	59.9	59.9

18-Nov-75	4:00	59.6	59.6
18-Nov-75	5:00	59.3	59.3
18-Nov-75	6:00	59	59
18-Nov-75	7:00	58.7	58.7
18-Nov-75	8:00	58.4	58.4
18-Nov-75	9:00	58.1	58.1
18-Nov-75	10:00	57.8	57.8
18-Nov-75	11:00	57.4	57.4
18-Nov-75	12:00	57.1	57.1
18-Nov-75	13:00	56.8	56.8
18-Nov-75	14:00	56.5	56.5
18-Nov-75	15:00	56.2	56.2
18-Nov-75	16:00	55.9	55.9
18-Nov-75	17:00	55.6	55.6
18-Nov-75	18:00	55.3	55.3
18-Nov-75	19:00	55.1	55.1
18-Nov-75	20:00	54.8	54.8
18-Nov-75	21:00	54.5	54.5
18-Nov-75	22:00	54.2	54.2
18-Nov-75	23:00	53.9	53.9
19-Nov-75	0:00	53.6	53.6
19-Nov-75	1:00	53.3	53.3
19-Nov-75	2:00	53	53

19-Nov-75	3:00	52.8	52.8
19-Nov-75	4:00	52.5	52.5
19-Nov-75	5:00	52.2	52.2
19-Nov-75	6:00	51.9	51.9
19-Nov-75	7:00	51.6	51.6
19-Nov-75	8:00	51.4	51.4
19-Nov-75	9:00	51.1	51.1
19-Nov-75	10:00	50.8	50.8
19-Nov-75	11:00	50.6	50.6
19-Nov-75	12:00	50.3	50.3
19-Nov-75	13:00	50	50
19-Nov-75	14:00	49.8	49.8
19-Nov-75	15:00	49.5	49.5
19-Nov-75	16:00	49.2	49.2
19-Nov-75	17:00	49	49
19-Nov-75	18:00	48.7	48.7
19-Nov-75	19:00	48.4	48.4
19-Nov-75	20:00	48.2	48.2
19-Nov-75	21:00	47.9	47.9
19-Nov-75	22:00	47.7	47.7
19-Nov-75	23:00	47.4	47.4
20-Nov-75	0:00	47.2	47.2
20-Nov-75	1:00	46.9	46.9

20-Nov-75	2:00	46.7	46.7
20-Nov-75	3:00	46.4	46.4
20-Nov-75	4:00	46.2	46.2
20-Nov-75	5:00	45.9	45.9
20-Nov-75	6:00	45.7	45.7
20-Nov-75	7:00	45.4	45.4
20-Nov-75	8:00	45.2	45.2
20-Nov-75	9:00	45	45
20-Nov-75	10:00	44.7	44.7
20-Nov-75	11:00	44.5	44.5
20-Nov-75	12:00	44.3	44.3
20-Nov-75	13:00	44	44
20-Nov-75	14:00	43.8	43.8
20-Nov-75	15:00	43.6	43.6
20-Nov-75	16:00	43.3	43.3
20-Nov-75	17:00	43.1	43.1
20-Nov-75	18:00	42.9	42.9
20-Nov-75	19:00	42.6	42.6
20-Nov-75	20:00	42.4	42.4
20-Nov-75	21:00	42.2	42.2
20-Nov-75	22:00	42	42
20-Nov-75	23:00	41.7	41.7
21-Nov-75	0:00	41.5	41.5

21-Nov-75	1:00	41.3	41.3
21-Nov-75	2:00	41.1	41.1
21-Nov-75	3:00	40.9	40.9
21-Nov-75	4:00	40.6	40.6
21-Nov-75	5:00	40.4	40.4
21-Nov-75	6:00	40.2	40.2
21-Nov-75	7:00	40	40
21-Nov-75	8:00	39.8	39.8
21-Nov-75	9:00	39.6	39.6
21-Nov-75	10:00	39.4	39.4
21-Nov-75	11:00	39.1	39.1
21-Nov-75	12:00	38.9	38.9
21-Nov-75	13:00	38.7	38.7
21-Nov-75	14:00	38.5	38.5
21-Nov-75	15:00	38.3	38.3
21-Nov-75	16:00	38.1	38.1
21-Nov-75	17:00	37.9	37.9
21-Nov-75	18:00	37.7	37.7
21-Nov-75	19:00	37.5	37.5
21-Nov-75	20:00	37.3	37.3
21-Nov-75	21:00	37.1	37.1
21-Nov-75	22:00	36.9	36.9
21-Nov-75	23:00	36.7	36.7

22-Nov-75	0:00	36.5	36.5
22-Nov-75	1:00	36.3	36.3
22-Nov-75	2:00	36.1	36.1
22-Nov-75	3:00	36	36
22-Nov-75	4:00	35.8	35.8
22-Nov-75	5:00	35.6	35.6
22-Nov-75	6:00	35.4	35.4
22-Nov-75	7:00	35.2	35.2
22-Nov-75	8:00	35	35
22-Nov-75	9:00	34.8	34.8
22-Nov-75	10:00	34.6	34.6
22-Nov-75	11:00	34.5	34.5
22-Nov-75	12:00	34.3	34.3
22-Nov-75	13:00	34.1	34.1
22-Nov-75	14:00	33.9	33.9
22-Nov-75	15:00	33.7	33.7
22-Nov-75	16:00	33.5	33.5
22-Nov-75	17:00	33.4	33.4
22-Nov-75	18:00	33.2	33.2
22-Nov-75	19:00	33	33
22-Nov-75	20:00	32.8	32.8
22-Nov-75	21:00	32.7	32.7
22-Nov-75	22:00	32.5	32.5

22-Nov-75	23:00	32.3	32.3
23-Nov-75	0:00	32.1	32.1

Input Hydrographs Iyidere River 50-Year Return Period of Flood

Date	Time	Inflow (m3/s)	Outflow (m3/s)
15-Nov-75	0:00	11	11
15-Nov-75	1:00	10.9	10.9
15-Nov-75	2:00	10.9	10.9
15-Nov-75	3:00	10.9	10.9
15-Nov-75	4:00	12.5	12.5
15-Nov-75	5:00	19.2	19.2
15-Nov-75	6:00	35.4	35.4
15-Nov-75	7:00	67.6	67.6
15-Nov-75	8:00	187	187
15-Nov-75	9:00	576.5	576.5
15-Nov-75	10:00	982.6	982.6
15-Nov-75	11:00	1093.1	1093.1
15-Nov-75	12:00	1118.1	1118.1
15-Nov-75	13:00	1120.9	1120.9
15-Nov-75	14:00	1116.3	1116.3
15-Nov-75	15:00	1105.8	1105.8
15-Nov-75	16:00	1094.6	1094.6

15-Nov-75	17:00	1077.6	1077.6
15-Nov-75	18:00	1056	1056
15-Nov-75	19:00	1034.3	1034.3
15-Nov-75	20:00	1007.3	1007.3
15-Nov-75	21:00	976.3	976.3
15-Nov-75	22:00	947.1	947.1
15-Nov-75	23:00	919.7	919.7
16-Nov-75	0:00	893.9	893.9
16-Nov-75	1:00	866.7	866.7
16-Nov-75	2:00	827.7	827.7
16-Nov-75	3:00	779.7	779.7
16-Nov-75	4:00	734.3	734.3
16-Nov-75	5:00	691.7	691.7
16-Nov-75	6:00	651.5	651.5
16-Nov-75	7:00	613.7	613.7
16-Nov-75	8:00	578.1	578.1
16-Nov-75	9:00	544.5	544.5
16-Nov-75	10:00	513	513
16-Nov-75	11:00	483.3	483.3
16-Nov-75	12:00	455.4	455.4
16-Nov-75	13:00	429.1	429.1
16-Nov-75	14:00	404.3	404.3
16-Nov-75	15:00	381	381

16-Nov-75	16:00	359.1	359.1
16-Nov-75	17:00	338.4	338.4
16-Nov-75	18:00	319	319
16-Nov-75	19:00	300.7	300.7
16-Nov-75	20:00	283.5	283.5
16-Nov-75	21:00	267.3	267.3
16-Nov-75	22:00	252	252
16-Nov-75	23:00	237.7	237.7
17-Nov-75	0:00	224.1	224.1
17-Nov-75	1:00	211.4	211.4
17-Nov-75	2:00	199.4	199.4
17-Nov-75	3:00	188.1	188.1
17-Nov-75	4:00	177.5	177.5
17-Nov-75	5:00	167.5	167.5
17-Nov-75	6:00	158.1	158.1
17-Nov-75	7:00	149.3	149.3
17-Nov-75	8:00	140.9	140.9
17-Nov-75	9:00	133.1	133.1
17-Nov-75	10:00	125.7	125.7
17-Nov-75	11:00	118.7	118.7
17-Nov-75	12:00	112.2	112.2
17-Nov-75	13:00	106	106
17-Nov-75	14:00	100.2	100.2

17-Nov-75	15:00	94.7	94.7
17-Nov-75	16:00	89.6	89.6
17-Nov-75	17:00	84.7	84.7
17-Nov-75	18:00	80.1	80.1
17-Nov-75	19:00	75.8	75.8
17-Nov-75	20:00	71.8	71.8
17-Nov-75	21:00	68	68
17-Nov-75	22:00	64.4	64.4
17-Nov-75	23:00	61.9	61.9
18-Nov-75	0:00	61.6	61.6
18-Nov-75	1:00	61.2	61.2
18-Nov-75	2:00	60.9	60.9
18-Nov-75	3:00	60.6	60.6
18-Nov-75	4:00	60.3	60.3
18-Nov-75	5:00	60	60
18-Nov-75	6:00	59.6	59.6
18-Nov-75	7:00	59.3	59.3
18-Nov-75	8:00	59	59
18-Nov-75	9:00	58.7	58.7
18-Nov-75	10:00	58.4	58.4
18-Nov-75	11:00	58.1	58.1
18-Nov-75	12:00	57.8	57.8
18-Nov-75	13:00	57.5	57.5

18-Nov-75	14:00	57.1	57.1
18-Nov-75	15:00	56.8	56.8
18-Nov-75	16:00	56.5	56.5
18-Nov-75	17:00	56.2	56.2
18-Nov-75	18:00	55.9	55.9
18-Nov-75	19:00	55.6	55.6
18-Nov-75	20:00	55.4	55.4
18-Nov-75	21:00	55.1	55.1
18-Nov-75	22:00	54.8	54.8
18-Nov-75	23:00	54.5	54.5
19-Nov-75	0:00	54.2	54.2
19-Nov-75	1:00	53.9	53.9
19-Nov-75	2:00	53.6	53.6
19-Nov-75	3:00	53.3	53.3
19-Nov-75	4:00	53	53
19-Nov-75	5:00	52.8	52.8
19-Nov-75	6:00	52.5	52.5
19-Nov-75	7:00	52.2	52.2
19-Nov-75	8:00	51.9	51.9
19-Nov-75	9:00	51.6	51.6
19-Nov-75	10:00	51.4	51.4
19-Nov-75	11:00	51.1	51.1
19-Nov-75	12:00	50.8	50.8

19-Nov-75	13:00	50.6	50.6
19-Nov-75	14:00	50.3	50.3
19-Nov-75	15:00	50	50
19-Nov-75	16:00	49.8	49.8
19-Nov-75	17:00	49.5	49.5
19-Nov-75	18:00	49.2	49.2
19-Nov-75	19:00	49	49
19-Nov-75	20:00	48.7	48.7
19-Nov-75	21:00	48.5	48.5
19-Nov-75	22:00	48.2	48.2
19-Nov-75	23:00	47.9	47.9
20-Nov-75	0:00	47.7	47.7
20-Nov-75	1:00	47.4	47.4
20-Nov-75	2:00	47.2	47.2
20-Nov-75	3:00	46.9	46.9
20-Nov-75	4:00	46.7	46.7
20-Nov-75	5:00	46.4	46.4
20-Nov-75	6:00	46.2	46.2
20-Nov-75	7:00	45.9	45.9
20-Nov-75	8:00	45.7	45.7
20-Nov-75	9:00	45.5	45.5
20-Nov-75	10:00	45.2	45.2
20-Nov-75	11:00	45	45

20-Nov-75	12:00	44.7	44.7
20-Nov-75	13:00	44.5	44.5
20-Nov-75	14:00	44.3	44.3
20-Nov-75	15:00	44	44
20-Nov-75	16:00	43.8	43.8
20-Nov-75	17:00	43.6	43.6
20-Nov-75	18:00	43.3	43.3
20-Nov-75	19:00	43.1	43.1
20-Nov-75	20:00	42.9	42.9
20-Nov-75	21:00	42.6	42.6
20-Nov-75	22:00	42.4	42.4
20-Nov-75	23:00	42.2	42.2
21-Nov-75	0:00	42	42
21-Nov-75	1:00	41.7	41.7
21-Nov-75	2:00	41.5	41.5
21-Nov-75	3:00	41.3	41.3
21-Nov-75	4:00	41.1	41.1
21-Nov-75	5:00	40.9	40.9
21-Nov-75	6:00	40.6	40.6
21-Nov-75	7:00	40.4	40.4
21-Nov-75	8:00	40.2	40.2
21-Nov-75	9:00	40	40
21-Nov-75	10:00	39.8	39.8

21-Nov-75	11:00	39.6	39.6
21-Nov-75	12:00	39.4	39.4
21-Nov-75	13:00	39.2	39.2
21-Nov-75	14:00	38.9	38.9
21-Nov-75	15:00	38.7	38.7
21-Nov-75	16:00	38.5	38.5
21-Nov-75	17:00	38.3	38.3
21-Nov-75	18:00	38.1	38.1
21-Nov-75	19:00	37.9	37.9
21-Nov-75	20:00	37.7	37.7
21-Nov-75	21:00	37.5	37.5
21-Nov-75	22:00	37.3	37.3
21-Nov-75	23:00	37.1	37.1
22-Nov-75	0:00	36.9	36.9
22-Nov-75	1:00	36.7	36.7
22-Nov-75	2:00	36.5	36.5
22-Nov-75	3:00	36.3	36.3
22-Nov-75	4:00	36.1	36.1
22-Nov-75	5:00	36	36
22-Nov-75	6:00	35.8	35.8
22-Nov-75	7:00	35.6	35.6
22-Nov-75	8:00	35.4	35.4
22-Nov-75	9:00	35.2	35.2

22-Nov-75	10:00	35	35
22-Nov-75	11:00	34.8	34.8
22-Nov-75	12:00	34.6	34.6
22-Nov-75	13:00	34.5	34.5
22-Nov-75	14:00	34.3	34.3
22-Nov-75	15:00	34.1	34.1
22-Nov-75	16:00	33.9	33.9
22-Nov-75	17:00	33.7	33.7
22-Nov-75	18:00	33.5	33.5
22-Nov-75	19:00	33.4	33.4
22-Nov-75	20:00	33.2	33.2
22-Nov-75	21:00	33	33
22-Nov-75	22:00	32.8	32.8
22-Nov-75	23:00	32.7	32.7
23-Nov-75	0:00	32.5	32.5

Input Hydrographs Iyidere River 100-Year Return Period of Flood

Date	Time	Inflow (m3/s)	Outflow (m3/s)
15-Nov-75	0:00	11	11
15-Nov-75	1:00	10.9	10.9
15-Nov-75	2:00	10.9	10.9
15-Nov-75	3:00	11	11
15-Nov-75	4:00	13.5	13.5
15-Nov-75	5:00	22.7	22.7
15-Nov-75	6:00	43.3	43.3
15-Nov-75	7:00	82.1	82.1
15-Nov-75	8:00	219.3	219.3
15-Nov-75	9:00	659.2	659.2
15-Nov-75	10:00	1112.9	1112.9
15-Nov-75	11:00	1234	1234
15-Nov-75	12:00	1260.2	1260.2
15-Nov-75	13:00	1261.9	1261.9
15-Nov-75	14:00	1255.4	1255.4
15-Nov-75	15:00	1242.4	1242.4
15-Nov-75	16:00	1228.7	1228.7
15-Nov-75	17:00	1208.7	1208.7
15-Nov-75	18:00	1183.8	1183.8
15-Nov-75	19:00	1158.6	1158.6

15-Nov-75	20:00	1127.8	1127.8
15-Nov-75	21:00	1092.5	1092.5
15-Nov-75	22:00	1059.2	1059.2
15-Nov-75	23:00	1028	1028
16-Nov-75	0:00	998.6	998.6
16-Nov-75	1:00	967.7	967.7
16-Nov-75	2:00	924	924
16-Nov-75	3:00	870.3	870.3
16-Nov-75	4:00	819.6	819.6
16-Nov-75	5:00	771.9	771.9
16-Nov-75	6:00	727	727
16-Nov-75	7:00	684.7	684.7
16-Nov-75	8:00	644.9	644.9
16-Nov-75	9:00	607.5	607.5
16-Nov-75	10:00	572.3	572.3
16-Nov-75	11:00	539.1	539.1
16-Nov-75	12:00	507.9	507.9
16-Nov-75	13:00	478.5	478.5
16-Nov-75	14:00	450.8	450.8
16-Nov-75	15:00	424.8	424.8
16-Nov-75	16:00	400.3	400.3
16-Nov-75	17:00	377.2	377.2
16-Nov-75	18:00	355.5	355.5

16-Nov-75	19:00	335	335
16-Nov-75	20:00	315.8	315.8
16-Nov-75	21:00	297.7	297.7
16-Nov-75	22:00	280.6	280.6
16-Nov-75	23:00	264.6	264.6
17-Nov-75	0:00	249.5	249.5
17-Nov-75	1:00	235.3	235.3
17-Nov-75	2:00	221.9	221.9
17-Nov-75	3:00	209.3	209.3
17-Nov-75	4:00	197.4	197.4
17-Nov-75	5:00	186.3	186.3
17-Nov-75	6:00	175.7	175.7
17-Nov-75	7:00	165.8	165.8
17-Nov-75	8:00	156.5	156.5
17-Nov-75	9:00	147.8	147.8
17-Nov-75	10:00	139.5	139.5
17-Nov-75	11:00	131.7	131.7
17-Nov-75	12:00	124.4	124.4
17-Nov-75	13:00	117.5	117.5
17-Nov-75	14:00	111	111
17-Nov-75	15:00	104.9	104.9
17-Nov-75	16:00	99.2	99.2
17-Nov-75	17:00	93.8	93.8

17-Nov-75	18:00	88.7	88.7
17-Nov-75	19:00	83.9	83.9
17-Nov-75	20:00	79.3	79.3
17-Nov-75	21:00	75.1	75.1
17-Nov-75	22:00	71.1	71.1
17-Nov-75	23:00	67.3	67.3
18-Nov-75	0:00	63.7	63.7
18-Nov-75	1:00	61.8	61.8
18-Nov-75	2:00	61.5	61.5
18-Nov-75	3:00	61.2	61.2
18-Nov-75	4:00	60.9	60.9
18-Nov-75	5:00	60.5	60.5
18-Nov-75	6:00	60.2	60.2
18-Nov-75	7:00	59.9	59.9
18-Nov-75	8:00	59.6	59.6
18-Nov-75	9:00	59.3	59.3
18-Nov-75	10:00	58.9	58.9
18-Nov-75	11:00	58.6	58.6
18-Nov-75	12:00	58.3	58.3
18-Nov-75	13:00	58	58
18-Nov-75	14:00	57.7	57.7
18-Nov-75	15:00	57.4	57.4
18-Nov-75	16:00	57.1	57.1

18-Nov-75	17:00	56.8	56.8
18-Nov-75	18:00	56.5	56.5
18-Nov-75	19:00	56.2	56.2
18-Nov-75	20:00	55.9	55.9
18-Nov-75	21:00	55.6	55.6
18-Nov-75	22:00	55.3	55.3
18-Nov-75	23:00	55	55
19-Nov-75	0:00	54.7	54.7
19-Nov-75	1:00	54.4	54.4
19-Nov-75	2:00	54.1	54.1
19-Nov-75	3:00	53.8	53.8
19-Nov-75	4:00	53.6	53.6
19-Nov-75	5:00	53.3	53.3
19-Nov-75	6:00	53	53
19-Nov-75	7:00	52.7	52.7
19-Nov-75	8:00	52.4	52.4
19-Nov-75	9:00	52.2	52.2
19-Nov-75	10:00	51.9	51.9
19-Nov-75	11:00	51.6	51.6
19-Nov-75	12:00	51.3	51.3
19-Nov-75	13:00	51.1	51.1
19-Nov-75	14:00	50.8	50.8
19-Nov-75	15:00	50.5	50.5

19-Nov-75	16:00	50.2	50.2
19-Nov-75	17:00	50	50
19-Nov-75	18:00	49.7	49.7
19-Nov-75	19:00	49.4	49.4
19-Nov-75	20:00	49.2	49.2
19-Nov-75	21:00	48.9	48.9
19-Nov-75	22:00	48.7	48.7
19-Nov-75	23:00	48.4	48.4
20-Nov-75	0:00	48.1	48.1
20-Nov-75	1:00	47.9	47.9
20-Nov-75	2:00	47.6	47.6
20-Nov-75	3:00	47.4	47.4
20-Nov-75	4:00	47.1	47.1
20-Nov-75	5:00	46.9	46.9
20-Nov-75	6:00	46.6	46.6
20-Nov-75	7:00	46.4	46.4
20-Nov-75	8:00	46.1	46.1
20-Nov-75	9:00	45.9	45.9
20-Nov-75	10:00	45.6	45.6
20-Nov-75	11:00	45.4	45.4
20-Nov-75	12:00	45.2	45.2
20-Nov-75	13:00	44.9	44.9
20-Nov-75	14:00	44.7	44.7

20-Nov-75	15:00	44.4	44.4
20-Nov-75	16:00	44.2	44.2
20-Nov-75	17:00	44	44
20-Nov-75	18:00	43.7	43.7
20-Nov-75	19:00	43.5	43.5
20-Nov-75	20:00	43.3	43.3
20-Nov-75	21:00	43.1	43.1
20-Nov-75	22:00	42.8	42.8
20-Nov-75	23:00	42.6	42.6
21-Nov-75	0:00	42.4	42.4
21-Nov-75	1:00	42.1	42.1
21-Nov-75	2:00	41.9	41.9
21-Nov-75	3:00	41.7	41.7
21-Nov-75	4:00	41.5	41.5
21-Nov-75	5:00	41.3	41.3
21-Nov-75	6:00	41	41
21-Nov-75	7:00	40.8	40.8
21-Nov-75	8:00	40.6	40.6
21-Nov-75	9:00	40.4	40.4
21-Nov-75	10:00	40.2	40.2
21-Nov-75	11:00	40	40
21-Nov-75	12:00	39.7	39.7
21-Nov-75	13:00	39.5	39.5

21-Nov-75	14:00	39.3	39.3
21-Nov-75	15:00	39.1	39.1
21-Nov-75	16:00	38.9	38.9
21-Nov-75	17:00	38.7	38.7
21-Nov-75	18:00	38.5	38.5
21-Nov-75	19:00	38.3	38.3
21-Nov-75	20:00	38.1	38.1
21-Nov-75	21:00	37.9	37.9
21-Nov-75	22:00	37.7	37.7
21-Nov-75	23:00	37.5	37.5
22-Nov-75	0:00	37.3	37.3
22-Nov-75	1:00	37.1	37.1
22-Nov-75	2:00	36.9	36.9
22-Nov-75	3:00	36.7	36.7
22-Nov-75	4:00	36.5	36.5
22-Nov-75	5:00	36.3	36.3
22-Nov-75	6:00	36.1	36.1
22-Nov-75	7:00	35.9	35.9
22-Nov-75	8:00	35.7	35.7
22-Nov-75	9:00	35.5	35.5
22-Nov-75	10:00	35.4	35.4
22-Nov-75	11:00	35.2	35.2
22-Nov-75	12:00	35	35

22-Nov-75	13:00	34.8	34.8
22-Nov-75	14:00	34.6	34.6
22-Nov-75	15:00	34.4	34.4
22-Nov-75	16:00	34.2	34.2
22-Nov-75	17:00	34.1	34.1
22-Nov-75	18:00	33.9	33.9
22-Nov-75	19:00	33.7	33.7
22-Nov-75	20:00	33.5	33.5
22-Nov-75	21:00	33.3	33.3
22-Nov-75	22:00	33.2	33.2
22-Nov-75	23:00	33	33
23-Nov-75	0:00	32.8	32.8

Appendix B

CORINE LAND COVER NOMENCLATURES

(European Environment Agency, 2012)

LEVEL 1	LEVEL 1	LEVEL 3
1. ARTIFICIAL SURFACES	1.1. Urban fabric 1.2. Industrial, commercial and transport units 1.3. Mine, dump and construction sites 1.4. Artificial, non-agricultural vegetated areas	1.1.1. Continuous urban fabric 1.1.2. Discontinuous urban fabric 1.2.1. Industrial or commercial units 1.2.2. Road and rail Networks and associated land 1.2.3. Port areas 1.2.4. Airports 1.3.1. Mineral extraction sites 1.3.2. Dump sites 1.3.3. Construction sites 1.4.1. Green urban areas 1.4.2. Sport and leisure facilities
2. AGRICULTURAL AREAS	2.1. Arable land	2.1.1. Non-irrigated arable land 2.1.2. Permanently

	2.2. Permanent crops 2.3. Pastures 2.4. Heterogeneous agricultural areas	irrigated land 2.1.3. Rice fields 2.2.1. Vineyards 2.2.2. Fruit trees and berry plantations 2.2.3. Olive groves 2.3.1. Pastures 2.4.1. Annual crops associated with permanent crops 2.4.2. Complex cultivation patterns 2.4.3. Land principally occupied by agriculture, with significant areas of natural vegetation 2.4.4. Agro-forestry areas
3. FOREST AND SEMI-NATURAL AREAS	3.1. Forests 3.2. Scrub and/or herbaceous associations	3.1.1. Broad-leaved forest 3.1.2. Coniferous forest 3.1.3. Mixed forest 3.2.1. Natural

	3.3. Open spaces with little or no vegetation	grassland 3.2.2. Moors and heathland 3.2.3. Sclerophyllous vegetation 3.2.4. Transitional woodland-scrub 3.3.1. Beaches, dunes, sands 3.3.2. Bare rocks 3.3.3. Sparsely vegetated areas 3.3.4. Burnt areas 3.3.5. Glaciers and perpetual snow
4. WETLANDS	4.1.Inland wetlands 4.2.Marine wetlands	4.1.1. Inland marshes 4.1.2. Peat bogs 4.2.1. Salt marshes 4.2.2. Salines 4.2.3. Intertidal flats
5. WATER BODIES	5.1. Inland waters 5.2. Marine waters	5.1.1. Water courses 5.1.2. Water bodies 5.2.1. Coastal lagoons 5.2.2. Estuaries 5.2.3. Sea and ocean